Role of Fibroblast Growth Factor Homologous Factors in Excitability of Hippocampal Neurons

BY

XIAO HUANG

A dissertation submitted to the Graduate Faculty in Biochemistry in partial fulfillment of the requirements for the degree of Doctor of Philosophy,

The City University of New York

2009

This manuscript has been read and accepted for the Graduate Faculty in Biochemistry in satisfaction of the dissertation requirement for the Doctor of Philosophy

Dr. Mitchell Goldfarb

_________________________ _________________________

Date Chair of Examining Committee

Dr. Edward J. Kennelly

_________________________ _________________________

Date Executive Officer

Dr. David A. Foster

____

Dr. Wilfredo Mellado

____

Dr. Probal Banerjee

____

Dr. Jonathan B. Levitt

____

Supervisory Committee

THE CITY UNIVERSITY OF NEW YORK

ABSTRACT

Role of Fibroblast Growth Factor Homologous Factors in Excitability of Hippocampal Neurons

By XIAO HUANG

Adviser: Professor Mitchell Goldfarb

Fibroblast growth factor homologous factors (FHFs) are a family of vertebrate neuronal proteins which function in manners distinct from fibroblast growth factors (FGFs). While bearing substantial sequence and structural homology to FGFs, FHFs reside intracellularly and bind targets unrelated to FGF receptors, which include voltage-gated sodium channels (Na_vs). FHFs have been shown to control excitability of cerebellar granule cells through modulation of channel inactivation. Since action potentials are initiated at axon initial segment (AIS), we suspected that at least some FHF isoforms would reside at AIS in association with Na_vs. As expected, a broad repertoire of FHF isoforms colocalizes with Na_vs at the AIS of cultured hippocampal neurons. Moreover, together with other studies in our laboratory, the present study shows that FHF "b" isoform associates with AIS to a far lesser extent than "a" isoform, demonstrating that there is isoform specificity in FHF targeting. AIS targeting of an FHF requires the

protein's channel binding surface, as a mutant derivative of FHF2a deficient for channel binding is also deficient in AIS targeting.

The association of FHFs with Na_vs at AIS suggests that FHFs may modulate channel physiology, thereby controlling the intrinsic excitability of hippocampal neurons in a manner similar to that which has been described for cerebellar granule neurons of *Fhf1*$^{-/-}$*Fhf4*$^{-/-}$ mice. Moreover, real time PCR shows that FHF2 is the most abundant of the FHFs expressed in hippocampal neurons. The requirement of FHF2 for hippocampal neuron excitability was analyzed using RNAi in conjunction with electrophysiological recordings. These studies have demonstrated that knockdown of *fhf2* in hippocampal neurons derived from *Fhf1*$^{-/-}$ mice impairs excitability, with less maximum spike frequency and elevated voltage thresholds for spike induction. Sodium channel inactivation parameters are altered in *Fhf1*$^{-/-}$*Fhf4*$^{-/-}$ granule neurons. In accordance, the colocalization and physical interaction of FHFs with Na_vs in hippocampal neurons suggest that excitability deficits could reflect altered channel physiology in cells lacking FHF1 and FHF2 function. These are the first data to indicate a role for FHF2 in neuronal excitability. These data suggest a widespread role for FHFs in the control of excitability across the central nervous system (CNS).

ACKNOWLEDGMENTS

I wish to express my sincere gratitude to my mentor, Dr. Mitchell Goldfarb, for his guidance, suggestions, tutoring and continuous encouragement throughout my Ph.D. studies at Hunter College, CUNY. I would not have been able to make this work a reality without his help. I also wish to thank my committee members: Dr. David A. Foster, Dr. Wilfredo Mellado, Dr. Probal Banerjee and Dr. Jonathan B. Levitt, for their time, helpful comments and suggestions.

I am also heartily grateful to Dr. Lesley Davenport and Ms. Judy Li, Assistant Program Officer of the Biochemistry Ph.D. Program, The Graduate Center, CUNY, for helping me in countless ways throughout my studies at CUNY.

Many thanks to Dr. Patricia Rockwell and Dr. Thomas Schmidt-Glenewinkel from Hunter College, CUNY for kindly providing working area and instruments needed for my experiments. Many thanks to Dr. Hualin Zhong from Hunter College, CUNY for her great suggestions at the start of my project. I wish to extend my thanks to Ms. Barbara Wolin, Ms. Sonia Acevedo, Ms. Sally Sockwell, and Ms. Patricia Caldwell, in Animal Facility from Hunter College, CUNY for the training I received from them and for their good care of my experimental mice. I also thank staffs in Hunter College Bio-Imaging Facility and FACS Facility for their help with the instruments.

I wish to thank the former and present members in our laboratory, Dr. Bhaswati Banerjee, Ms. Dafna Tchetchik, Ms. Nataly Shtraizent, Ms. Joanna Giza, Ms. Annie Yam, and Ms. Kasia Dover, for their support and help throughout my research. I would like to thank all the members of Dr. Patricia Rockwell, Dr. Thomas Schmidt-Glenewinkel, and Dr. Marie Filbin's laboratory for their support and help. I would like to give special thanks to Ms. Rena Quinlan for her time and patience to edit my thesis.

Finally, very special thanks to my husband and my soul mate, Faqiang Li, for his invaluable love and support in my life and my research. Very special thanks to my parents for their unconditional love and continuous encouragement. This manuscript is dedicated to my son Yuhuang Li, who was born during my dissertation study, and who made me discover an inner strength I never thought I had.

This work was supported by PHS grant R01-NS39906 and CUNY Graduate Research Grants Program (February 1, 2005-January 31, 2006).

TABLE OF CONTENTS

LIST OF TABLES

LIST OF FIGURES

LIST OF ABBREVIATIONS

AIS	axon initial segment
AnkG	ankyrin G
AraC	cytosine arabinoside
BAC	bacterial artificial chromosome
bp	base pair
cDNA	complementary deoxyribonucleic acid
CIP	calf intestinal phosphatase
CNS	central nervous system
DAPI	4', 6-diamidino-2-phenylindole dihydrochloride
DNA	deoxyribonucleic acid
dC	deoxycytidine
DIV	days *in vitro*
DRG	dorsal root ganglion
ds	double-stranded
E18	embryonic day 18
EGFP	enhanced green fluorescent protein
ES	mouse embryonic stem
FGF	fibroblast growth factor
FHF	fibroblast growth factor homologous factor
GFP	green fluorescent protein
HEK	human embryonic kidney cell
HEPES	N-2-Hydroxyethylpiperazine-N'-2-Ethanesulfonic Acid
hr	hour
IB2	islet brain 2
kb	kilo base
MAP2	microtubule-associated protein 2
MEF	mouse embryonic fibroblast

min	minute
Na_v	voltage-gated sodium channel
nt	nucleotide
PBS	phosphate-buffered saline
PCR	polymerase chain reaction
PGK	phosphoglycerate kinase
RNA	ribonucleic acid
RNAi	RNA interference
RT-PCR	reverse transcription-PCR
S.D.	standard deviation
sec	second
siRNA	small interfering RNA
SNT2	suc1-associated neurotrophic factor target 2

CHAPTER 1

BACKGROUND AND INTRODUCTION

1.1 Expression and requirement of FHFs in the nervous system

Fibroblast growth factor homologous factors (FHFs) are a family of vertebrate neuronal proteins with an unusual mechanism of action. FHFs were identified through searches of expressed sequence tag databases for sequences with homology to the core region of fibroblast growth factors (FGFs) (Smallwood et al., 1996; Coulier et al., 1997; Verdier et al., 1997). FHFs are related to FGFs by substantial sequence and structural homology (**Figure 1-1**), but they have unrelated functions. FGFs bind to the extracelluar domain of cell surface receptor tyrosine kinases (Ornitz and Itoh, 2001), whereas FHFs bind to an intracellular kinase scaffold protein, islet brain 2 (IB2) (Schoorlemmer and Goldfarb, 2001) or to the voltage-gated sodium channels (Na_vs) (Liu et al., 2001b; Liu et al., 2003). Recombinant FHFs can bind heparin with high affinity like classical FGFs, but fail to activate any of the seven principal FGF receptors. FHFs also lack a recognizable secretory signal sequence, and remain intracellular when transfected into two cultured cell lines (Smallwood et al., 1996; Wang et al., 2000).

The crystal structures for the FGF-homologous portion of human FHF1b and FHF2a have been solved, and reveal remarkable structural similarity to FGFs (Olsen et al., 2003; Goetz et al., manuscript submitted). The homologous sequence of FHF and FGF spans a region encoding 120-130 amino acids, a core domain which adopts a β-trefoil fold (**Figure 1-1**). The core domain consists of 12 antiparallel β strands (β1 through β12). A common binding surface for interaction with a segment of Na_v C-terminal tails was determined on the FHF β-trefoil fold (Goetz et al., manuscript submitted).

In mammals, four distinct genes encode FHFs. FHF 1, 2, 3, and 4, were also known as FGF12, 13, 11, and 14, respectively. Proteins within the FHF family show striking amino acid identity between 58% and 71% (Smallwood et al., 1996). For each FHF, multiple isoforms differing only in the N-terminal region are generated through alternative promoter usage and differential splicing of 5'- exons (**Figure 1-2**) (Hartung et al., 1997; Munoz-Sanjuan et al., 2000b; Yamamoto et al., 2000), giving rise to ten FHF splice isoforms in humans. The "a" isoforms for all 4 FHFs are very homologous in their N-terminal extensions. The "b" isoform N-termini are variable in sequence, and are very short in FHF1b and FHF2b (**Figure 1-2**). These FHF isoforms are evolutionarily well conserved and exhibit distinct tissue distribution and subcellular localization, implicating the N-terminus as an intracellular trafficking signal (Munoz-Sanjuan et al., 1999; Munoz-Sanjuan et al., 2000b; Wang et al., 2000). When expression vectors for FHF1a, FHF2a, or FHF4a are transfected into non-neuronal cultured cells, the proteins are predominantly

nuclear in distribution (Smallwood et al., 1996; Wang et al., 2000). Nuclear localization is mediated by a bipartite translocation signal sequence located in the N-terminal region unique to the "a" isoform (Smallwood et al., 1996). By contrast, "b" isoforms of FHFs expressed following transfection are almost exclusively cytoplasmic in distribution (Wang et al., 2000).

In situ hybridization studies in mice have revealed prominent expression of FHFs in developing and mature neurons of the central and peripheral nervous systems (**Table 1-1**). *Fhf2* is expressed in dorsal root ganglia (DRG), all cranial ganglia, and ganglia of the enteric nervous system (Smallwood et al., 1996; Hartung et al., 1997), and is detected in skeletal muscle by Northern blot hybridization (Gecz et al., 1999). Specially, FHF2b is abundantly expressed in the hippocampus and colocalizes with $Na_v1.6$ at mature nodes of Ranvier in myelinated sensory fibers in the dorsal root of the sciatic nerve (Wittmack et al., 2004). Murine *fhf1* and *fhf2* are also expressed in connective tissue and heart (Smallwood et al., 1996; Hartung et al., 1997; Munoz-Sanjuan et al., 1999). In chickens, FHFs are expressed in the developing limbs and face (Munoz-Sanjuan et al., 2000a; Munoz-Sanjuan et al., 2001). The expression patterns of FHF genes suggest that FHFs function in the development of the central and peripheral nervous systems, connective tissue of the skeleton, and the myocardia of the heart. Importantly, FHF genes share overlapping but non-identical expression patterns (Smallwood et al., 1996; Hartung et al., 1997). *Fhf1* and *fhf4* are expressed in partially overlapping sets in adult spinal motor neurons and cerebellar granule neurons (Smallwood et al., 1996; Wang et al., 2000). In

the spinal cord and DRG of embryonic day 10.5, the domains of *fhf1* and *fhf2* expression are overlapping (Smallwood et al., 1996; Hartung et al., 1997), and overlap persists in adult sensory neurons (Pardee and Goldfarb, unpublished data).

The importance of FHFs for the performance of the mammalian nervous system is now evident through genetic analysis in mice and human. To date, only *fhf1* and *fhf4* of the four *fhf* genes have been disrupted in mice. *Fhf*-mutant mice have failed to show detectable neuroanatomical abnormalities, but do show several behavior deficits. General brain and spinal cord histologies are normal, as are myelination and the ultrastructure of neuromuscular synapses (Wang et al., 2002; Goldfarb et al., 2007). Mice lacking FHF4 have mild reduction in grip strength, and suffer from ataxia and paroxysmal dyskinesia, and a loss of function mutation in FHF4 has been detected in patients with autosomal dominant cerebellar ataxia (Wang et al., 2002; van Swieten et al., 2003). *Fhf4*$^{-/-}$ mice also show sensorimotor and cognitive abnormalities that resemble symptoms seen in ataxia patients carrying *fhf4* mutations. *Fhf1*$^{-/-}$ knockout mice are less severely affected, having only a modest reduction in grip strength (Goldfarb et al., 2007). However, *Fhf1*$^{-/-}$ *Fhf4*$^{-/-}$ double knockout mice show enhanced and novel phenotypes not seen in mice with either individual gene mutated. These mice have more severe ataxia, muscle weakness, and locomotor hyperactivity (Goldfarb et al., 2007). Syndromic and non-specific forms of X-linked mental retardation have been mapped to the *fhf2* gene locus, making the *fhf2* gene a positional candidate gene for these disorders (Shiloh et al., 1990; Malmgren et al., 1993; Gedeon et al., 1996; Ferrero et al., 1997; Gecz et al., 1999).

1.2 Mechanisms involved in Na_v localization and modulation

A highly conserved segment in the cytoplasmic tail of Na_v α subunits interacts with FHFs when ectopically expressed by transfection of non-neuronal cells (Liu et al., 2001a; Liu et al., 2003). The association of FHFs with Na_vs suggests that FHFs may be involved in channel localization and modulation.

A variety of different sodium channels have been identified by electrophysiological recording, biochemical purification, and molecular cloning (Goldin, 2001), but the functional properties of the known sodium channels are relatively similar. The nine mammalian sodium channel isoforms ($Na_v1.1$-$Na_v1.9$) that have been identified and functionally expressed are all greater than 50% identical in amino acid sequence in transmembrane and extracellular domains. However, their expression profiles are different. $Na_v1.5$ is exclusively expressed in cardiac muscle (Gee et al., 1998), $Na_v1.4$ is expressed in skeletal muscle (Goldin et al., 2000), and the other seven sodium channel alpha subunits are expressed in neuronal cells. Expression of these neuronal sodium channel isoforms vary with respect to neuronal cell identities, developmental time course of expression, and subcellular distribution. $Na_v1.7$, $Na_v1.8$, and $Na_v1.9$ are almost exclusively expressed in developing and adult unmyelinated sensory neurons (Herzog et al., 2003; Benn et al., 2001; Dib-Hajj et al., 1998), $Na_v1.3$ expression is restricted to embryonic neurons (Beckh et al., 1989), and $Na_v1.2$ is preferentially expressed in postnatal juvenile neurons, while $Na_v1.1$ and $Na_v1.6$ are abundant in adult neurons (Gong

et al., 1999). $Na_v1.6$ is the major channel expressed within specialized axonal compartments, including the axon initial segment (AIS) and nodes of Ranvier along myelinated fibers (Burgess et al., 1995; Schaller et al., 1995). $Na_v1.6$ largely replaces $Na_v1.2$ at these axonal sites as the nervous system matures (Boiko et al., 2001).

Na_v consists of an α subunit associated with smaller auxiliary β subunits (Catterall, 2000). The pore-forming α subunit is sufficient for functional expression (Noda et al., 1986), but the kinetics and voltage dependence of channel gating are modified by Na_v β subunits (Isom, 2001). Na_v α subunits are organized in four internally repeated homologous domains (I-IV), each of which contains six transmembrane segments (S1-S6) and an additional pore loop located between the S5 and S6 segments. The pore loops line the outer, narrow entry to the pore, whereas the S5 and S6 segments line the inner, wider exit from the pore. The S4 segments in each domain contain positively charged amino acid residues at every third position. These residues serve as gating charges and move across the membrane to initiate channel activation in response to depolarization of the membrane. The short intracellular loop connecting homologous domains III and IV serves as the inactivation gate, folding into the channel structure and blocking the pore from the inside during sustained depolarization of the membrane (Catterall, 2000). The Ile-Phe-Met (IFM) motif located in the III-IV linker of Na_vs has been identified as a major component of the fast inactivation gate (McPhee et al., 1995). The C-terminal tail of Na_vs has multiple functions, and is required for the activation (Sugawara et al., 2003) and inactivation (Benhorin et al., 1998; Abriel et al., 2001) of the channel. The

contribution of the Na_v C-terminal tail to these processes still remains to be investigated in detail.

One of the major physiological roles of the neuronal Na_vs is to generate action potentials at the axon hillock or AIS, and to ensure propagation along myelinated or unmyelinated fibers to nerve termini (Stuart et al., 1997; Catterall, 2000). These processes require a precise distribution of sodium channels accumulated at high density in discrete subdomains of the nerve membrane. In neurons, information relevant to ion channel trafficking and compartmentalization into subdomains of the plasma membrane is far from being elucidated (Winckler and Mellman, 1999; Burack et al., 2000). Several proteins have been found to bind to Na_vs and affect channel trafficking, anchoring at the cell surface, and channel biophysical properties. Sodium channel β1 and 3 subunits link the channel to extracellular matrix proteins via neurofascin-186 and may play a role in retaining sodium channels at the nodes of Ranvier (Ratcliffe et al., 2001). Biochemical, developmental and genetic studies also suggest that the cytoskeletal linker protein ankyrin G (AnkG) could play an important role in sodium channel clustering at the initial segment (Bennett and Lambert, 1999). During the early stages of the establishment of neuronal polarity, $Na_v1.2$ is found to be preferentially distributed on axons of developing hippocampal neurons, and to display a high density at the AIS (Dargent, 1998). Subsequent studies show that the cytoplasmic regions of neuronal sodium channel $Na_v1.2$ contain a dendritic retrieval signal for axonal compartmentalization (Garrido et al., 2001).

However, the upstream mechanisms that initially direct sodium channels to the axonal membrane remain poorly understood.

1.3 Interaction between FHFs and Na_vs

FHFs may contribute to essential neurological functions through their interactions with IB2 and Na_vs. Both the core domain and C-terminal tail are required for FHFs binding IB2 and Na_vs (Olsen et al., 2003). My work focuses on the interaction between FHFs and Na_vs and its consequences.

An FHF interaction with a Na_v was first described by Liu et al (2001a), wherein FHF1b was identified in a yeast two-hybrid cDNA library screen using the C-terminal tail of $Na_v1.9$ as "bait". Although this first description suggested a high degree of specificity between FHF and channel isoforms for interaction, more recent findings have proven otherwise. FHFs share a common binding surface for interaction with a segment of Na_v C-terminal tails that is highly conserved among channel isoforms (Goetz et al., manuscript submitted). In this study, any combination of recombinant FHF and channel isoforms could bind *in vitro*. Several examples of native FHF/channel complexes have been described. Native complexes of FHF2 in association with Na_vs have been detected in extracts from whole rat brain (Wittmack et al., 2004), and complexes of FHF1 and Na_vs have been detected in extracts from mouse cerebellum (Goldfarb et al., 2007).

Many more combinations of FHF/channel complexes have been reported by coimmunoprecipitation of transfected FHFs and Na_vs in non-neuronal cells (Liu et al., 2003; Lou et al., 2005; Laezza et al., 2007). These limited examples among the potentially 50 possible FHF/channel combinations probably reflect the limited availability of isoform-specific FHF and sodium channel antibodies.

FHFs bind to the C-terminal tail region of Na_v α subunits. The FHF binding domain has been mapped to the proximal segment of the tail in $Na_v1.5$ and $Na_v1.9$ (Liu et al., 2001b; Liu et al., 2003) which is a region of the channel dedicated to activation (Sugawara et al., 2003), inactivation (Benhorin et al., 1998; Abriel et al., 2001), and subcellular distribution (Garrido et al., 2001). Liu et al (2003) showed that FHF1b induces a significant hyperpolarizing shift in the voltage dependence of $Na_v1.5$ channel inactivation in an ectopic expression system. This is the only reported example where FHF shifts channel inactivation to more negative potential. By contrast, all other studies to date (Wittmack et al., 2004; Lou et al., 2005; Rush et al., 2006; Goldfarb et al., 2007) describe FHFs inducing depolarizing shifts of voltage-dependent inactivation of the channels.

1.4 Hippocampal neuron was chosen as a model system in this study

FHF1, 2, 3, and 4 are normally expressed in hippocampal neurons (Goldfarb, 2005). The hippocampus is a source of a relatively homogeneous population of neurons with well-characterized properties typical of central nervous system (CNS) neurons in general (Banker et al., 1998). Hippocampal cell culture contains several types of neurons: pyramidal, multipolar, fusiform, and small round cells (soma diameter < 10 μm) (Brown and Zador, 1990). Pyramidal neurons, the principal cell type in the hippocampus, have been estimated to account for 85% to 90% of the total neuronal population. Hippocampal pyramidal cells have a characteristic, well-defined shape. Like most CNS neurons, they have a single axon and several dendrites, thus offering a nice model to study the localization and interaction of FHF proteins and Na_vs. FHF proteins are anticipated to colocalize with Na_vs at the AIS of hippocampal neurons, as resting Na_vs concentrate at AIS, where action potentials are generated.

1.5 Objectives

FHFs are widely expressed in neurons of the central and peripheral nervous systems. The importance of FHF function is illustrated by the detection of behavioral deficits in mice lacking *fhf4* and *fhf1* genes (Wang et al., 2002; Goldfarb et al., 2007; Xiao et al., 2007), and by association of a human mutation in the *fhf4* gene with spinocerebellar ataxia (Wang et al., 2002; van Swieten et al., 2003). *Fhf4*$^{-/-}$ and *Fhf1*$^{-/-}$

Fhf4$^{-/-}$ cerebellar granule cells exhibit impaired intrinsic excitability (Goldfarb et al., 2007).

Since excitability in CNS neurons is induced at the AIS where Na_vs cluster, I anticipated that one or more FHFs may reside at the AIS in association with Na_vs. One of my research objectives has been to determine whether FHFs localize to AIS, and if so, which FHFs specifically localize to AIS. My findings are presented in **Chapter 3**.

While the functional importance of FHF1 and FHF4 has been established through gene knockout studies, the roles of FHF2 and FHF3 have not been elucidated. My other research efforts have focused on defining functional requirements for the FHF2 protein. Following my unsuccessful efforts to generate an *fhf2* knockout mouse (see **Appendix**), I focused on the potential role of FHF2 in hippocampal neuron excitability. My studies demonstrated that the FHF2 protein resides at the AIS of hippocampal neurons (**Chapter 3**). I have analyzed the relative expression of FHF genes in hippocampal neurons, and have shown that among *fhf* genes, *fhf2* is the most abundantly expressed (**Chapter 4**). I have gone on to analyze the requirement of FHF2 for hippocampal neuron excitability using siRNA gene knockdown technology in conjunction with electrophysiological recordings. These studies have demonstrated that siRNA knockdown of *fhf2* expression in hippocampal neurons derived from *Fhf1*$^{-/-}$ mice impairs excitability (**Chapter 5**).

Figure 1-1. FHFs are related to FGFs by substantial sequence and structural homology

The homologous sequence of FHF and FGF spans a region encoding 120-130 amino acids, a core domain which adopts a β-trefoil fold. The core domain consists of 12 antiparallel β strands (β1 through β12). FGFs bind to the extracelluar domain of cell surface receptor tyrosine kinases, whereas FHFs bind to an intracellular kinase scaffold protein, islet brain 2 (IB2) or to the cytoplasmic tail of voltage-gated sodium channels (Na_vs).

(Reprinted with permission from Goldfarb, 2005)

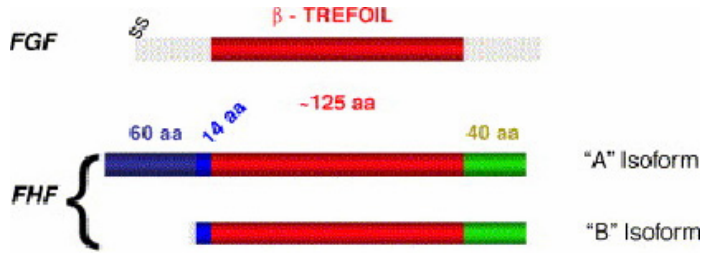
FGF
β - TREFOIL
-125 aa
60 aa
14 aa
40 aa
FHF
"A" Isoform
"B" Isoform

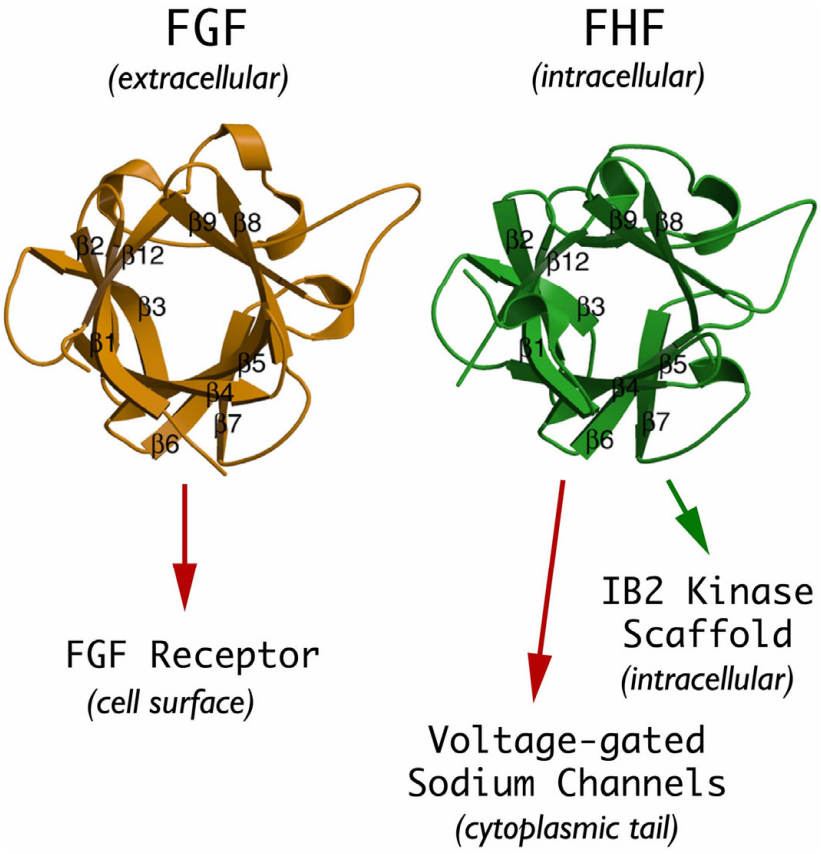
FGF
(extracellular)
FHF
(intracellular)
β9
β8
β2
β12
β3
β1
β5
β4
β7
β6
FGF Receptor
(cell surface)
IB2 Kinase
Scaffold
(intracellular)
Voltage-gated
Sodium Channels
(cytoplasmic tail)

Figure 1-1.

Figure 1-2. Structure-based sequence alignment of the four human FHF family members and their splice isoforms

For comparison, the sequence of FGF2 is included in the alignment. Residue numbers are in parenthesis to the left of the alignment. Secondary structure elements are denoted on top of the sequence alignment. The locations and lengths of the secondary structure elements are indicated by boxes in the sequences. A slash has been introduced into the sequence to mark the junction between alternatively spliced N-terminal FHF region and FHF homology core region. A dash in the sequence represents a gap introduced to optimize the alignment. The FHF homology core region is highlighted by grey background. Residues, which are engaged in channel binding, are colored grey. Residues, which are engaged in anti-FHF2 antibody generation, are highlighted by black background. Note that these residues map to the FHF homology core region, and are conserved among all four FHFs. Also note that except for three, these residues have diverged from FGFs.

Modified from (Goetz et al., manuscript submitted)

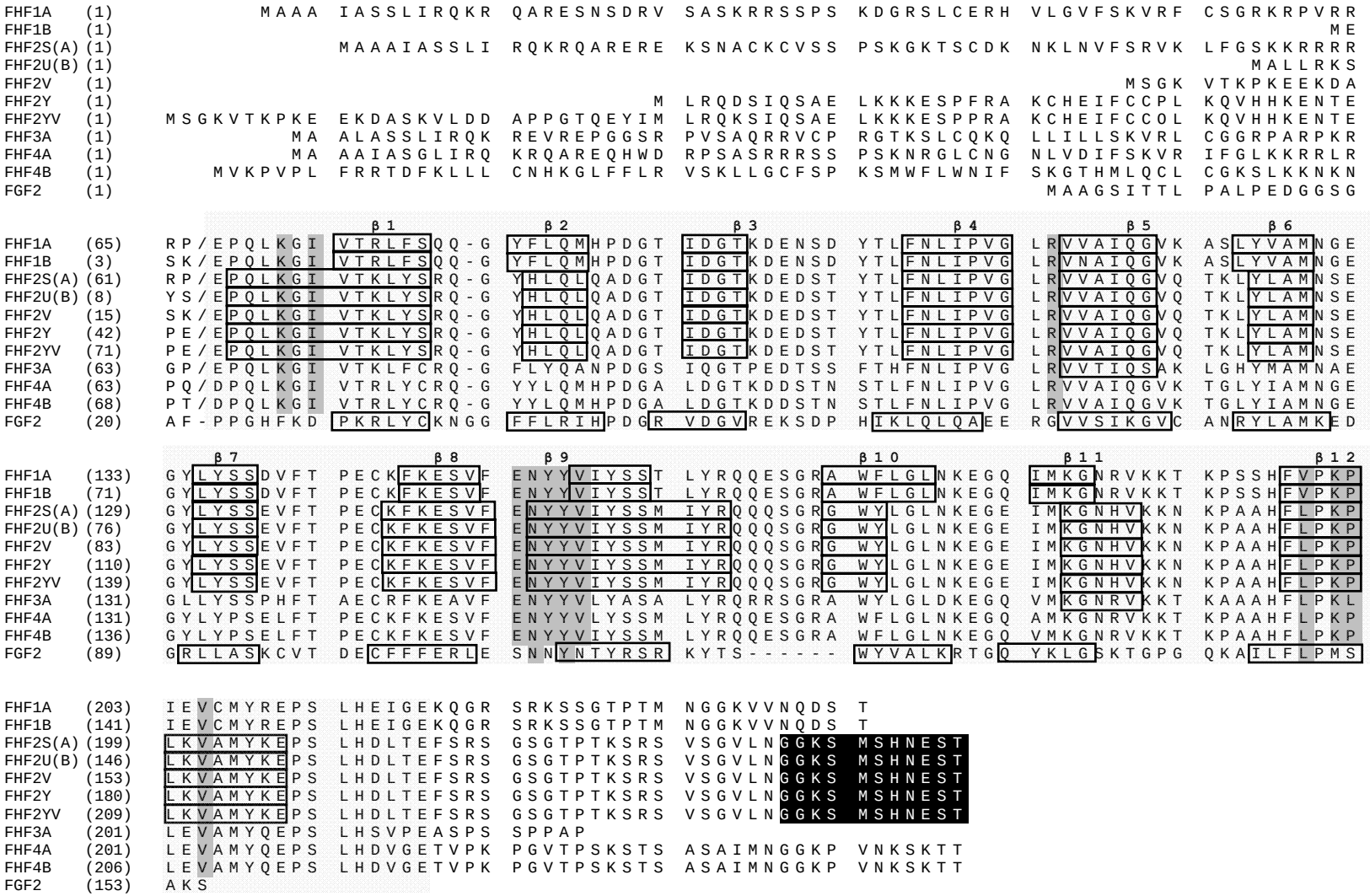
FHF1A (1) MAAA IASSLIRQKR QARESNSDRV SASKRRSSPS KDGRSLCERH VLGVFSKVRF CSGRKRPVRR
FHF1B (1) ME
FHF2S(A) (1) MAAAIASSLI RQKRQARERE KSNACKCVSS PSKGKTSCDK NKLNVFSRVK LFGSKKRRRR
FHF2U(B) (1) MALLRKS
FHF2V (1) MSGK VTKPKEEKDA
FHF2Y (1) M LRQDSIQSAE LKKKESPFRA KCHEIFCCPL KQVHHKENTE
FHF2YV (1) MSGKVTKPKE EKDASKVLDD APPGTQEYIM LRQKSIQSAE LKKKESPPRA KCHEIFCCOL KQVHHKENTE
FHF3A (1) MA ALASSLIRQK REVREPGGSR PVSAQRRVCP RGTKSLCQKQ LLILLSKVRL CGGRPARPKR
FHF4A (1) MA AAIASGLIRQ KRQAREQHWD RPSASRRRSS PSKNRGLCNG NLVDIFSKVR IFGLKKRRLR
FHF4B (1) MVKPVPL FRRTDFKLLL CNHKGLFFLR VSKLLGCFSP KSMWFLWNIF SKGTHMLQCL CGKSLKKNKN
FGF2 (1) MAAGSITTL PALPEDGGSG
β1 β2 β3 β4 β5 β6
FHF1A (65) RP/EPQLKGI VTRLFSQQ-G YFLQMHPDGT IDGTKDENSD YTLFNLIPVG LRVVAIQGVK ASLYVAMNGE
FHF1B (3) SK/EPQLKGI VTRLFSQQ-G YFLQMHPDGT IDGTKDENSD YTLFNLIPVG LRVNAIQGVK ASLYVAMNGE
FHF2S(A) (61) RP/EPQLKGI VTKLYSRQ-G YHLQLQADGT IDGTKDEDST YTLFNLIPVG LRVVAIQGVQ TKLYLAMNSE
FHF2U(B) (8) YS/EPQLKGI VTKLYSRQ-G YHLQLQADGT IDGTKDEDST YTLFNLIPVG LRVVAIQGVQ TKLYLAMNSE
FHF2V (15) SK/EPQLKGI VTKLYSRQ-G YHLQLQADGT IDGTKDEDST YTLFNLIPVG LRVVAIQGVQ TKLYLAMNSE
FHF2Y (42) PE/EPQLKGI VTKLYSRQ-G YHLQLQADGT IDGTKDEDST YTLFNLIPVG LRVVAIQGVQ TKLYLAMNSE
FHF2YV (71) PE/EPQLKGI VTKLYSRQ-G YHLQLQADGT IDGTKDEDST YTLFNLIPVG LRVVAIQGVQ TKLYLAMNSE
FHF3A (63) GP/EPQLKGI VTKLFCRQ-G FLYQANPDGS IQGTPEDTSS FTHFNLIPVG LRVVTIQSAK LGHYMAMNAE
FHF4A (63) PQ/DPQLKGI VTRLYCRQ-G YYLQMHPDGA LDGTKDDSTN STLFNLIPVG LRVVAIQGVK TGLYIAMNGE
FHF4B (68) PT/DPQLKGI VTRLYCRQ-G YYLQMHPDGA LDGTKDDSTN STLFNLIPVG LRVVAIQGVK TGLYIAMNGE
FGF2 (20) AF-PPGHFKD PKRLYCKNGG FFLRIHPDGR VDGVREKSDP HIKLQLQAEE RGVVSIKGVC ANRYLAMKED
β7 β8 β9 β10 β11 β12
FHF1A (133) GYLYSSDVFT PECKFKESVF ENYYVIYSST LYRQQESGRA WFLGLNKEGQ IMKGNRVKKT KPSSHFVPKP
FHF1B (71) GYLYSSDVFT PECKFKESVF ENYYVIYSST LYRQQESGRA WFLGLNKEGQ IMKGNRVKKT KPSSHFVPKP
FHF2S(A) (129) GYLYSSEVFT PECKFKESVF ENYYVIYSSM IYRQQQSGRG WYLGLNKEGE IMKGNHVKKN KPAAHFLPKP
FHF2U(B) (76) GYLYSSEVFT PECKFKESVF ENYYVIYSSM IYRQQQSGRG WYLGLNKEGE IMKGNHVKKN KPAAHFLPKP
FHF2V (83) GYLYSSEVFT PECKFKESVF ENYYVIYSSM IYRQQQSGRG WYLGLNKEGE IMKGNHVKKN KPAAHFLPKP
FHF2Y (110) GYLYSSEVFT PECKFKESVF ENYYVIYSSM IYRQQQSGRG WYLGLNKEGE IMKGNHVKKN KPAAHFLPKP
FHF2YV (139) GYLYSSEVFT PECKFKESVF ENYYVIYSSM IYRQQQSGRG WYLGLNKEGE IMKGNHVKKN KPAAHFLPKP
FHF3A (131) GLLYSSPHFT AECRFKEAVF ENYYVLYASA LYRQRRSGRA WYLGLDKEGQ VMKGNRVKKT KAAAHFLPKL
FHF4A (131) GYLYPSELFT PECKFKESVF ENYYVLYSSM LYRQQESGRA WFLGLNKEGQ AMKGNRVKKT KPAAHFLPKP
FHF4B (136) GYLYPSELFT PECKFKESVF ENYYVIYSSM LYRQQESGRA WFLGLNKEGQ VMKGNRVKKT KPAAHFLPKP
FGF2 (89) GRLLASKCVT DECFFERLES NNYNTYRSRK YTS------ WYVALKRTGQ YKLGSKTGPG QKAILFLPMS
FHF1A (203) IEVCMYREPS LHEIGEKQGR SRKSSGTPTM NGGKVVNQDS T
FHF1B (141) IEVCMYREPS LHEIGEKQGR SRKSSGTPTM NGGKVVNQDS T
FHF2S(A) (199) LKVAMYKEPS LHDLTEFSRS GSGTPTKSRS VSGVLNGGKS MSHNEST
FHF2U(B) (146) LKVAMYKEPS LHDLTEFSRS GSGTPTKSRS VSGVLNGGKS MSHNEST
FHF2V (153) LKVAMYKEPS LHDLTEFSRS GSGTPTKSRS VSGVLNGGKS MSHNEST
FHF2Y (180) LKVAMYKEPS LHDLTEFSRS GSGTPTKSRS VSGVLNGGKS MSHNEST
FHF2YV (209) LKVAMYKEPS LHDLTEFSRS GSGTPTKSRS VSGVLNGGKS MSHNEST
FHF3A (201) LEVAMYQEPS LHSVPEASPS SPPAP
FHF4A (201) LEVAMYQEPS LHDVGETVPK PGVTPSKSTS ASAIMNGGKP VNKSKTT
FHF4B (206) LEVAMYQEPS LHDVGETVPK PGVTPSKSTS ASAIMNGGKP VNKSKTT
FGF2 (153) AKS

Table 1-1. Some neuronal sites of *fhf* gene expression

Site	FHF1	FHF2	FHF3	FHF4
Cerebral cortical neurons	Yes	Yes	Yes	Yes
Hippocampal pyramidal neurons	Yes	Yes	Yes	Yes
Cerebellar granule neurons	Yes	No	Yes	Yes
Spinal motor neurons	Yes	No	Not tested	Yes
Peripheral sensory neurons	Yes	Yes	Not tested	No

(Reprinted with permission from Goldfarb, 2005)

CHAPTER 2

MATERIALS AND METHODS

2.1 Rats and mice in this study

Timed-pregnant SpragueDawley rats were purchased from Charles River Laboratories. Wild-type mice (C57BL/6 strain) were maintained in Animal Facilities of Hunter College. A null allele for the *fhf1* gene was produced through standard gene targeting technology. Resulting *Fhf1*$^{-/-}$ mice were viable, and fertile (Goldfarb et al., 2007). *Fhf1*$^{-/-}$ mice were also maintained in Animal Facilities of Hunter College. Timed-pregnant wild-type and *Fhf1*$^{-/-}$ mice were checked for plugs every morning.

2.2 Hippocampal neuron cell culture

Hippocampal neuron culture was prepared from embryonic day 18 (E18) rat (SpragueDawley, Charles River Labs) or mouse (C57BL/6) hippocampus according to Winckler *et al.* (1999) with slight modifications. The hippocampi were dissected and individual cells were dissociated by trituration with papain (Sigma) treatment. Cells were plated at a density of $4.5X10^4$ cells/cm^2 on poly-D-lysine-coated 12-mm coverslips in 4-well culture dishes, and maintained at 37 ^{0}C in a humidified incubator under an

atmosphere of 95% air and 5% CO_2. Cells were first plated in minimum essential medium supplemented with 10% horse serum, 20% glucose and 1% sodium pyruvate. Four hours later, the medium was changed to Neurobasal medium containing B27 and glutamine, and exchanged once a week thereafter. 10 μM cytosine arabinoside (AraC) and 10 μM deoxycytidine (dC) were added the next day to obtain glia-free cultures.

2.3 Hippocampal neuron transfection

Neurons were transfected at 9 DIV using Lipofectamine™ 2000 according to the manufacturer's instructions (Invitrogen). Briefly, 2 μl Lipofectamine™ 2000 was diluted in 50 μl Neurobasal medium and mixed with 1 μg plasmids, and the formulation was continued for 20 min at room temperature. The mixture then was applied to the cells incubated in fresh Neurobasal medium. After 2 hr, coverslips with cells on the top were transferred back to the conditioned medium. Transfected cells were processed for immunofluorescence 24-48 hr after transfection.

2.4 Generation of anti-FHF2 antibody and peptide interference experiment

Anti-FHF2 antibody was prepared as described previously (Schoorlemmer and Goldfarb, 2002): Rabbits were immunized against peptides corresponding to mouse FHF2 residues 234–244 (GGKSMSHNEST) synthesized with added N-terminal cysteine

for sulfhydryl-mediated directional coupling to carrier protein (Research Genetics). Antibodies were affinity-purified with corresponding peptides immobilized on activated agarose (Pierce). FHF2 antibodies recognized FHF2, but not FHF1, in lysates from expression vector-transfected 293T cells (Schoorlemmer and Goldfarb, 2002).

Peptide interference was performed as follows: 100 fold diluted P1 (FHF2 residues 234–244, 1 mg/ml) and 200 fold diluted P2 (IB2 residues 117-128, 2 mg/ml) were used. Rabbit anti-FHF2 antibody was mixed with anti-AnkG antibody. Peptides were added to the final mix, and preincubated at room temperature for 20 min before adding to the neurons fixed on coverslips. Bound antibodies were visualized by indirect immunofluorescence with biotinylated donkey anti-mouse IgG (Jackson) + streptavidin Alexa 594 (Molecular Probes) and goat anti-rabbit IgG 488 antibody (Molecular Probes).

2.5 Generation of C-terminal GFP-tagged FHFs

The *fhf1a-gfp*, *fhf1b-gfp* and *fhf4b-gfp* fusion constructs were amplified using PCR primers designed based on DNA sequences of mouse *fhf1a* (GenBank accession number NM_183064), human *fhf1b* (GenBank accession number NM_004113), and human *fhf4b* (GenBank accession number NM_175929), respectively. Then the amplified sequences were subcloned into the pEGFP-vector (Clontech) between the *Xho*I and *Hind*III restriction sites. PCR of construct fragments with the following primers:

mfhf1a-Xho-sense: ggCACACTCgAgCCATggCTgCggCgATAgCCA;

mfhf1a-Hind-antisense: ggCACCAAgCTTTgTAgAATCTTgATTCACgACTTTgCCT;

hfhf1b-Xho-sense: ggCACACTCgAgCCATggAgAgCAAAgAACCCCA;

hfhf1b-Hind-antisense: ggCACCAAgCTTTgTTgAATCTTgATTCACAACTTTgCCT;

hfhf4b-Xho-sense: ggCACACTCgAgCCATggTAAAACCggTgCCCCT;

hfhf4b-Hind-antisense: ggCACCAAgCTTTgTTgTCTTACTCTTgTTgACTggT. *Fhf2a-gfp* was engineered by ligated products of PCR amplification for exon1a of *mfhf2a*, exons 2-5 of *hfhf2b*, and pEGFP-N1 vector by our laboratory.

2.6 Generation of mutant GFP-tagged FHFs

The R114G and Y155N mutations in mouse *fhf1a* were introduced into the *fhf1a-gfp* construct by our laboratory and verified by sequencing. The numbering used for the FHF1a protein sequence is based on the numbering system for mouse FHF1a (GenBank accession number NP_034328). *Fhf2a*$_{octamutant}$*-gfp* was engineered by ligated products of PCR amplification for exon1a of mouse *fhf2a*, exons 2-5 of human *fhf2b-octamutant*, and pEGFP-N1 vector by our laboratory. The 8 missense mutations: K14F/I16R/Y98N/ Y99H/L142R/K144M/P145S/V148S were then introduced into the constructed *fhf2a-gfp* construct (Goetz et al., manuscript submitted).

2.7 Immunocytochemistry

For immunostaining, neurons on coverslips were fixed for 20 min with 4% formaldehyde and 4% sucrose in phosphate-buffered saline (PBS) on ice. After fixation cells were permeabilized with 0.5% Triton X-100 for 10 min, and blocked with 5% fetal calf serum at room temperature. Primary and secondary antibody incubations were carried out in PBS containing 1% BSA and 0.25% Triton-X 100. Primary incubations are carried out overnight at 4 ^{0}C. After three washes in PBS for 15 min at room temperature, cells are incubated in fluorescent secondary antibodies for 3 hr at room temperature. After three washes in PBS, cells were stained with 4', 6-diamidino-2-phenylindole dihydrochloride (DAPI). Coverslips were mounted with Vectashield (Vector Laboratories) onto slides and sealed with nail polish. Green and red fluorescence are detected using a Zeiss Axiophot microscope with a 40X or 60X objective lens.

Primary antibodies used in this study include anti-AnkG antibody (Santa Cruz Biotech), rabbit anti-MAP2 polyclonal antibody (Chemicon), anti-GFP antibody (Jackson Immuno), and monoclonal anti-sodium channel Pan antibody (Sigma). Secondary antibodies used in this study include streptavidin Alexa Fluor 488 anti-rabbit antibody (CALTAG), ALEXA Fluor 594 goat anti-mouse IgG1 (Molecular Probes), Alexa Fluor 488 goat anti-mouse IgG1 (Molecular Probes), and Alexa Fluor 594 goat anti-mouse IgG (H+L) (Molecular Probes).

2.8 Total RNA preparation

Total RNA was prepared from extracts of a certain number of cells or tissues using Trizol (Life Technologies) without further treatment. RNA was transcribed into cDNA using Omniscript Reverse Transcription Kit (Qiagen) by adding 20 µl of a mixed solution containing specific *fhf* inner primer pair, 2 µl of dNTP mix, 0.5 µl of RNase inhibitor (40U/µl), and 1 µl of Reverse Transcriptase.

2.9 One-step RT-PCR

Total RNA was subjected to One-step RT-PCR with β-actin primer pair and an equal mix of four *fhf* outer primer pairs. The 50 µl One-step RT-PCR system (QIAGEN) contains 10 µl 5X QIAGEN OneStep RT-PCR Buffer, 2 µl QIAGEN OneStep RT-PCR Enzyme Mix, 2 µl dNTP mix, 0.2 µl RNase inhibitor (40U/µl), and β-actin primer pair (final concentration 0.6 mM) and mixture of *fhf* outer primer pairs (final concentration 0.6 mM each). The reaction was performed at 50 ^{0}C for 30 min, then heated at 95 ^{0}C for 15 min, and followed by 28 cycles with 94 ^{0}C for 45 sec, 56 ^{0}C for 45 sec, and 72 ^{0}C for 1 min, and ended by 72 ^{0}C for 8 min.

2.10 Real time PCR

The Applied Biosystems 7500 Real-Time PCR System was used in this study. Real time PCR was performed with 30 μl reaction mixtures containing 1 μl of 1:100 dilutions of the first round One-step RT-PCR products, specific *fhf* inner primer pair or β-actin primer pair (final concentration 0.6 mM), and 15 μl SYBR Green PCR Master Mix (Applied Biosystems) as follows: 95 ^{0}C for 3 min, then 40 cycles with 94 ^{0}C for 45 sec, 55 ^{0}C for 45 sec, and 72 ^{0}C for 1 min. A melt curve analysis was performed on each run immediately after the last step to determine product presence and purity. The products were also confirmed by electrophoresis and compared to the melt curve analysis.

All quantifications were normalized to the signal of β-actin cDNA for the same sample. The fold change of transcript abundance of target genes was first calculated as $2^{-\Delta Ct}$, where ΔC_t is the number of PCR cycles required to reach the log phase of amplification for the target gene minus the same measure for β-actin. Transcript abundance of *fhf2* was then adjusted to 100% and fold changes of transcripts from other *fhf* genes from the same sample were normalized via comparison with that of *fhf2*. Values represent the mean of three real time PCR replicates ± S.D.

2.11 Single-cell RT-PCR

Single-cell RT-PCR was performed essentially as described (Lambolez et al., 1992; Bochet et al., 1994; Tsuzuki et al., 2000). Following whole-cell recording, as

much as possible of the cell's content was aspirated into the patch-pipette. The contents of the pipette (~8 µl) were expelled into a PCR tube. Then, 42 µl of a solution were added containing 10 µl 5X QIAGEN OneStep RT-PCR Buffer, 2 µl QIAGEN OneStep RT-PCR Enzyme Mix, 2 µl dNTP mix, 0.2 µl RNase inhibitor (40U/µl), and β-actin primer pair and mixture of *fhf* outer primer pairs (final concentration 0.6 mM each). The reaction was performed at 50 ^{0}C for 30 min, then heated at 95 ^{0}C for 15 min, and followed by 28 cycles with 94 ^{0}C for 45 sec, 56 ^{0}C for 45 sec, and 72 ^{0}C for 1 min, and ended by 72 ^{0}C for 8 min. Subsequent real time PCR amplifications were performed as described in 2.10.

2.12 Measurement of real time PCR amplification efficiencies

The efficiency values of real time PCR primers were measured using the C_t slope method according to the Amplification Efficiency of TaqMan® Gene Expression Assays: Application Note (Applied Biosystems). This method involves generating a dilution series of the target template and determining the C_t value for each dilution. A plot of C_t versus log cDNA concentration is constructed. Amplification efficiency was calculated from the slope using the equation: $Ex = 10^{(-1/slope)} - 1$. With this method, the expected slope for a 10-fold dilution series of template DNA is -3.32, when Ex = 1.0. In this study, a 3-log or 4-log dilution range (with 4 or 5 concentration points at 5, 0.5, 0.05, 0.005, and 0.0005 ng/µl) was generated using 10-fold serial dilutions of the outer primer PCR

product, respectively. Each of these dilutions was subjected to real time PCR amplification with each *fhf* inner primer pair using SYBR Green PCR Master Mix (Applied Biosystems) on an Applied Biosystems 7500 Real-Time PCR System. The C_t values obtained over this 3-log or 4-log dilution range were plotted against log cDNA concentration.

2.13 Generation of the *fhf2*-siRNA constructs

The *fhf2*-siRNA constructs were generated based on the pSUPER.neo+gfp vector (OligoEngine) with GFP expressed as a fusion protein to help identify positive transfectants. Oligos that contain the siRNA-expressing sequence were dissolved in sterile, nuclease-free H_2O to a concentration of 3 mg/ml. Assemble the annealing reaction by mixing 1 µl of each oligo (forward + reverse) with 48 µl Annealing Buffer (5M NaCl; 1M HEPES, pH 7.4). Incubate the mixture at 94 ^{0}C for 4 min, and then 80 ^{0}C for 4 min. Slowly cool the annealed oligos to 75 ^{0}C for 4 min, then down to 70 ^{0}C. Continue step-cooling to 37 ^{0}C for 15-20 min, then to 10 ^{0}C, and further to 4 ^{0}C. The annealed oligos were stored at –20 ^{0}C for further use.

The pSUPER.neo+gfp vector was linearized by *Bgl*II and *Hind*III digestion. The annealed oligos were ligated into the linearized vector to generate pSUPER.neo+gfp-

FHF2, which was transformed into E. *coli* strain DH10B. The positive clones were confirmed with *EcoR*I and *Sal*I digestion, and by sequencing using T3 primers.

2.14 Electrophysiological recording on hippocampal neurons

Patch-clamp recordings were conducted using an Axonpatch 200B amplifier, a Digidata 1322 digital-analog interface, and Clampex external command and data acquisition software (all from Axon Instruments). Coverslips of cultured hippocampal cells were placed in the perfusion chamber on the fixed stand of an upright Nikon EF600 microscope equipped with DIC optics for bright-field cell visualization and fluorescence optics for identifying transfected GFP-expressing cells. Patch pipettes are pulled with a P-97 Micropipette Puller (Sutter Instruments). Whole-cell currents of hippocampal cells were recorded with patch-pipettes filled with 8 μl of internal solution containing 126 mM K Gluconate, 4 mM NaCl, 5 mM HEPES, 15 mM glucose and 1 mM $MgSO_4$. The resistance of the patch-pipette in working solutions was about 5 GΩ. The external solution contained 120 mM NaCl, 3 mM KCl, 1.2 mM KH_2PO_4, 26 mM $NaHCO_3$, 1.19 mM $MgSO_4$, 2 mM $CaCl_2$, 3 mM glucose and 5 mM HEPES.

In glia-free cultures, the overwhelming majority of cells displayed triangular-shaped somata bearing morphological resemblance to pyramidal neurons. The intrinsic excitability of hippocampal neurons was examined by whole cell patch clamp in both

current-clamp mode and voltage-clamp mode. Patched cells were confirmed as hippocampal neurons by their resting membrane potential, and their demonstration of a prominent afterhyperpolarization (a negative membrane potential relative to baseline) following a train of action potentials. For each neuron, the membrane resistance and capacitance determined through this analysis would confirm the relative size of neuron being patched, and the inward and outward currents would confirm the health and neural identity of the patched cell. pCLAMP (Axon Instruments, CA) software was used for acquisition and analysis. Voltage clamp step depolarization of neurons was from -70 mV holding potential to -30 mV. The *I-V* plot of the current was fit by a Goldman-Hodgkin-Katz current equation.

The recording data measured up to the following standards were taken into analysis: Cm > 15 pF, R_{leak} > 0.3 GΩ, and $-I_{(peak\text{-}10\ mV)}$ > 1000 pA. Membrane capacitance (Cm) was calculated from measurement of the area under current transients induced by 10 mV voltage-clamp steps (-70 to -80 mV). Input resistance was calculated from change in leak current using formula $R_{leak} = \Delta V_m/\Delta_{leak}$. Measured membrane voltages from current-clamp recordings were corrected by -10 mV to offset the liquid junction potential (LJP) ($Vm = V_{record} + LJP$), which was measured empirically as -10.1± 0.3 mV using the agar-bridge reference electrode method (Nether, 1992) Cumulative results from *n* cells are given as means ± S.D. Significant statistical differences between data from various experimental groups were determined using two-tailed Student's *t*-test.

CHAPTER 3

LOCALIZATION OF FHF PROTEINS IN HIPPOCAMPAL NEURONS

Summary

FHFs interact with Na_vs and have been shown to control excitability of cerebellar granule cells through modulation of channel inactivation. Since action potentials are initiated at the AIS, we suspected that at least some FHF isoforms would colocalize with Na_vs at the AIS. I have investigated the localization of endogenous FHFs for which antibodies are available and the localization of FHF-GFP fusion proteins transfected into neurons. Endogenous FHF2 and FHF4 proteins colocalize at the AIS of hippocampal neurons. Transfected FHF1a, FHF2a, and FHF4b GFP fusion proteins also localize to the AIS in both hippocampal and cerebellar granule neurons. By contrast, FHF1b-GFP associates with AIS to a far lesser extent, demonstrating that there is isoform specificity in FHF targeting. AIS targeting of an FHF requires the protein's sodium channel binding surface, as a mutant derivative of FHF2a deficient for channel binding is also deficient in AIS targeting.

3.1 Introduction

FHFs are expressed in neurons and certain other excitable cells from early in development through adulthood (Smallwood et al., 1996; Hartung et al., 1997; Munoz-Sanjuan et al., 1999). Inside these excitable cells, FHFs are in native complexes with IB2 (Schoorlemmer and Goldfarb, 2001) or Na_v (Liu et al., 2001b; Liu et al., 2003). The importance of FHF for the performance of the nervous system is revealed by the detection of behavioral deficits in *Fhf1*$^{-/-}$*Fhf4*$^{-/-}$ mice (Wang et al., 2002; Goldfarb et al., 2007; Xiao et al., 2007), and by association of a human mutation in the *fhf4* gene with spinocerebellar ataxia (Wang et al., 2002; van Swieten et al., 2003). *Fhf4*$^{-/-}$ and *Fhf1*$^{-/-}$ *Fhf4*$^{-/-}$ cerebellar granule neurons show impaired intrinsic excitability, characterized by failure of mutant neurons to generate repetitive action potentials and elevated voltage thresholds for spiking in response to inwardly injected current. Underlying the excitability deficits are the altered physiological responses of Na_vs (Goldfarb et al., 2007). Na_vs cluster at high density at the AIS (Matsumoto and Rosenbluth, 1985), and are responsible for the rapid inward sodium currents and the consequent depolarization required for the induction of the action potential and saltatory conduction (Catterall, 2000; Hille, 2001). AIS of pyramidal cells is a critical region for the generation of action potentials and for the control of pyramidal cell excitability (Inda et al., 2006). Consistent with its interaction with Na_v, one or more FHFs are anticipated to reside at the AIS in association with Na_vs, thereby modulating the channel physiology.

Factors involved in FHF subcellular localization are not fully understood. FHF isoforms are evolutionarily well conserved and exhibit distinct tissue distribution and subcellular localization, implicating the N-terminus as an intracellular trafficking signal (Munoz-Sanjuan et al., 1999; Munoz-Sanjuan et al., 2000b; Wang et al., 2000). When expression vectors for FHF1a, FHF2a, or FHF4a are transfected into human embryonic kidney cells (HEK) (293), the proteins are predominantly nuclear in distribution (Smallwood et al., 1996; Wang et al., 2000). Nuclear localization is mediated by a bipartite translocation signal sequence located in the N-terminal region unique to the "a" isoform (Smallwood et al., 1996). By contrast, "b" isoforms of FHFs expressed following transfection are almost exclusively cytoplasmic in distribution (Wang et al., 2000). The FHF4b N-terminus contains two leucine-based motifs which have been implicated in protein trafficking (Bonifacino and Traub, 2003).

If FHFs were to localize to the AIS of neurons, this may be mediated by the affinity of FHFs for the cytoplasmic tails of Na_vs (Liu et al., 2001a; Liu et al., 2003). The recent acquisition of a crystal structure for a full-length FHF and the determination of the channel-binding surface on the FHF β-trefoil fold (Goetz et al., manuscript submitted) could allow us to test whether sodium channel binding is necessary for FHF subcellular localization (**Figure 3-1**). A further question is whether channel binding is a sufficient determinant of FHF targeting. If so, we would predict that all FHF isoforms capable of binding Na_vs would share similar subcellular distribution.

I have investigated the ability of endogenous and transfected FHF proteins to target to the AIS of hippocampal neurons and cerebellar granule neurons. I find that several, but not all, FHF isoforms can target to the AIS. I further show that a mutant derivative of FHF2a deficient in channel binding is also deficient for AIS targeting. These findings show that sodium channel interaction is necessary, but not sufficient, for FHFs colocalization with channels to the AIS.

3.2 Results

3.2.1 Optimization of hippocampal neuron culture conditions for localization studies

In order to investigate FHF localization in cultured hippocampal neurons, I first tested the differentiation time frame of hippocampal neurons under our current culture conditions ($4.5X10^4$ cells/cm^2). When E18 hippocampal neurons are plated into culture, they acquire their characteristic polarized morphology in a series of well-defined developmental stages (Dotti et al., 1988). After being plated, the cells form several short neurites that cannot be distinguished as axons or dendrites. After 12-36 hr in culture, one of these neurites enters a prolonged period of growth and acquires axonal characteristics, thus defining the polarity of the cell. In the next few days, the remaining neurites acquire dendritic characteristics. The efficiency of sorting integral membrane proteins in hippocampal neurons reaches mature levels only toward the end of the first week in culture (Banker et al., 1998). The membrane proteins I chose to visualize the regions of

hippocampal neuron include AnkG and microtubule-associated protein 2 (MAP2). AnkG defines the AIS of mature neurons (Kordeli et al., 1995). MAP2 is initially present throughout the cell (Caceres et al., 1986), becoming restricted to the dendrites only during the stage of dendritic outgrowth. In the following experiments, axons were identified as neuronal processes possessing little or no MAP2 immunofluorescence.

Hippocampal neurons at 9 days *in vitro* (DIV) show AnkG immunostaining concentrated at the AIS and MAP2 immunostaining present throughout the dendrites, ending just proximal to the growth cones (**Figure 3-2A**). The AIS was readily identified as a short, thin, and smooth process with a characteristic "eyelash-like" appearance. Moreover, immunolabelling with a pan-Na_v α subunit-specific antibody revealed that robust Na_v expression is in the AIS of 9 DIV hippocampal neurons (**Figure 3-2B**). The anti-pan-Na_v antibody used in the present study recognizes all of the known vertebrate Na_vs (Rasband et al., 1999), and, therefore, it is thought to reflect the complete repertoire of Na_vs in the AIS, where they are distributed along its whole length. These findings suggested that the hippocampal neurons under the current culture conditions are fully differentiated at 9 DIV. **Figure 3-2C** shows the Na_v and MAP2 immunostaining of the 11 DIV hippocampal neurons. The increase in cell size and the complexity of the neuronal network in the 11 DIV hippocampal neurons are apparent compared with the 9 DIV culture. Therefore, in the following experiments, I studied the localization of the native FHF proteins in the hippocampal neurons at or after 9 DIV, or transfected the

hippocampal neurons at 9 DIV, and fixed 24 hr (10 DIV) or 48 hr (11 DIV) after transfection to investigate the localization of the FHF constructs fused to GFP.

3.2.2 Endogenous FHF2 and FHF4 localize to AIS and colocalize with Na_vs

When I started to investigate the localization of FHFs in hippocampal neurons, the anti-FHF2 antibody was the only anti-FHF antibody generated and available in our laboratory (Schoorlemmer and Goldfarb, 2002). The anti-FHF2 antibody was raised against peptides corresponding to the residues 234–244 (GGKSMSHNEST) at the C-terminal of mouse FHF2a, which does not share any similarity with other FHF paralogs (**Figure 1-2**). To verify the specificity of FHF2 immunoreactivity, two peptides were used. P1 peptide is the FHF2 immunizing peptide, and as a negative control, P2 peptide contains the residues 117-128 of IB2 (FHF2 interacts with the residues 212-471 of IB2). 12 DIV rat hippocampal neurons were fixed and double immunostained with antibodies against native FHF2 and either AnkG or Na_vs. Before being added to the fixed neurons on coverslips, the P1 and P2 peptides were preincubated with the anti-FHF2 antibody, respectively. Accordingly, the P1 peptide competed for binding with the anti-FHF2 antibody, and 3 out of the 57 neurons with AnkG immunostaining analyzed (5.3%) had strong FHF2 immunostaining in the soma and the AIS. Conversely, the P2 peptide had no suppressed effect, and 77 out of the 121 neurons with AnkG immunostaining analyzed (63.6%) had FHF2 immunostaining in the soma and the AIS. These data demonstrated the specificity of the FHF2 immunostaining in cultured hippocampal neurons. As shown

in **figure 3-3**, robust expression of FHF2 is evident in the soma and the AIS of hippocampal neurons. In addition, FHF2 expression is colocalized with Na_vs at the AIS.

Later, we obtained the mouse monoclonal antibody against FHF4 from NeuroMab (NIH/NINDS). To investigate whether FHF2 and FHF4 localize to the same localization, I performed the immunostaining on 12 DIV mouse hippocampal neurons with antibodies against native FHF2 and FHF4, respectively. **Figure 3-4** shows that FHF2 and FHF4 immunostaining overlap in the soma and the AIS of hippocampal neurons, which suggests no substantive difference in the distributions of endogenous FHF2 and FHF4 in hippocampal neurons.

3.2.3 Localization of FHF-GFP fusion proteins in transfected neurons

Transfection of neurons with FHF-GFP fusion proteins enables us to examine the subcellular localization of FHFs for which antibodies are unavailable or are not isoform-specific. I generated DNA vectors for expression of FHF1a, FHF1b, FHF2a, or FHF4b bearing C-terminal GFP fusions. 10 DIV rat hippocampal neurons were transfected with these vectors or a vector expressing GFP alone served as a negative control. After 48 hr, cells were fixed and double immunostained with antibodies against GFP and either MAP2 or Na_vs. For all FHFs tested, I could find examples of neurons with FHF in the soma and concentrated at the AIS together with Na_vs in hippocampal neurons (**Figure 3-**

5). This AIS concentration of FHFs was visually self-evident, but in some experiments, the AIS enrichment was quantitated (see below).

Although examples of cells showing AIS enrichment could be found for all FHFs tested, we noticed that among FHF1b-GFP transfected cells, it was more difficult to find cells with clear AIS localization. Therefore, I repeated the transfections with FHF1a-GFP versus FHF1b-GFP and determined what fraction of GFP-expressing neurons showed AIS localization of FHFs. As shown in **figure 3-5**, the immunostaining signals of FHF1b-GFP at the AIS are weaker than those of FHF1a-GFP, which suggests that more FHF1a concentrated in the AIS than FHF1b. 24 hr after transfection, 3 out of the 6 (50%) transfected hippocampal neurons showed FHF1a-GFP expression restricted to the soma and the AIS, while the remaining 50% showed that FHF1a-GFP was expressed throughout the entire neuron rather than being localized to any particular regions of the neuron. On the contrary, FHF1b-GFP was expressed in all the regions of cells in all of the transfected hippocampal neurons (n=7, 100%). However, 50 hr after transfection, all of the transfected hippocampal neurons (n=7, 100%) had FHF1a-GFP restricted to the soma and the AIS, while only 1 out of the 8 (12.5%) transfected neurons had FHF1b-GFP enriched in the soma and the AIS. Therefore, these experiments demonstrate that FHF1a has a far greater propensity for AIS localization than does FHF1b (**Figure 3-6**).

To see whether the cellular localization of FHF1 in other types of neurons is the same as in hippocampal neurons, I transfected 18 DIV mouse cerebellar granule neurons

with *fhf1a-gfp* or *fhf1b-gfp*, and 48 hr after transfection double immunostained fixed neurons with antibodies against GFP and Na_vs. As with their localization in hippocampal neurons, I could identify cerebellar granule neurons in which FHF1a-GFP or FHF1b-GFP was detectable in the soma and the AIS together with Na_vs (**Figure 3-7**). Although I did not undertake a rigorous quantitation, it was clear that among transfected granule neurons, many could be found showing that FHF1a accumulated at the AIS, whereas very few FHF1b-transfected cells showed such enrichment. These experiments provide support for FHF localization in the AIS that can account for the ability of FHFs to modulate cerebellar granule neuron excitability (Goldfarb et al., 2007). Additionally, my data suggest that FHF1b is unlikely to contribute to modulation of neuronal excitability. One possibility is that this FHF concentrates elsewhere in the neuron to modulate other sodium channel-dependent processes (see Discussion).

3.2.4 Residues affecting the subcellular targeting of FHFs

The crystal structure of the FHF homology core domain of FHF2a has been determined (Goetz et al., manuscript submitted). FHF2a formed a non-crystallographic dimer with a buried surface under the crystallization condition employed. Most of the residues buried in the FHF2a dimer interface are highly conserved among FHFs, but are diverged in FGFs. It is likely that divergence at this surface contributes to the functional divergence of FHFs from FGFs, including the specific ability of FHFs to interact with Na_vs. Our laboratory substituted residues on this FHF surface in FHF2a and FHF1a with

the corresponding residues of FGFs (**Figure 1-2**) and examined the effect of these mutations on channel binding. In the case of FHF2a, our laboratory generated a mutant in which eight of the conserved surface residues were substituted (K67F/I69R/Y151N/Y152H/L195R/K197M/P198S/V201S) (**Figure 3-1**). Vectors expressing wild-type or mutant FHF2a as GFP fusion proteins or a vector expressing GFP alone were transfected into mouse hippocampal neurons. 48 hr after transfection, cells were fixed and double immunostained with antibodies against AnkG and GFP. As illustrated in **figure 3-8A**, hippocampal neurons expressing wild-type FHF2a showed prominent fluorescence in the AIS, as judged by co-staining with AnkG. Although detectable in the soma of hippocampal neurons, $FHF2a_{octamutant}$-GFP was not enriched in the AIS (**Figure 3-8B**). Thus, in contrast to wild-type FHF2a-GFP, $FHF2a_{octamutant}$-GFP does not colocalize with native Na_vs at the AIS of hippocampal neurons. These data show that the channel-binding surface in the FHF homology core domain is essential for FHF2a targeting to the AIS.

To evaluate the contribution of individual residues, our laboratory made two single mutants for FHF1a (R114G and Y155N). Wild-type FHF1a and its mutant variants were expressed as GFP fusion proteins in mouse hippocampal neurons. After 48 hr, cells were fixed and double immunostained with antibodies against GFP and AnkG. As shown in **figure 3-9**, in all GFP-expressing neurons with localized AnkG immunostaining, the GFP signal was restricted to the soma and the AIS. These data

demonstrated that the single mutation R114G or Y155N does not affect the targeting of FHF1a in the AIS of hippocampal neurons.

3.3 Discussion

As shown in the present study, endogenous FHF2, labeled with anti-FHF2 antibody, was detected in the soma and the AIS together with Na_vs in hippocampal neurons (**Figure 3-3**). Endogenous FHF4, detected with a newly obtained anti-FHF4 antibody, overlapped with endogenous FHF2 in the soma and the AIS of hippocampal neurons (**Figure 3-4**). When expressed in hippocampal neurons, FHF1a-GFP, FHF2a-GFP, or FHF4b-GFP was found highly enriched at the AIS, and colocalized with endogenous Na_vs (**Figure 3-5**). Similar to their localization in hippocampal neurons, FHF1a-GFP and FHF1b-GFP were detectable in the soma and the AIS together with Na_vs in cerebellar granule neurons (**Figure 3-7**). In aggregate, these findings show that a broad repertoire of FHF isoforms colocalizes with Na_vs at the AIS of hippocampal neurons. The association of FHFs with Na_vs at the AIS suggests that FHFs may modulate channel physiology, thereby controlling the intrinsic excitability of hippocampal neurons in a manner similar to that which has been described for cerebellar granule neurons of *Fhf1*$^{-/-}$*Fhf4*$^{-/-}$ mice (Goldfarb et al., 2007). This hypothesis was tested and will be discussed in **Chapter 5**.

A differential subcellular localization of FHF1a and 1b was also observed in the present study. FHF1a-GFP tends to concentrate in the AIS of hippocampal neurons, while FHF1b-GFP does not (**Figure 3-6**). FHF1b-GFP does, however cluster at the node of Ranvier in the transfected and myelinated DRG/Schwann coculture (Dover, et al., unpublished data). Moreover, differential subcellular localizations are also observed in FHF2a and 2b (Goldfarb, unpublished data). Together with my findings, our results suggest that different FHF isoforms are differentially targeted along axons, perhaps to differentially modulate sodium channels in different axonal compartments.

The crystal structure of the FHF homology core domain of FHF2a unveils conserved surface regions implicated in sodium channel binding (Goetz et al., manuscript submitted). Eight of the conserved surface residues were substituted with its most common FGF counterpart (K67F/I69R/Y151N/Y152H/L195R/K197M/P198S/V201S) (**Figure 3-1**) in the FHF2a core domain. Wild-type FHF2a and its octa-mutant were expressed as GFP fusion proteins in mouse hippocampal neurons. The pattern of endogenous FHF2 expression (**Figure 3-3**), together with the observation that the $FHF2a_{octamutant}$-GFP does not interact with Na_vs or localize at the AIS (**Figure 3-8B**), strongly suggested that the eight mutations in the Na_v binding site act by disrupting the interaction between FHF2 and Na_vs at the AIS of hippocampal neurons. Additional experiments are needed to test this hypothesis directly. The distribution of Na_vs in the AIS of $FHF2a_{octamutant}$-GFP expressing cells will be further investigated. To further corroborate this channel-binding surface, these eight mutations were also introduced into

the wild-type *fhf2b-gfp* construct to generate *fhf2b*$_{octamutant}$*-gfp*. The effects of these mutations on FHF2b localization and channel binding will be investigated in hippocampal neurons.

Furthermore, these eight mutations (K67F/I69R/Y151N/Y152H/L195R/K197M/P198S/V201S) also disabled FHF modulation of voltage-dependent fast inactivation of Na_vs in neuronal cells (Goetz et al., manuscript submitted). Voltage-dependence of channel fast inactivation was recorded in Neuro2A cells expressing wild-type FHF2a, FHF2a octa-mutant, wild-type FHF2b, and FHF2b octa-mutant. The results show that wild-type FHF2a and FHF2b but not the octa-mutant variants caused depolarizing shifts in the voltage-dependence of channel inactivation (Goetz et al., manuscript submitted). These data are consistent with my results that the channel-binding surface in the FHF homology core domain is essential for FHF2a targeting to the AIS.

Two corresponding single mutants (R114G and Y155N) in the FHF1a core domain were generated to evaluate the contribution of individual surface residues for FHF targeting to the AIS. However, neither of these mutations affect FHF1a targeting to the AIS of hippocampal neurons (**Figure 3-9**), which suggests that these mutations in the Na_v binding site do not disrupt the interaction between FHF1a and Na_vs at the AIS of hippocampal neurons. By contrast, the corresponding single mutant (R52G) in the FHF1b core domain has been reported to prevent FHF1b binding to either IB2 or to Na_vs

in gel filtration chromatography (Olsen et al., 2003). Since FHF 1a and 1b differ only in the N-terminal region, and exhibit distinct subcellular localization (**Figure 3-6**), the lack of effect of the R114G mutant in FHF1a and channel interaction (**Figure 3-9**) suggests that the N-terminal region of FHF 1a may contribute to sodium channel binding together with the core domain. More site-directed mutants of FHF1a in both the N-terminal region and the core domain are needed to study the role of the N-terminal region in channel binding or AIS targeting. Moreover, these single mutants of FHF1a fail to associate with Na_vs in the co-immnuoprecipitation (Dover, et al., unpublished data). These findings show that sodium channel interaction is necessary, but not sufficient, for FHF colocalization with channels to the AIS.

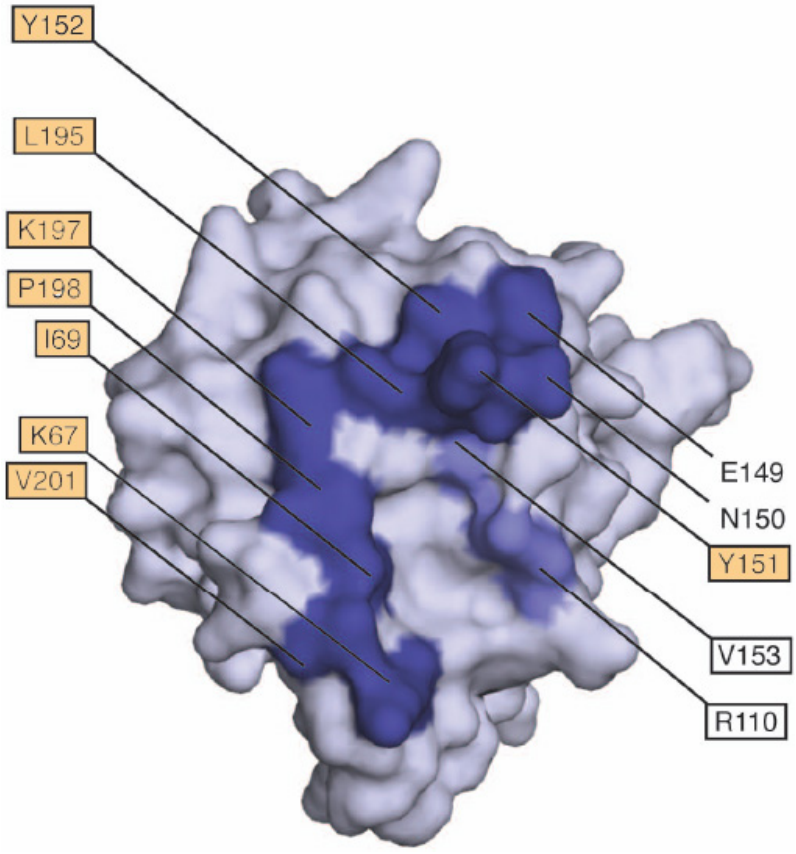

Figure 3-1. The crystal structure of FHF2a unveils conserved surface regions implicated in channel binding

Channel-binding residues buried in the FHF2a dimer interface are colored deep blue. The eight residues engaged in site-directed mutagenesis are marked by a black box highlighted in orange.

Modified from (Goetz et al., manuscript submitted)

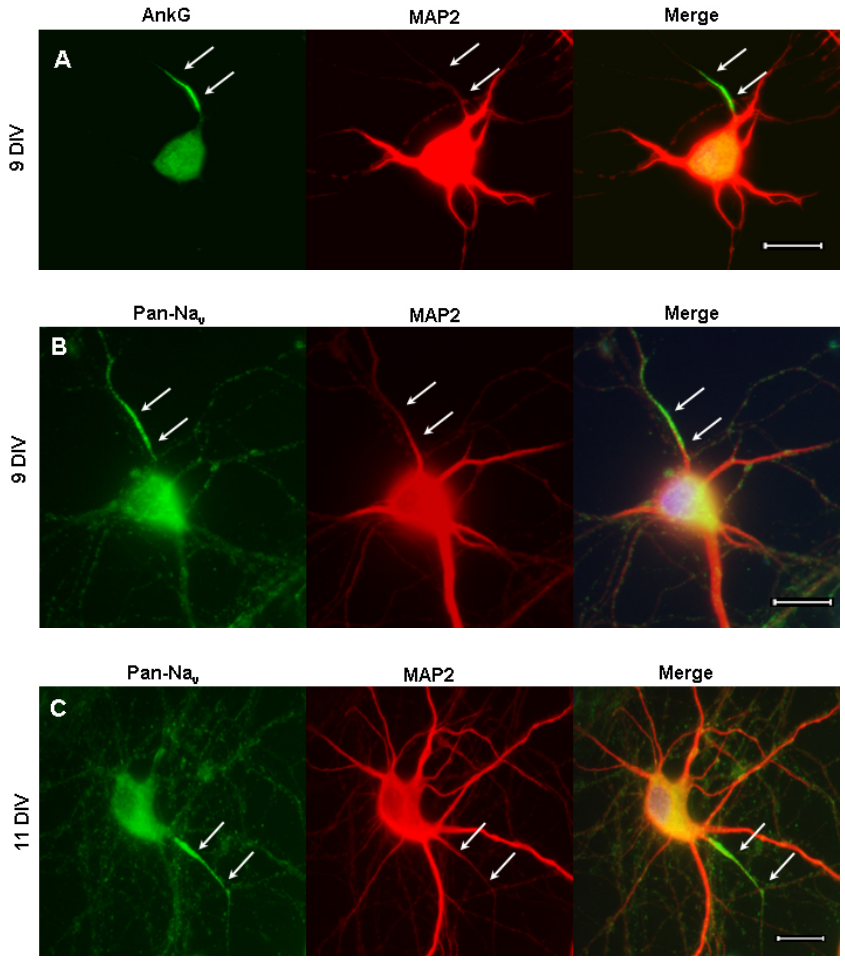

Figure 3-2. Localization of AnkG, MAP2, and Na_v in cultured hippocampal neurons

Rat hippocampal neurons cultured for 9 (A and B) and 11 (C) days were fixed and double immunostained with antibodies against AnkG (green), or sodium channels (Pan-Na_v, green), and MAP2 (red). Merged images include DAPI stain. Arrows denote axon initial segments. Scale bar, 10 µm. Note that AnkG and Na_v immunostaining concentrate at the AIS and MAP2 immunostaining is present throughout the dendrites.

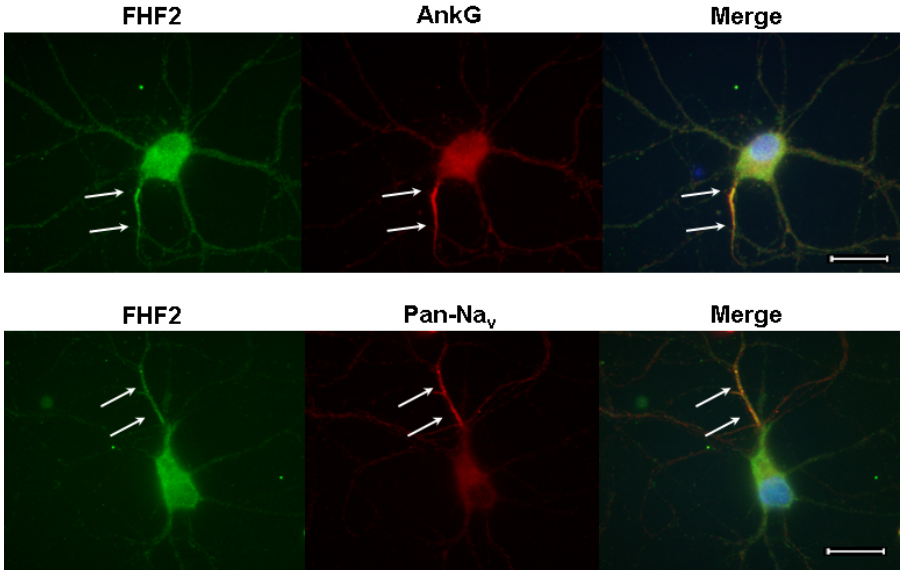

Figure 3-3. Endogenous FHF2 localizes in the soma and the AIS, and colocalizes with Na_vs at the AIS of cultured hippocampal neurons

12 DIV rat hippocampal neurons were fixed and double immunostained with antibodies against native FHF2 (green) and either ankyrin G (AnkG, red) or sodium channels (Pan-Na_v, red). Merged images include DAPI stain. Arrows denote axon initial segments. Scale bar, 10 μm.

(Reprinted with permission from Goldfarb et al., 2007)

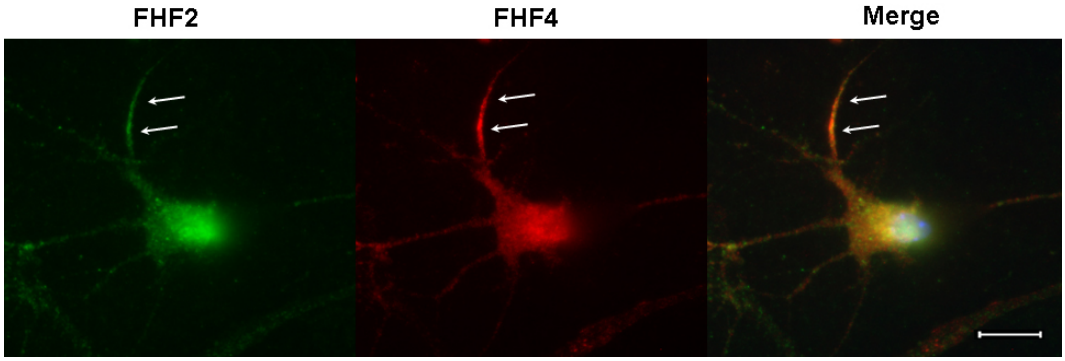

Figure 3-4. FHF2 and FHF4 immunostaining overlap in the soma and the AIS of cultured hippocampal neurons

12 DIV mouse hippocampal neurons were fixed and double immunostained with antibodies against native FHF2 (green) and FHF4 (red). Merged images include DAPI stain. Arrows denote axon initial segments. Scale bar, 5 μm.

Figure 3-5. FHF-GFP fusion proteins localize in the soma and the AIS, and colocalize with Na_vs at the AIS of cultured hippocampal neurons

10 DIV rat hippocampal neurons were transfected with FHF1a-GFP, FHF1b-GFP, FHF2a-GFP, and FHF4b-GFP, respectively. After 48 hr, cells were fixed and immunostained with antibodies against GFP (green) and either MAP2 (red) or sodium channels (Pan-Na_v, red); for FHF2a, cell was double immunostained with antibodies against GFP (red) and AnkG (green). Merged images include DAPI stain. Arrows denote axon initial segments. Scale bar, 5 μm.

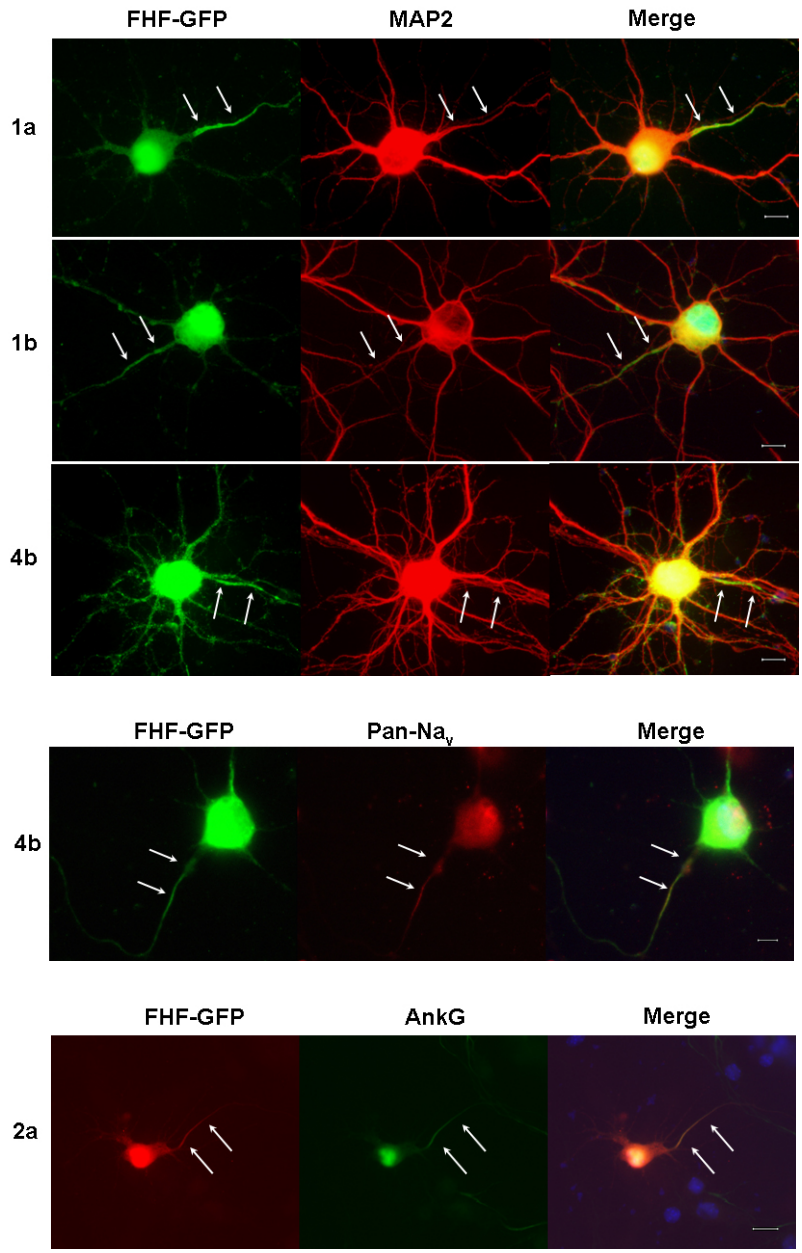
FHF-GFP
MAP2
Merge
1a
1b
4b
FHF-GFP
Pan-Na$_v$
Merge
4b
FHF-GFP
AnkG
Merge
2a

Figure 3-5.

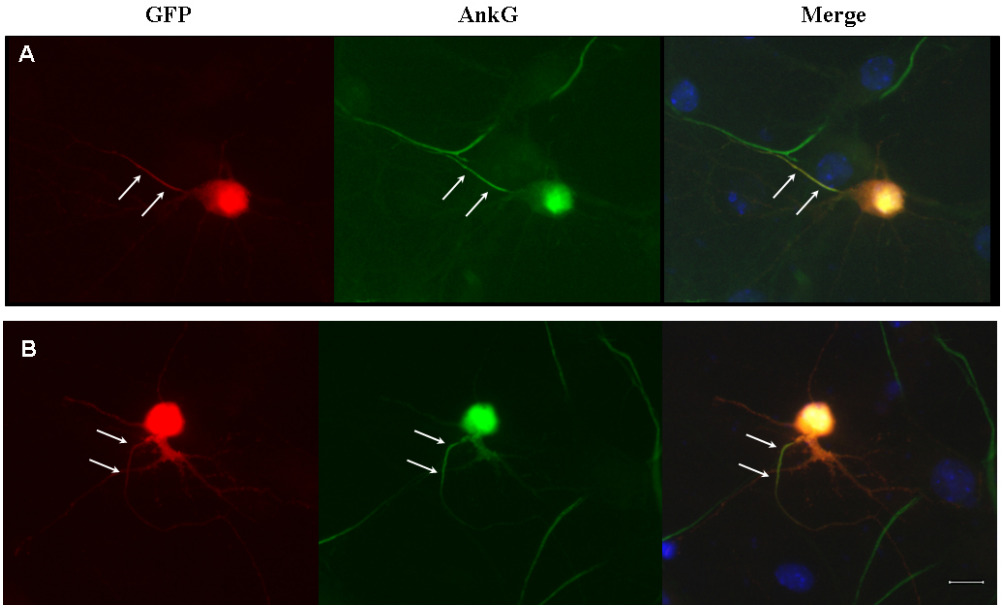

Figure 3-6. Differential subcellular localization of FHF1a and 1b in cultured hippocampal neurons

10 DIV mouse hippocampal neurons were transfected with FHF1a-GFP (A) and FHF1b-GFP (B), respectively. After 50 hr, cells were fixed and double immunostained with antibodies against GFP (red) and AnkG (green). Merged images include DAPI stain. Arrows denote axon initial segments. Scale bar, 10 μm.

Note that FHF1a-GFP tends to concentrate in the AIS of hippocampal neurons, while FHF1b-GFP does not.

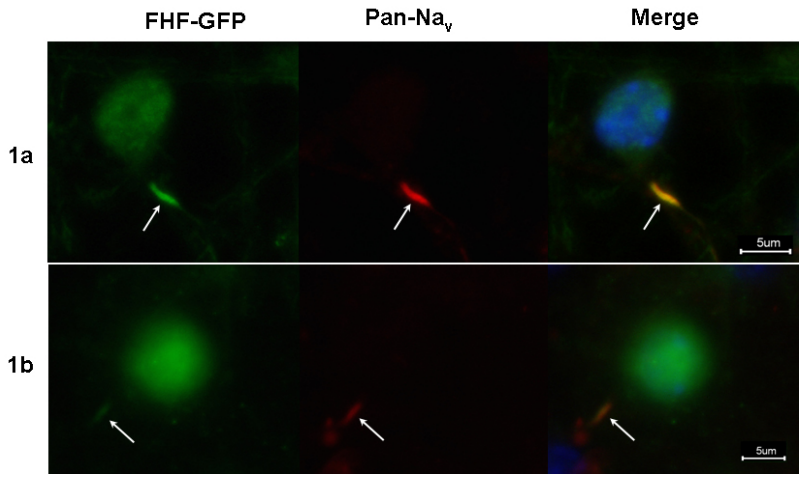

Figure 3-7. FHF 1a and FHF1b GFP fusion proteins localize in the soma and the AIS, and colocalize with Na$_v$s at the AIS of cultured cerebellar granule neurons

18 DIV mouse cerebellar granule neurons were transfected with FHF1a-GFP and FHF1b-GFP, respectively. After 48 hr, cells were fixed and double immunostained with antibodies against GFP (green) and sodium channels (Pan-Na$_v$, red). Merged images include DAPI stain. Arrows denote axon initial segments. Scale bar, 5 µm.

(Reprinted with permission from Goldfarb et al., 2007)

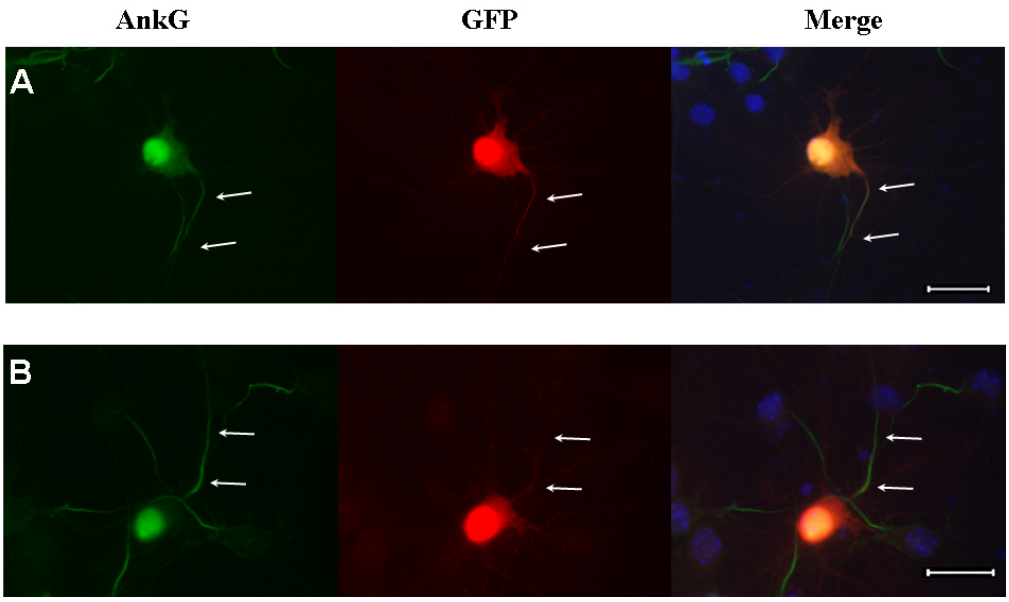

Figure 3-8. Eight mutations in the Na_v binding site disable FHF2a targeting to the AIS of cultured hippocampal neurons

9 DIV mouse hippocampal neurons were transfected with FHF2a-GFP (A) and $FHF2a_{octamutant}$-GFP (B), respectively. After 48 hr, cells were fixed and double immunostained with antibodies against AnkG (green) and GFP (red). Merged images include DAPI stain. Arrows denote AIS. Scale bar, 10 μm. Note that in contrast to wild-type FHF2a, the FHF2a octa-mutant is not targeted to the AIS.

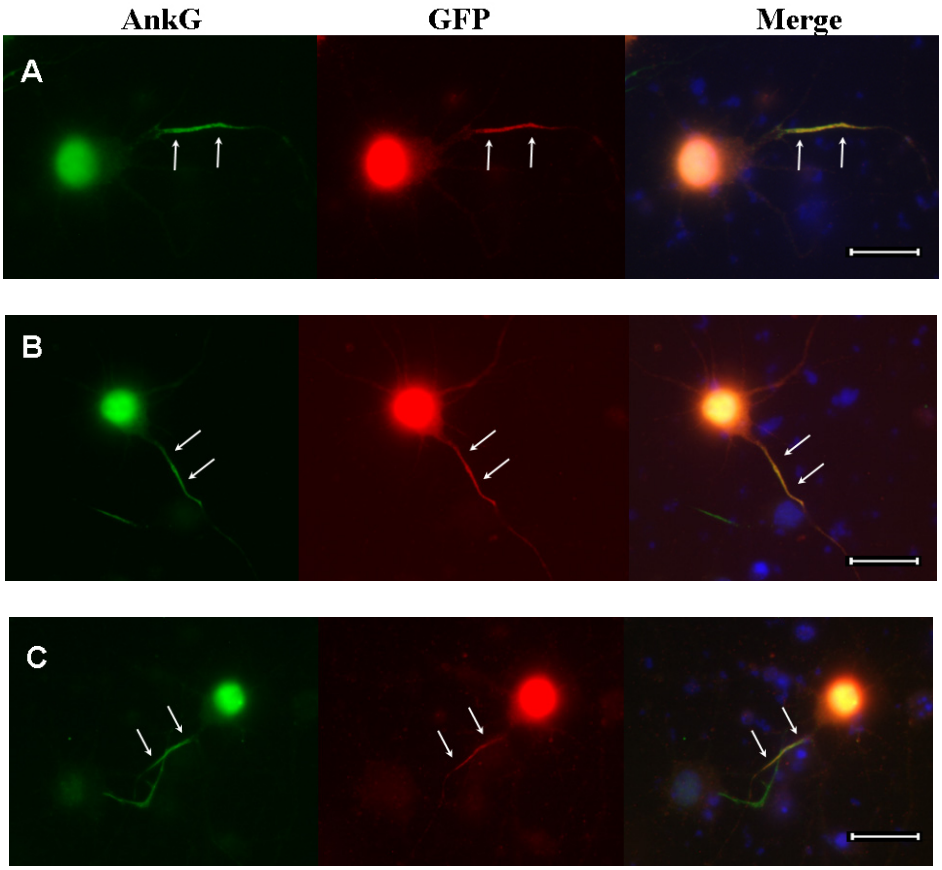

Figure 3-9. Single mutant (R114G or Y155N) in the Na_v binding site does not disrupt FHF1a targeting to the AIS of cultured hippocampal neurons

9 DIV mouse hippocampal neurons were transfected with FHF1a-GFP (A), FHF1a $_{R114G}$-GFP (B), and FHF1a $_{Y155N}$-GFP (C), respectively. After 48 hr, cells were fixed and double immunostained with antibodies against AnkG (green) and GFP (red). Merged images include DAPI stain. Arrows denote axon initial segments. Scale bar, 10 µm. Note that the single mutation R114G or Y155N does not affect the localization of FHF1a in the AIS of hippocampal neurons.

CHAPTER 4

REAL TIME PCR ANALYSIS OF RELATIVE FHF EXPRESSION

Summary

The functional redundancy reflected in FHF1 and FHF4 knockout mice studies makes it intriguing to investigate the relative expression levels of FHFs in different neurons and tissues. Using real time PCR, I established a sensitive system which can detect four FHFs simultaneously in different cells and tissues. The simultaneous amplification of the four FHFs reflects the initial proportions of their mRNA levels. Real time PCR reveals that FHF2 is the most abundant among the FHF mRNAs in hippocampal neurons, making these cells attractive candidates for examining the potential role of FHF2 in neuronal excitability. Furthermore, I have confirmed earlier findings that FHF expression in the brain is far higher than in non-neuronal tissues. The present study also demonstrates the tissue-specific expression patterns of FHFs.

4.1 Introduction

Individual FHFs are expressed in overlapping, but distinct, cell- and tissue-specific patterns. *In situ* hybridization studies in mice have revealed prominent expression of FHFs in developing and adult neurons of the central and peripheral nervous systems (Smallwood et al., 1996; Hartung et al., 1997; Wang et al., 2000 and Allen Brain Atlas: http://www.brain-map.org/). FHFs are also expressed to a limited degree in non-neuronal tissues, including connective tissue of the skeleton and the myocardia of the heart (Smallwood et al., 1996; Hartung et al., 1997; Munoz-Sanjuan et al., 1999). *Fhf1* and *fhf4* are normally expressed in adult spinal motor neurons and cerebellar granule neurons (Smallwood et al., 1996; Wang et al., 2000). *Fhf1* and *fhf2* are expressed in neurons of all spinal and cranial sensory ganglia (Smallwood et al., 1996; Hartung et al., 1997). Coexpression of multiple FHFs in specific neurons could result in functional redundancy. For example, there are only subtle motor deficits of $Fhf1^{-/-}$ mice, greater deficits in $Fhf4^{-/-}$ mice, and much more severe deficits in $Fhf1^{-/-}Fhf4^{-/-}$ mice (Goldfarb et al., 2007). We anticipate that neurological deficits in other combinations of *fhf* gene mutations will reflect the expression profiles of the four *fhf* genes across the nervous system.

I have been interested in determining neurological functions for FHF2, for which no genetic data are yet available. As a first step, I looked for FHF2 in specific neurons

and compared FHF2 expression to that of other FHFs. Until now, few data are available on the relative expression levels of FHFs in tissues or cells. The regional distribution of FHFs in the nervous system can be mapped by *in situ* hybridization. However, this technique requires relatively large amounts of RNA and provides only qualitative or semiquantitative information regarding mRNA levels. Thus, *in situ* hybridization does not allow one to determine the actual composition of different FHFs in the same tissue or cell, and does not provide the molecular analysis with functional correlates. Moreover, the limited availability of antibodies to specific FHFs has prevented the visualization of all specific endogenous FHFs in tissues or cells. Therefore, I chose real time PCR to solve this question.

Real time PCR is used for gene-specific amplification as this technology is capable of detecting product well below the amount required for visualizing amplicons using agarose gel electrophoresis, and generating quantitative data for later analysis (Nolan et al., 2006). The real time PCR system is based on the detection and quantitation of a fluorescent reporter. In the present study, SYBR green was used to monitor DNA synthesis. The higher the copy of template, the faster it reaches the detectable threshold (threshold cycle $C_{t)}$. After the last stage of the PCR, a melt curve analysis is performed, and the melting temperature of the product is noted, which is subsequently used to identify positive transcripts from single neurons or in different tissues (Nolan et al., 2006).

Using real time PCR, I developed a strategy which allowed me to detect four FHFs simultaneously in different cells and tissues. The simultaneous amplification of the four FHFs was designed to maintain the initial proportions of their mRNA level. The present study shows that FHF2 is the most abundant among the FHF mRNAs in hippocampal neurons, making these cells attractive candidates for examining the potential role of FHF2 in electrical excitability. Furthermore, I have confirmed earlier findings that FHF expression in the brain is far higher than in non-neuronal tissues.

4.2 Results

4.2.1 Primer design and PCR system set up

FHF1 to 4 are known to be expressed in the hippocampal neurons by *in situ* hybridization (Goldfarb, 2005). To determine the relative expression levels of FHFs, specific primers for each FHF gene were designed based on the FHF cDNA sequences as shown in **table 4-1**, **table 4-2**, and **figure 4-1**. These primers span two different exons, and have minimal primer-dimer formation, high sequence specificity, and melting temperatures within 55-60 ^{0}C. Since the transcript level of each FHF is very low, the expression profile analysis was carried out in two rounds of PCR amplification. The initial RT-PCR amplification was performed to produce sufficient template in the form of PCR product to enable the quantitative analysis of four FHFs in the second round real time PCR. The primers used in the first round of PCR are termed outer primers, and the

primers used in the second round of PCR are termed inner primers. The concomitant β-actin amplification was used as a positive control (Li et al., 2004) for RNA extraction from tissue or cell aspiration, allowing us to remove undesirable samples, and to ensure that PCR products were detected within the exponential phase of amplification. All PCRs were performed following procedures designed to minimize the chances of cross-contamination. To ensure that genomic DNA does not contribute to the PCR products, control experiments were performed in which total RNA is harvested and processed in the normal manner, except that the reverse transcriptase is omitted. Contamination from extraneous sources was checked by replacing the cellular template with the background solution. These negative controls for contamination from extraneous and genomic DNA were performed for every patch of neurons.

First, the specificity and sensitivity of PCR amplifications using different pairs of primers were tested on total RNA isolated from cultured rat hippocampal neurons. The molecular identities of the outer primer products were confirmed by direct sequencing. The specificity of each inner primer pair was tested with equal amounts of purified products from the first round of PCR as templates (**Figure 4-2A**). The molecular identities of these inner primer products were also confirmed by direct sequencing. These results demonstrate that the primers chosen specifically amplify cDNA for FHFs and that mRNA for all four FHFs is present in the hippocampal neurons. The PCR products were confirmed by electrophoresis together with the melt curve analysis on each run (**Figure 4-2B**).

Second, the PCR amplification efficiency with each *fhf* inner primer pair was measured using the Ct slope method (see Materials and Methods 2.12). A 3-log or 4-log dilution range (with 4 or 5 concentration points at 5, 0.5, 0.05, 0.005, and 0.0005 ng/µl) was generated using 10-fold serial dilutions of the outer primer PCR product, respectively. Each of these dilutions was subjected to real time PCR amplification with each *fhf* inner primer pair using SYBR Green PCR Master Mix on an Applied Biosystems 7500 Real-Time PCR System. The C_t values obtained over this 3-log or 4-log dilution range were plotted against log cDNA concentration (**Figure 4-3**). Amplification efficiency was calculated from the slope of **figure 4-3** using the equation: $Ex = 10^{(-1/slope)} - 1$. As summarized in **table 4-3**, the amplification efficiency with the inner primer pair is sufficient high to perform analysis of the *fhf* expression profile. To obtain a more reliable estimation of the 'real expression ratio', a correction for the differences in PCR efficiencies will be performed in the analysis of the fold-differences in *fhf* expression.

4.2.2 Relative FHF mRNA abundance in hippocampal neurons

Table 4-4 presents data from real time PCR where the relative expression levels of FHFs in rat hippocampal neurons are evaluated. The levels of FHF amplicons in a total RNA sample prepared from 14 DIV rat hippocampal neurons were compared to equal molar *fhf* DNA control to eliminate any differences in PCR efficiencies. By

optimizing the PCR conditions, I was able to detect transcripts of all four FHFs down to 12 pg (single cell level) of total RNA from hippocampal neurons. Total RNA was serially diluted to 12 pg, and subjected to the first round One-step RT-PCR with an equal mix of four outer primer pairs (28 cycles). In the same experiment, equal molar of individual FHF DNAs (outer primer products) were serially diluted to a level approximating potential abundance in a single cell (0.8 fg), and subjected to the first round of PCR with an equal mix of four outer primer pairs (28 cycles). Aliquots of each first PCR product were diluted 100-fold, and subjected to a second round real time PCR (40 cycles) with the inner primer pairs, respectively. For reactions where total RNA template was omitted, no bands were detected (data not shown). Fold-differences calculated are expressed as a range, which is a result of incorporating the standard deviation of the ΔC_t value into the fold-difference calculation. As shown in **table 4-4** and **figure 4-4**, FHF2 is the most abundant among the FHF mRNAs in hippocampal neurons.

4.2.3 Relative expression of FHFs in mouse tissues

To investigate the transcript levels of FHFs in various mouse tissues, total RNA was extracted from the cerebral cortex, skeletal muscle, and kidney of wild-type 9-month old mouse using TRizol (Life Technologies). 1 μg of each total RNA was reverse transcribed into cDNA with a β-actin primer pair and a specific *fhf* inner primer pair using Omniscript Reverse Transcription Kit (Qiagen). FHF3 expression was not tested in this experiment. 0.5 μl of each 20 μl product was subjected to real time PCR

amplification with a specific *fhf* inner primer pair. All quantifications were normalized to β-actin according to the $\Delta\Delta C_t$-method. For reactions where total RNA template was omitted, no bands were detected (data not shown). As illustrated in **figure 4-5**, high levels of expression of FHF1, 2, and 4 were detected in the cerebral cortex, whereas FHF1 and FHF4 were under detectable levels in the skeletal muscle and kidney. Comparatively low levels of FHF2 expression were detected in the skeletal muscle and kidney.

4.3 Discussion

The co-expression of four FHFs has been largely described in the central and peripheral nervous tissues. The present real time PCR system has been successfully used to detect different FHF mRNAs from cells and tissues. It is important to ensure that the relative abundances of the FHF1-4 amplified products reflected the relative abundances of their corresponding mRNAs level in tissues or cells. Different mRNAs for different FHFs may be reverse transcribed at different efficiencies. However, the amplification efficiency with the inner primer pair was sufficient high to perform analysis (**Table 4-3**), and the levels of FHF amplicons in a total RNA sample prepared from hippocampal neurons were compared to equal molar *fhf* DNA control to eliminate any differences in PCR efficiencies (**Table 4-4**). Taken together, it can be concluded that FHF2 is the most abundant compared to other FHFs in hippocampal neurons (**Figure 4-4**). These data

provide a strong foundation for the project described in **Chapter 5**, which examines the requirement of FHF2 for hippocampal neuron excitability using gene knockdown technology.

Further studies will be needed to explore the exact contribution at the functional level of each FHF and especially of FHF2, which is the most highly expressed in hippocampal neurons. The present method provides a convenient way to link electrophysiological recordings to the actual composition of native FHFs expressed by a given neuron, which will be further described in **Chapter 5**. The experimental design is outlined in **figure 4-6** to correlate the degree of neuronal excitability to its FHF expression level for individual cells.

In the present study, real time PCR revealed that high levels of FHF1, 2, and 4 were expressed in the cerebral cortex, which is consistent with published expression patterns (Smallwood et al., 1996; Hartung et al., 1997; Wang et al., 2000 and Allen Brain Atlas: http://www.brain-map.org/) showing that FHF expression in the brain is far higher than in non-neuronal tissues. Low levels of FHF2 were detected in total RNA sample from the skeletal muscle, which may attribute to FHF2 expression in Schwann cells in the motor axons innervating the muscle. The low levels of FHF2 expression in kidney may be due to the contamination from the adrenal gland. These data demonstrate the tissue-specific expression pattern of FHFs, which is in consistence to previous reports (Smallwood et al., 1996; Hartung et al., 1997; Munoz-Sanjuan et al., 1999).

Table 4-1. PCR Primers for *fhf* amplification from rat hippocampal neurons

Gene		Position	Sequence (5'-3')	Product length (bp)	Accession No.
fhf1	outer	201-226	ACCCCAGCTGAAAGGGATTGTGACAA	381	NM_130814
		556-581	GGCTTGGTTTTCTTCACTCTGTTCCC		
	inner	286-306	ACCAAGGACGAAAACAGCGAC	211	
		474-496	GGCGATACAGGGTTGAGGAATAG		
fhf2	outer	155-180	GCCTCAGCTTAAGGGGATAGTCACCA	406	NM_053428
		540-560	TGGTTTGGGCAGAAAATGTGC		
	inner	240-260	ACCAAAGACGAGGACAGCACT	150	
		367-389	GCACTCAGGTGTGAAATGTTCCG		
fhf3	outer	195-220	GCCTCAGCTCAAAGGCATCGTCACCA	404	NM_130816
		579-598	GCTTGGGCACAAAGTGGGCA		
	inner	280-300	ACCCCAGAGGACACCAGCTCC	211	
		468-490	GGCGGTAGAGAGCGGAGGCATAC		
fhf4	outer	195-220	TCCCCAGCTCAAGGGCATAGTGACCA	381	NM_022223
		550-575	GGTTTGGTTTTCTTTACTCTGTTTCC		
	inner	277-299	GGAACTAAGGATGACAGCACCAA	214	
		468-490	GCCTGTACAGCATGGATGAGTAG		
β-actin		1547-1570	CACGGCATTGTAACCAACTGGGAC	288	V01217
		2275-2298	ACCCTCATAGATGGGCACAGTGTG		

Table 4-2. PCR Primers for *fhf* amplification from mouse hippocampal neurons

Gene	Position		Sequence (5'-3')	Product length (bp)	Accession No.
fhf1	outer	201-226	ACCCCAGCTGAAAGGGATTGTGACAA	381	NM_010199
		556-581	GGCTTGGTTTTCTTCACTCTGTTCCC		
	inner	286-306	ACCAAGGACGAAAACAGCGAC	211	
		474-496	GGCGATACAGGGTTGAGGAATAG		
fhf2	outer	155-180	GCCTCAGCTTAAGGGTATAGTTACCA	381	NM_010200
		510-535	GGCTTGTTCTTCTTCACATGGTTGCC		
	inner	240-260	ACCAAAGACGAGGACAGCACT	150	
		367-389	GCACTCAGGTGTGAAATGTTCCG		
fhf3	outer	195-220	GCCTCAGCTCAAAGGCATCGTCACCA	381	NM_010198
		550-575	GCCTTGGTCTTCTTGACTCGGTTTCC		
	inner	280-300	ACCCCAGAGGACACCAGCTCC	211	
		468-490	GACGGTAGAGAGCAGAGGCATAC		
fhf4	outer	195-220	TCCCCAGCTCAAGGGCATAGTGACCA	381	NM_207667
		550-575	GGTTTGGTTTTCTTTACTCTGTTTCC		
	inner	271-295	CTCGATGGAACCAAGGATGACAGCA	123	
		370-393	ACCTTCTCCATTCATTGCTATGTA		
β-actin	1547-1570		CATGGCATTGTTACCAACTGGGAC	288	NM_007393
	2275-2298		GCCCTCGTAGATGGGCACAGTGTG		

Figure 4-1. PCR primer positions in the cDNA sequence alignment of four rat *fhf*s

The sequences were aligned using *Vector NTI*® software. The GenBank accession numbers of the cDNA sequences are listed in Table 4-1. Residue numbers are in parenthesis to the left of the alignment. A dash in the sequence represents a gap introduced to optimize the alignment. The outer primer pairs are highlighted in black background, and the inner primer pairs are highlighted in grey background.

Figure 4-2. **The specificity of each *fhf* inner primer pair was confirmed by traditional PCR and real time PCR**

A, The specificity of each inner primer pair was tested with equal amount of purified outer primer products (5 ng) from the first round of PCR as templates and amplified with each inner primer pair for 20 cycles. Products were resolved in 2% agarose gel containing ethidium bromide. M, 100 bp DNA ladder; 1-4, rat *fhf1* outer primer products amplified with rat *fhf1-4* inner primer pairs, respectively; 5-8, rat *fhf2* outer primer products amplified with rat *fhf1-4* inner primer pairs, respectively; 9-12, rat *fhf3* outer primer products amplified with rat *fhf1-4* inner primer pairs, respectively; 13-16, rat *fhf4* outer primer products amplified with rat *fhf1-4* inner primer pairs, respectively; 17-20, negative control without rat *fhf* outer primer products as template amplified with rat *fhf1-4* inner primer pairs, respectively.

B, representative melt curve of each rat FHF inner primer products after real time PCR amplification. Melt temperature: FHF1 85.5 ^{0}C, FHF2 84.5 ^{0}C, FHF3 88 ^{0}C, FHF4 83.5 ^{0}C. Melt curve was generated by iCycler Thermal Cycler (Bio-Rad).

A

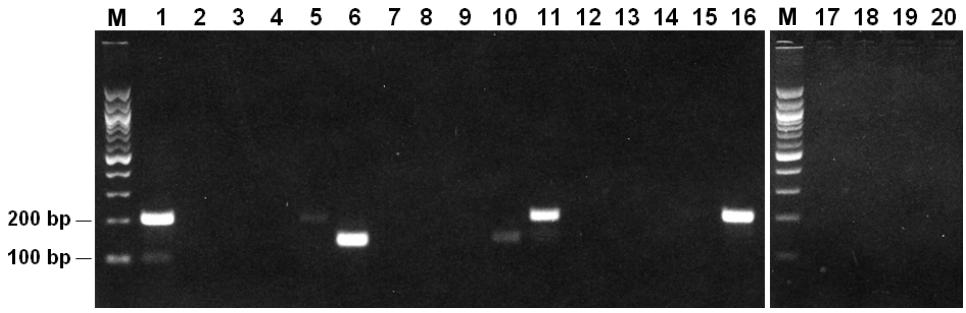
M 1 2 3 4 5 6 7 8 9 10 11 12 13 14 15 16 M 17 18 19 20
200 bp
100 bp

B

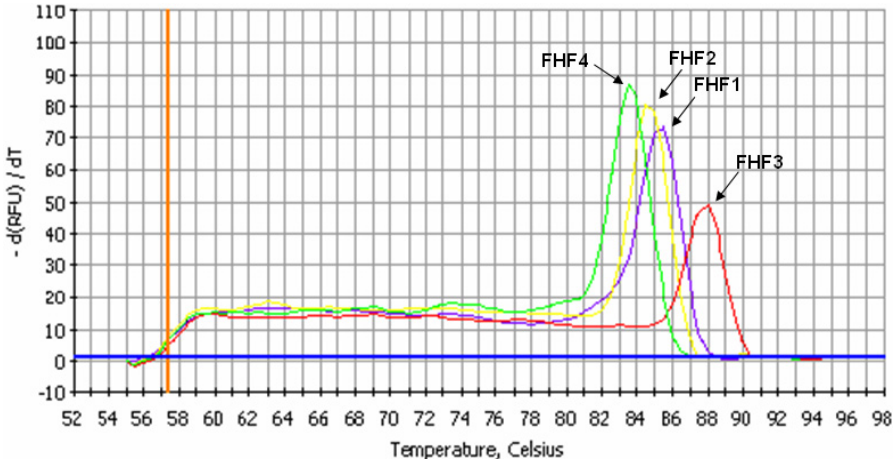
FHF4
FHF2
FHF1
FHF3
- d(RFU) / dT
Temperature, Celsius

Figure 4-2.

Figure 4-3. **The rat *fhf* inner primer pair efficiencies of PCR amplification were measured using the C_t slope method**

A dilution series of β-actin or each rat FHF cDNA was generated with 4 or 5 concentrations covering a 3-log or 4-log dilution range, and the C_t value for each dilution was determined (see Materials and Methods 2.12). A plot of C_t versus log cDNA concentration was constructed. The data points are indicated by black triangles. The trend line is indicated by a black line. Amplification efficiency (Ex) is calculated from the slope using the equation: $Ex = 10^{(-1/slope)} - 1$. The calculated efficiency for each inner primer pair is listed in Table 4-3.

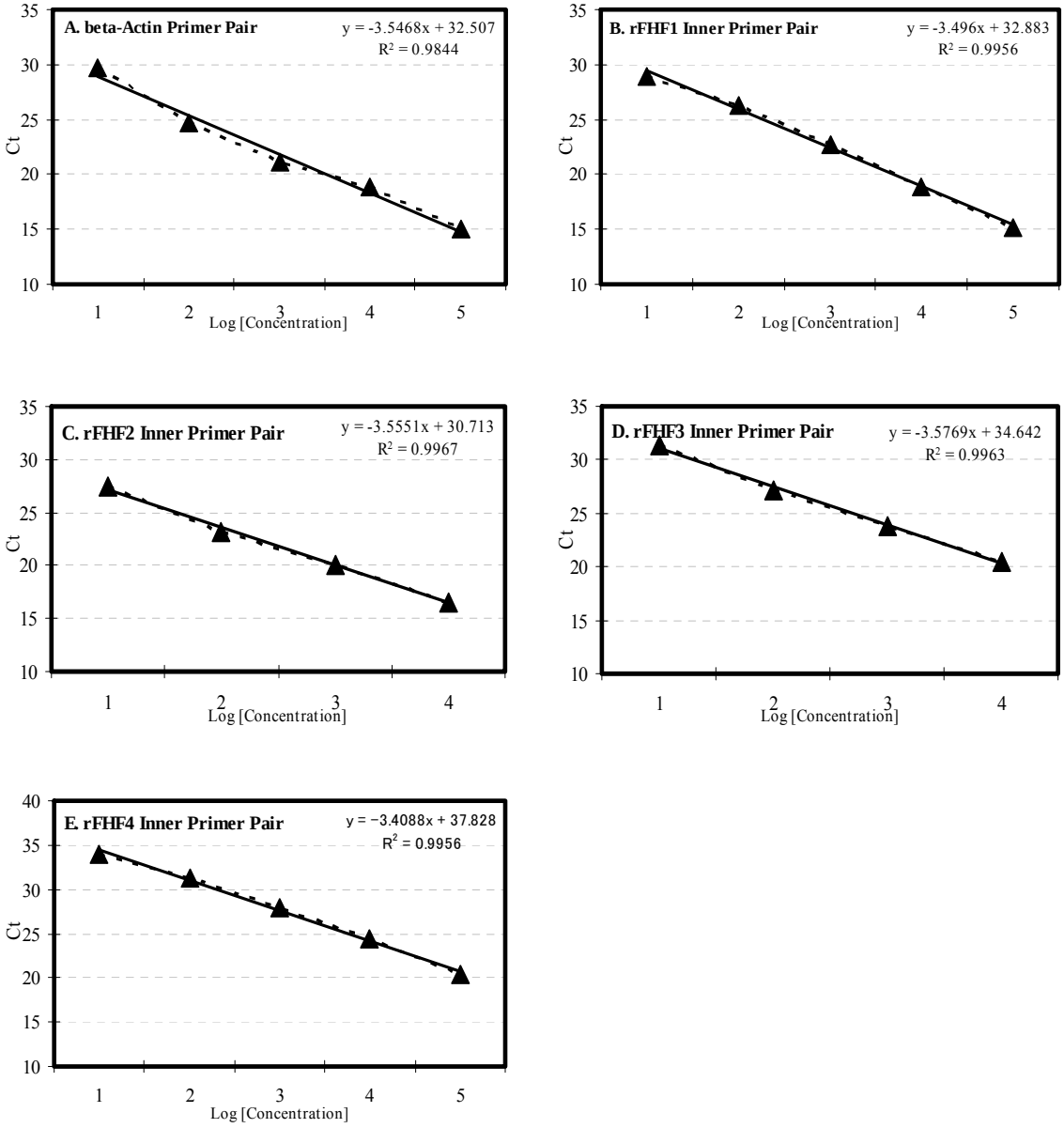
A. beta-Actin Primer Pair
y = -3.5468x + 32.507
R² = 0.9844
B. rFHF1 Inner Primer Pair
y = -3.496x + 32.883
R² = 0.9956
C. rFHF2 Inner Primer Pair
y = -3.5551x + 30.713
R² = 0.9967
D. rFHF3 Inner Primer Pair
y = -3.5769x + 34.642
R² = 0.9963
E. rFHF4 Inner Primer Pair
y = −3.4088x + 37.828
R² = 0.9956
Ct
Log [Concentration]

Figure 4-3.

Table 4-3. The real time PCR amplification efficiencies with β-actin primer pair and rat *fhf* inner primer pairs

Inner primer pair	Log [concentration]	C_t	Efficiency	Slope
β-actin	1	29.753	91.40%	-3.5468
	2	24.698		
	3	21.106		
	4	18.812		
	5	14.962		
rFHF1	1	28.931	93.22%	-3.496
	2	26.32		
	3	22.712		
	4	18.804		
	5	15.209		
rFHF2	1	27.382	91.11%	-3.5551
	2	23.223		
	3	20.132		
	4	16.562		
rFHF3	1	31.333	90.36%	-3.5769
	2	27.14		
	3	23.804		
	4	20.522		
rFHF4	1	34.002	96.50%	-3.4088
	2	31.3		
	3	27.923		
	4	24.35		
	5	20.433		

Table 4-4. Fold difference in rat FHFs relative to FHF2

Average C_t	FHF1	FHF2	FHF3	FHF4
Total RNA sample	**19.341 ± 0.049**	**18.527 ± 0.107**	**22.887 ± 0.028**	**22.247 ± 0.126**
Equal molar *fhf* DNA control	**13.893 ± 0.091**	**15.917 ± 0.044**	**15.953 ± 0.032**	**18.731 ± 0.007**
sample - control	**5.448 ± 0.103**	**2.610 ± 0.116**	**6.934 ± 0.043**	**3.516 ± 0.126**
Difference relative to FHF2	**-2.838 ± 0.103**	**0.000 ± 0.116**	**-4.324 ± 0.043**	**-0.906 ± 0.126**
Fold difference relative to FHF2	**0.140 (0.130-0.150)**	**1.000 (0.923-1.084)**	**0.050 (0.048-0.051)**	**0.536 (0.489-0.582)**

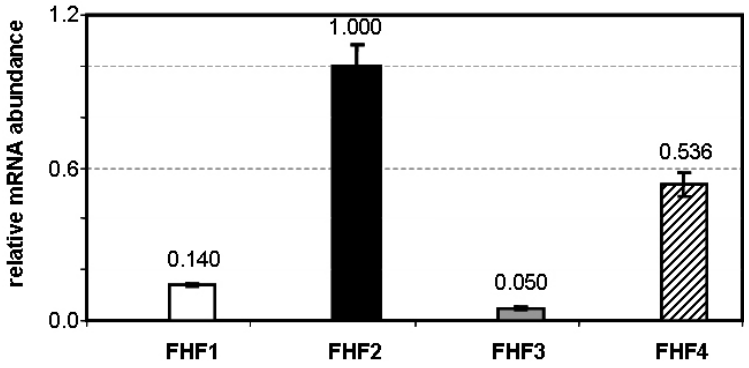

Figure 4-4. Relative amounts of FHF mRNAs amplified by real time PCR from rat hippocampal neurons in primary culture for 14 days

Transcript levels of rat *fhf* genes were normalized to the individual cDNA control measured in the same conditions and were relevant to rat *fhf2* transcript level (see Table 4-4). Values represent the mean of three real time PCR replicates ± S.D. Note that FHF2 is the most abundant among the FHF mRNAs in hippocampal neurons.

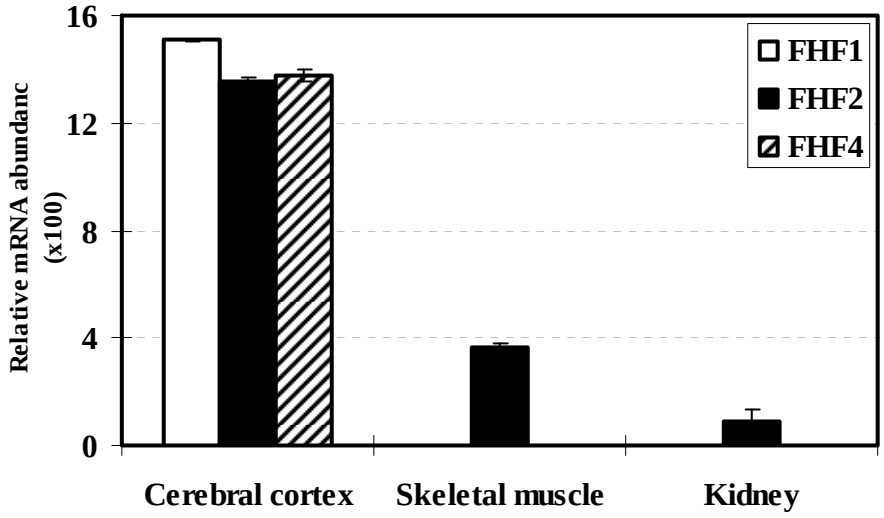

Figure 4-5. Relative expression of FHFs in mouse tissues

Relative amounts of FHF mRNAs amplified by combination of Omniscript reverse transcription and real time PCR from cerebral cortex, skeletal muscle, and kidney of wild-type 9-month old mouse. Transcript levels of mouse *fhf* genes were normalized to the expression β-actin measured in the same samples according to the $\Delta\Delta C_t$-method. Values represent the mean of three real time PCR replicates ± S.D. Note that FHF expression in the brain is far higher than in non-neuronal tissues.

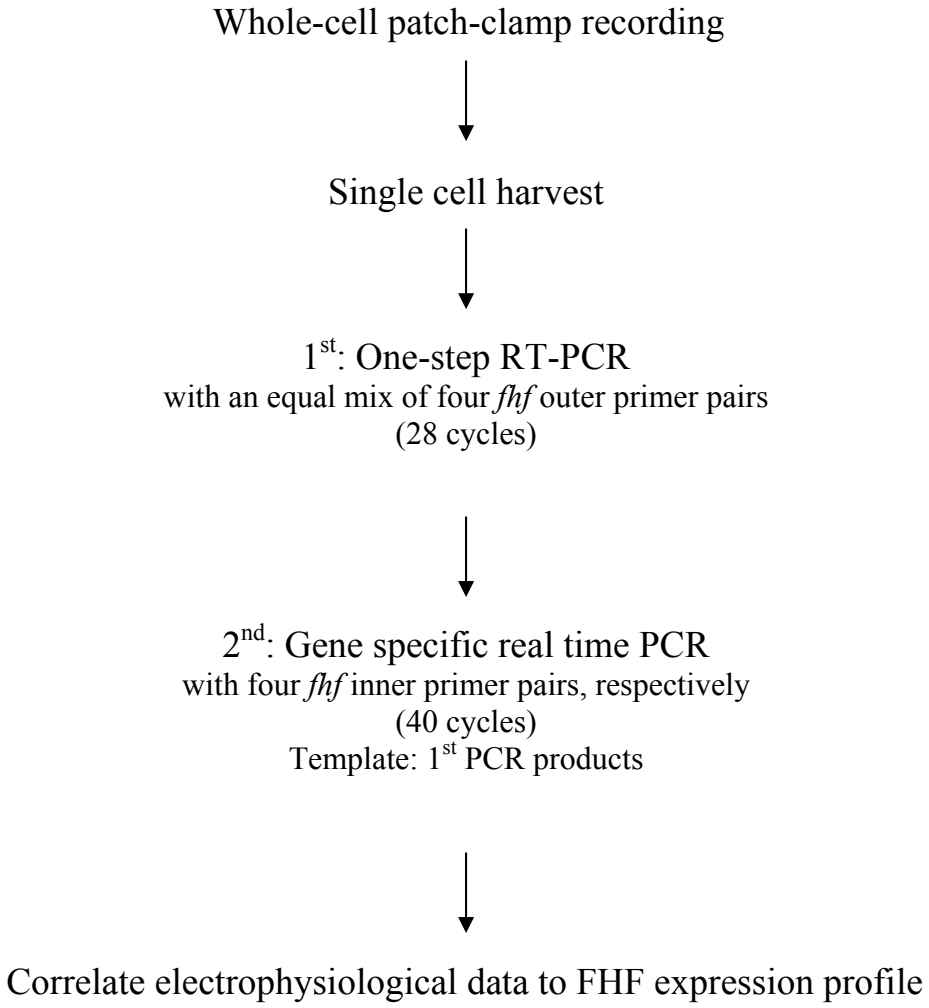

Figure 4-6. Schematic overview of the experimental design to correlate the degree of neuronal excitability to its FHF expression level for individual cells

CHAPTER 5

FHF2 MODULATION OF HIPPOCAMPAL NEURON EXCITABILITY

Summary

The association of FHFs with Na_vs in the AIS raises the possibility that FHFs play roles in neuronal excitability through modulation of Na_vs. We proposed that abnormal intrinsic excitability of hippocampal neurons would be expected when the *fhf2* gene is disrupted since FHF2 is the most abundant among the four FHF mRNAs in hippocampal neurons. The requirement of FHF2 for hippocampal neuron excitability was analyzed using siRNA gene knockdown technology in conjunction with electrophysiological recordings. Loss of FHF1 or FHF2 function alone does not impair the intrinsic excitability of hippocampal neurons in terms of both maximum spike frequency and voltage threshold for spike induction. Hippocampal neurons of *Fhf1*$^{-/-}$ mice were transfected with the *fhf2*-siRNA constructs to generate a model imitating a double knockout of both genes. Hippocampal neurons lacking functional alleles for both of these genes display excitability deficits, with less maximum spike frequency and elevated voltage thresholds for spike induction. Sodium channel inactivation parameters are altered in *Fhf1*$^{-/-}$*Fhf4*$^{-/-}$ granule neurons (Goldfarb et al., 2007). In accordance, the colocalization and physical interaction of FHFs with sodium channels in hippocampal

neurons suggest that intrinsic excitability deficits could reflect altered sodium channel physiology in cells lacking FHF1 and FHF2 function. These are the first data to indicate a role for FHF2 in neuronal excitability. These data suggest a widespread role for FHFs in the control of excitability across the CNS.

5.1 Introduction

FHFs share overlapping but non-identical expression patterns in the developing CNS and nonneuronal tissues (Smallwood et al., 1996; Hartung et al., 1997), which suggests the possible functional redundancy of FHFs. To date, only the functional importance of *fhf1* and *fhf4* of the four *fhf* genes has been established by gene knockout in mice (Wang et al., 2002; Goldfarb et al., 2007). The functional requirements of FHF1 in the absence of FHF4 have been revealed in these studies of knockout mice. *Fhf4*$^{-/-}$ knockout mice have mild reduction in grip strength, and suffer from ataxia and paroxysmal dyskinesia (Wang et al., 2002). *Fhf1*$^{-/-}$ knockout mice have only a modest reduction in grip strength, however, *Fhf1*$^{-/-}$*Fhf4*$^{-/-}$ double knockout mice show enhanced and novel phenotypes not seen in mice with either individual gene mutated. These mice have more severe ataxia, muscle weakness, and locomotor hyperactivity (Goldfarb et al., 2007). Similarly, functional redundancy may limit the breadth and severity of deficits in *fhf2* or *fhf3* single mutant mice. Mice with *fhf2* or *fhf3* disrupted in combination with *fhf1* or *fhf4* are expected to display accentuated and novel deficits.

Fhf-mutant mice have failed to show detectable neuroanatomical abnormalities (Wang et al., 2002; Goldfarb et al., 2007), which suggests that FHFs more directly control the physiological behavior of neurons. Therefore, electrophysiological experiments hold promise for elucidating FHF functions. The association of FHFs with Na_vs in the AIS raises the possibility that FHFs play roles in neuronal excitability through modulation of Na_vs (Goldfarb et al., 2007). Some experiments reported to date have examined the relationship between FHFs and Na_v function in neurons. Using HEK or ND7/23 cells transfected with specific Na_v isoforms alone or in conjunction with FHF gene transfection, FHFs have been shown to have effects on channel inactivation gating and on maximal sodium current influx (Liu et al., 2003; Wittmack et al., 2004). In cerebellar granule cells of *Fhf1*$^{-/-}$*Fhf4*$^{-/-}$ mice, altered sodium channel physiology accounts for a failure of neurons to fire repetitively and raises the voltage thresholds for spike initiation (Goldfarb et al., 2007). *Fhf4* mutation also alters the firing properties of cerebellar Purkinje neurons (Shakkottai et al., 2009).

The results presented in **Chapter 3** demonstrate that there is a broad repertoire of FHF isoforms including FHF2 colocalized with Na_vs at the AIS of hippocampal neurons, which suggests that FHFs may modulate channel physiology, thereby controlling the intrinsic excitability of hippocampal neurons in a manner similar to that which has been described for cerebellar granule neurons of *Fhf1*$^{-/-}$*Fhf4*$^{-/-}$ mice (Goldfarb et al., 2007). Moreover, the results presented in **Chapter 4** show that FHF2 is the most abundant

among the four FHF mRNAs in hippocampal neurons. Thus, we proposed that abnormal intrinsic excitability of hippocampal neurons would be expected when the *fhf2* gene is disrupted in isolation or in combination with *fhf1* and/or *fhf4*.

Knockout mice and RNA interference (RNAi) are two alternative strategies to characterize the function of FHF2. At first, I tried to establish a germ-line mutation of the *fhf2* gene, but failed at the stage of gene targeting in murine ES cells (see **Appendix**). RNAi, mediated by 21- to 22-nucleotide double-stranded (ds)-RNA (called small interfering RNA, or siRNA), has been proven effective in determining gene function in cultured mammalian cells (Elbashir et al., 2001). Considering the difficulties faced in generating *fhf2* knockout mice, RNAi may be more applicable for studying FHF2 function in cultured hippocampal neurons.

In the present study, to determine whether FHF2 expression is necessary for the excitability of hippocampal neurons, RNAi was used to knockdown the expression of FHF2 in cultured hippocampal cells. Intrinsic excitability of hippocampal neurons in culture was examined by whole-cell patch-clamp in terms of both maximum spike frequency and voltage threshold for spike induction. Similar to the slight effect observed in *Fhf1*$^{-/-}$ knockout mice, the knockdown of FHF2 alone does not impair the intrinsic excitability of hippocampal neurons in terms of both maximum spike frequency and voltage threshold for spike induction. Further experiments were performed to knockdown FHF2 in the hippocampal neurons of *Fhf1*$^{-/-}$ mice. Neurons lacking both

FHF1 and FHF2 display excitability deficits, with less maximum spike frequency and elevated voltage thresholds for spike induction.

5.2 Results

5.2.1 siRNA-mediated knockdown of FHF2 gene from wild-type rat hippocampal neurons

5.2.1.1 Generation of the *fhf2*-siRNA constructs

The siRNA specific for *fhf2* was designed to target for both *fhf2a* and *fhf2b*. The automated siRNA prediction software from Whitehead (http://jura.wi.mit.edu/bioc/siRNA/home.php) was used to define sequence motifs and G/C content with rat *fhf2* cDNA sequence (GenBank accession number AF271786) as the input. Two regions downstream of *fhf2* exon 1 were predicted as target sequences; 5' AAGAACAAGCCTGCAGCACATTT 3' and 5' AACTGCAGGCAGATGGAACCATT 3', respectively (**Figure 5-1**). To validate the target specificity of these predicted *fhf2*-siRNAs, a BLAST search was performed using the selected sequences as the input against the NCBI genome databases, and only the rat and mouse *fhf2* genes were targeted. Thus, the chosen *fhf2*-siRNA sequences target the same mRNA sequences of both the rat and the mouse.

The MFOLD program, which predicts RNA secondary structure based on free energy calculations, was used to simulate accessible sites on the siRNA targeting region of *fhf2* mRNA (**Figure 5-1**) (see http://bioweb.pasteur.fr/seqanal/interfaces/infold-simple.html). Luo and Chang found that the gene-silencing efficiency of siRNA is strongly dependent on the local structure of mRNA at the targeted region (Chang et al., 2004). The number of hydrogen bonds formed by the target region is a useful parameter to evaluate the suppression efficiency of designed siRNA. According to their hypothesis, the presence of a large number of unpaired nucleotides would indicate a better accessibility of the siRNA to the targeted mRNA. As shown in **figure 5-1**, there is a hairpin structure within the *fhf2*-siRNA#1 target region, while a loop structure is seen within the *fhf2*-siRNA#2 target region. Thus, the *fhf2*-siRNA#2 is predicted to be more effective than the *fhf2*-siRNA#1 in silencing the *fhf2* gene.

A DNA plasmid (pSUPER)-based method was used to introduce the *fhf2*-siRNA into cultured cells (**Figure 5-2**). The *fhf2*-siRNA constructs were made as follows. For each target site two complementary 60-mer oligonucleotides were prepared containing 5' *Bgl*II and *Hind*III ends (OligoEngine). The oligonucleotides encode two 19 nucleotide (nt) reverse complements homologous to the *fhf2* mRNA target sequence separated by a short spacer region which has no homology to either of the 19 nt sequences. The complementary oligonucleotides were annealed and placed into the pSUPER.neo+gfp vector between *Bgl*II and *Hind*III. Then the resulting construct pSUPER.neo+gfp-siFHF2 was transformed in DH10B. The pSUPER.neo+gfp vector express a fusion of

the neomycin resistance gene with enhanced GFP under control of the phosphoglycerate kinase (PGK) promoter (**Figure 5-2**). GFP expression can help identify positive transfectants. Negative controls were also made by scrambling the nucleotide sequence targeted by the *fhf2*-siRNA#1 or the *fhf2*-siRNA#2 (**Figure 5-1**). The presence of the correct inserts within the *fhf2*-siRNA constructs were confirmed with restriction enzyme digestion (**Figure 5-3**) and DNA sequencing. When expressed under the control of the RNA polymerase-III based expression system, the RNA transcript forms a short hairpin structure with a 19 base-pair double-stranded region and a short loop formed by the space region. The insert is designed such that the first two 5' bases of the spacer region (loop) are expressed as uridines and includes a specific T5 terminator sequence that incorporates two final uridines to the 3' end of the transcript. The hairpin has been designed to be an optimal substrate for the enzyme Dicer, which cleaves the hairpins to generate the short dsRNA, both strands having the two-uridine 3' overhang (**Figure 5-2**).

5.2.1.2 *Fhf2*-siRNA efficacy in rat hippocampal neurons

Traditionally, the suppression of target gene mRNA levels is evaluated by Northern blot, and the suppression of protein levels is evaluated by Western blot. The transfection efficiency reported is relatively low in hippocampal neurons (at most 1% to 2%) (Craig, 1998). Especially in the fully-mature hippocampal neurons (> 10 DIV) in my study, the transfection efficiency is about 0.1% (data not shown). Thus, the suppressed expression level of FHF2 would be too low to be evaluated by Northern blot

or Western blot. In this study, I chose anti-FHF2 antibody immunostaining in conjunction with single-cell real time PCR to evaluate the suppressed expression of FHF2 at protein and RNA levels.

The *fhf2*-siRNA constructs and the nonspecific controls were transfected into hippocampal neurons using Lipofectamine 2000 (Invitrogen). Cells were analyzed 24, 48, 72, and 96 hr from the start of transfection, and GFP-expressing cells were detected. 48 hr after transfection, FHF2 immunostaining remained in the soma and the AIS of hippocampal neurons transfected with the *fhf2*-siRNA or its negative-construct (data not shown). However, 72 hr after transfection, no prominent FHF2 immunostaining in the processes was detected in the *fhf2*-siRNA transfected cells (**Figure 5-4A**), while the AIS of the negative-construct transfected cells (**Figure 5-4B**) or the non-treated cells were positive for FHF2 immunostaining. The FHF2 immunostaining results of the transfected GFP-expressing cells are summarized in **table 5-1**. These data indicate that GFP-expressing cells were positive transfectants of the *fhf2*-siRNA or its negative construct. Therefore, both *fhf2*-siRNA#1 and *fhf2*-siRNA#2 worked successfully. FHF2 immunostaining disappeared in the AIS of the *fhf2*-siRNA transfected cells as early as 56 hr after transfection (**Table 5-1**).

Moreover, as illustrated in **figure 5-4C** and **D**, a well-formed AIS immunolabeled with AnkG antibody remained in the hippocampal neuron transfected with the *fhf2*-

siRNA or its negative-construct. Thus, the *fhf2*-siRNA constructs suppressed *fhf2* expression without disrupting the AIS morphology in hippocampal neurons.

As shown in the immunostaining pictures, transfected hippocampal neurons show higher background in the soma than nontransfected cells. To see if this is a generalized background for any antibodies, transfected GFP-expressing cells were double immunostained with anti-$SNT2_{356}$ (suc1-associated neurotrophic factor target 2) antibody (generated by our laboratory). **Figure 5-5** shows that anti-$SNT2_{356}$ antibody stained all areas of the cells, and a stronger immunostaining signal was detected in transfected cells than that in nontransfected cells. Immunostaining results of transfected cells described in previous chapters also have a high background in the soma of hippocampal neurons. Lipofectamine 2000 may promote penetration of DNA through intact cell membrane in the transfected cells, which may increase the accessibility of the intracellular proteins to the antibody. Thus, the absence of FHF2 immunostaining at the AIS in the *fhf2*-siRNA transfected cells can be taken as strong evidence of the successful knockdown of FHF2.

Suppression of FHF2 mRNA was further confirmed by single-cell real time PCR, which was performed on cell contents harvested into the patch pipette at the end of each recording (Lambolez et al., 1992) (see Materials and Methods 2.11). The continuous perfusion of the external solution prevented the accumulation of contaminating material. 72 hr after transfection, the collected single cell contents were subjected to the first round One-step RT-PCR with an equal mix of *fhf1* and *fhf2* outer primer pairs (28 cycles). For

reactions where cell content template was omitted, no bands were detected. Negative controls performed on the internal solution or the external solution removed from the bath did not show specific amplification (data not shown). Aliquots of each first PCR product were diluted 100-fold, and subjected to a second round real time PCR (40 cycles) with the *fhf1* and *fhf2* inner primer pairs, respectively. β-actin was simultaneously amplified as a positive control in both rounds of PCR to assess the quality of the harvesting and of subsequent steps. FHF2 was undetectable in cells transfected with the *fhf2*-siRNA, while FHF2 was still detected in cells transfected with the *fhf2*-siRNA negative construct (**Figure 5-6**). This finding demonstrated that FHF2 was successfully knocked down in the *fhf2*-siRNA transfected hippocampal neurons.

5.2.1.3 Electrophysiological recordings on *fhf2*-knockdown rat hippocampal neurons

Intrinsic excitability of hippocampal neurons in culture was examined by whole-cell patch-clamp first in a multisweep voltage-clamp mode, then in current-clamp mode, applying inward current of various amplitudes for the duration of 800 ms. The cell was again analyzed by voltage clamp to confirm that active currents had not substantially degraded. Threshold voltage for spike generation ($V_{threshold}$) was determined from recorded voltage traces as the inflection point of accelerating spike upstroke.

To determine directly the effects of *fhf2*-siRNA on excitability of hippocampal neurons, whole-cell patch-clamp recordings were obtained from rat hippocampal neurons 48-115 hr after transfection with the *fhf2*-siRNA and its negative construct. Representative recordings from the transfected GFP-expressing cells are illustrated in **figure 5-10**. Only the data measured up to the following standards were taken into analysis: $R_{leak} > 0.3$ GΩ, Cm > 15 pF, and $-I_{(peak\text{-}10\ mV)} > 1000$ pA. 72 hr after transfection, the $V_{threshold}$ of cells (n=8) transfected with the *fhf2*-siRNA (-43.8 ± 7.2 mV) was indistinguishable from that of the cells (n=7) transfected with the *fhf2*-siRNA negative construct (-48.3 ± 6.4 mV) (**Table 5-2** and **Figure 5-11**). GFP-expressing hippocampal neurons fired repetitively and at frequencies that varied with the stimulus strength. In cells (n=8) transfected with the *fhf2*-siRNA, the maximum number of spikes in 800 ms was also indistinguishable from that of the cells (n=7) transfected with the *fhf2*-siRNA negative construct (**Table 5-2** and **Figure 5-11**).

Taken together, these results demonstrate that knockdown of FHF2 alone does not affect the intrinsic excitability of hippocampal neurons in terms of both maximum spike frequency and voltage threshold for spike induction, which is similar to the studies which showed that *Fhf1*$^{-/-}$ knockout mice had slight demonstrable phenotype. Accordingly, we reasoned that enhanced or novel phenotypes in hippocampal neurons may be expected when *fhf2* is disrupted in combination with *fhf1*. Since *Fhf1*$^{-/-}$ mice were available in our lab, subsequent experiments were focused on knockdown of FHF2 in hippocampal

neurons of *Fhf1*$^{-/-}$ mice, which generates a model imitating a double knockout of both genes.

5.2.2 siRNA-mediated knockdown of FHF2 gene from *Fhf1*$^{-/-}$ mouse hippocampal neurons

Hippocampal neurons from *Fhf1*$^{-/-}$ embryos maintained in culture were indistinguishable from wild-type cultured cells in terms of both gross morphology under phase contrast microscopy (**Figure 5-7A**) and the presence of a well-formed AIS bearing Na_vs that colocalized with AnkG (**Figure 5-7B**). Hippocampal neurons from *Fhf1*$^{-/-}$ mice (n=7) showed normal excitability (**Table 5-2** and **Figure 5-10**). Repetitive firing was readily evoked in *Fhf1*$^{-/-}$ hippocampal neurons, and the maximum spike frequency was similar to that recorded in wild-type hippocampal neurons.

To determine the effects of loss of both FHF1 and FHF2 on the excitability of hippocampal neurons, *Fhf1*$^{-/-}$ hippocampal neurons in culture at 11 DIV were transfected with the *fhf2*-siRNA constructs and the nonspecific controls using Lipofectamine 2000 (Invitrogen). 48 hr after transfection, FHF2 immunostaining remained in the soma and the AIS of hippocampal neurons transfected with the *fhf2*-siRNA or its negative-construct (**Figure 5-8A** and **B**). However, 72 hr after transfection, no prominent FHF2 immunostaining in the processes was detected in the *fhf2*-siRNA transfected cells

(**Figure 5-8C**), while the AIS of the negative-construct transfected cells (**Figure 5-8D**) or the non-treated cells were positive for FHF2 immunostaining. Thus, FHF2 was successfully knocked down in the *fhf2*-siRNA transfected *Fhf1*$^{-/-}$ hippocampal neurons.

The distribution of Na_vs was also analyzed in the transfected GFP-expressing cells. As illustrated in **figure 5-8E** and **F**, a robust Na_v signal remained in the AIS of hippocampal neurons transfected with the *fhf2*-siRNA or its negative-construct. Thus, *fhf2* knockdown did not affect the distribution of Na_vs in hippocampal neurons.

Suppression of FHF2 mRNA was further confirmed by single-cell real time PCR. Following the protocol described for detecting FHF2 knockdown in rat hippocampal neurons, 72 hr after transfection, cell contents harvested into the patch pipette at the end of each recording were subjected to a first round One-step RT-PCR followed by a second round real time PCR. The second round PCR products obtained from four representative transfected cells were visualized on agarose gel (**Figure 5-9A**). No FHF2 band was detected in the *fhf2*-siRNA transfected cells, while the *fhf2*-siRNA negative construct transfected cells still showed the FHF2 band. These findings further demonstrated that FHF2 was successfully knocked down in the *fhf2*-siRNA transfected *Fhf1*$^{-/-}$ hippocampal neurons.

Whole-cell patch-clamp recordings were obtained from *Fhf1*$^{-/-}$ hippocampal neurons transfected with the *fhf2*-siRNA construct and its negative construct, respectively.

Representative recordings from the GFP-expressing *Fhf1*$^{-/-}$ hippocampal cells are illustrated in **figure 5-9B**. 48 hr after transfection, the $V_{threshold}$ and the maximum spike frequency of the *Fhf1*$^{-/-}$ hippocampal cells (n=5) transfected with the *fhf2*-siRNA construct were similar ($p < 0.5$) to those of the cells (n=5) transfected with the *fhf2*-siRNA negative construct (-45.0 ± 2.2 mV versus -47.0 ± 3.6 mV, and 28.6 ± 3.4 versus 31.0 ± 7.2). This finding suggested that *fhf2*-siRNA did not have any effect at 48 hr after transfection, which is consistent with the FHF2 immunostaining results at 48 hr after transfection in *Fhf1*$^{-/-}$ hippocampal neurons (**Figure 5-8A** and **B**).

By contrast, 72 hr after transfection, the $V_{threshold}$ was significantly ($p < 0.005$) elevated in *Fhf1*$^{-/-}$ hippocampal cells (n=5) transfected with the *fhf2*-siRNA (-36.1 ± 7.0 mV) compared to cells (n=5) transfected with the *fhf2*-siRNA negative construct (-49.6 ± 3.8 mV) (13.5 mV shift) (**Table 5-2** and **Figure 5-11**). Furthermore, repetitive firing was markedly attenuated in *Fhf1*$^{-/-}$ hippocampal cells (n=5) transfected with the *fhf2*-siRNA (**Figure 5-9**), and the maximum number of spikes in 800 ms (11.6 ± 8.0) was significantly reduced ($p < 0.05$) compared with the cells (n=5) transfected with the *fhf2*-siRNA negative construct (25.4 ± 10.3) (**Table 5-2** and **Figure 5-11**). This finding suggested that *fhf2*-siRNA had effect at 72 hr after transfection, which is consistent with the FHF2 immunostaining results at 72 hr after transfection in *Fhf1*$^{-/-}$ hippocampal neurons (**Figure 5-8C** and **D**). Therefore, hippocampal neurons lacking functional alleles for both FHF1 and FHF2 display excitability deficits. As illustrated in **figure 5-9**, the electrophysiological recordings were consistent with the actual composition of native

FHFs expressed by a transfected *Fhf1*$^{-/-}$ neuron in which FHF2 was successfully knocked down. These findings show a correlation between the degree of hippocampal neuron excitability deficits and the level of FHF expression.

5.3 Discussion

Since the biochemical functions of FHFs are quite similar, functional redundancy may have limited the breadth and severity of deficits in the single FHF mutants so far described (Goldfarb et al., 2007). Thus, the excitability of hippocampal neurons was not affected with only FHF2 knockdown or FHF1 knockout (**Figure 5-10**). However, hippocampal neurons lacking both of these genes have higher voltage spike thresholds and cannot fire action potentials repetitively (**Figure 5-10**). Based on the present experimental design, the electrophysiological recordings and the real time PCR results successfully correlated the degree of neuronal excitability to its FHF expression level for a transfected *Fhf1*$^{-/-}$ neuron (**Figure 5-9**). Since the primers designed for *fhf1* amplification did not locate in the gene targeting region to generate a null allele for the *fhf1* gene (Goldfarb et al., 2007), the present real time PCR method could still detect an FHF1 band in a transfected *Fhf1*$^{-/-}$ neuron (**Figure 5-9**).

As shown in **figure 5-6** and **figure 5-9**, the present real time PCR method is sensitive enough to be applied in single hippocampal neurons. I confined my analysis to

those cell samples positive for β-actin amplification, and normalized all quantifications to β-actin according to the *ΔΔCt*-method. Since single cell analysis is performed mostly with material harvested by somatic patch-clamp, this may result in underestimation of individual cell's contents. Despite this possible limitation, the obtained data demonstrate that the transcript level of FHF2 in single hippocampal pyramidal neurons was different from cell to cell (**Figure 5-6**). Moreover, heterogeneity of Na_v expression has been found in hippocampal neurons (Mechaly et al., 2005). Future experiments focused on linking the expression profiles of FHFs with those of Na_v will be of considerable interest. To see whether FHFs compensate for each other in terms of their function, it will be necessary to investigate the expression profiles of FHF1, 3, and 4 in transfected FHF2-knocked down cells compared to those of control cells.

The colocalization and physical interaction of FHFs with Na_vs suggested that intrinsic excitability deficits in *fhf* mutant granule neurons could reflect altered sodium channel physiology (Goldfarb et al., 2007). Na_vs in *Fhf1*$^{-/-}$*Fhf4*$^{-/-}$ cerebellar granule neurons are more sensitive to inactivation than channels in wild-type cells. In these neurons, Na_vs inactivate at more negative voltages and more rapidly, and are slower to recover from inactivation. As a biological consequence, *Fhf1*$^{-/-}$*Fhf4*$^{-/-}$ cerebellar granule neurons have higher voltage spike thresholds and cannot fire action potentials repetitively (Goldfarb et al., 2007). Hippocampal neurons lacking both FHF1 and FHF2 have similar, though less severe, deficits in intrinsic excitability as *Fhf1*$^{-/-}$*Fhf4*$^{-/-}$ cerebellar granule neurons, which could also reflect altered sodium channel physiology. However,

hippocampal neurons at the current developmental stage (> 10 DIV) have numerous neurites and more remote localization of Na_vs in the AIS (**Figure 3-1**). It does not allow good spatial control of the membrane voltage and the clear resolution of sodium current. Therefore, it is not practical to perform sodium current only recordings on fully differential *Fhf1*$^{-/-}$ hippocampal neurons in which FHF2 has been knocked down under the present experimental design.

FHF2 expression was not detected in cerebellar granule neurons (Goldfarb, 2005). Thus, the *Fhf1*$^{-/-}$*Fhf4*$^{-/-}$ cerebellar granule neuron is a model imitating a triple knockout of FHF1, 2, and 4 genes. It would be interesting to knockdown FHF2 in hippocampal neurons of *Fhf1*$^{-/-}$*Fhf4*$^{-/-}$ mice. With only FHF3 functioning, new or severe neuronal deficits would be expected in these hippocampal neurons.

Based on the present study and the gene localization and tissue-specific expression pattern of FHF1 and FHF2 (Smallwood et al., 1996; Hartung et al., 1997), *Fhf1*$^{-/-}$*Fhf2*$^{-/-}$ double mutant animals would be expected to have impaired neuronal excitability in the brain and the spinal and cranial sensory ganglia. However, RNAi only affect the transcriptional level of FHF2. The complex pattern of processing and control of expression of *fhf2*detected might reflect different spatial and temporal expression of the *fhf2* gene during development of the CNS (Smallwood et al., 1996). Despite prior technical difficulties, further efforts to generate *Fhf2*$^{-/-}$ mice and *Fhf1*$^{-/-}$*Fhf2*$^{-/-}$mice are still of critical importance for uncovering the overall repertoire of FHF functions.

Figure 5-1. The secondary structures of the *fhf2*-siRNA target regions in the *fhf2* mRNA and the sequences of the *fhf2*-siRNA duplexes

The top panel shows the energetically optimal local secondary structures of *fhf2* mRNA at the regions targeted by the *fhf2*-siRNA#*1* (A) or the *fhf2*-siRNA#2 (B) as determined by MFOLD program (http://bioweb.pasteur.fr/seqanal/interfaces/infold-simple.html). The regions targeted by the *fhf2*-siRNAs are indicated by the red dots next to the bases. The lower panel shows the target regions of the *fhf2*-siRNA*s*, the *fhf2*-siRNA duplexes and their scrambled sequences of negative controls.

A

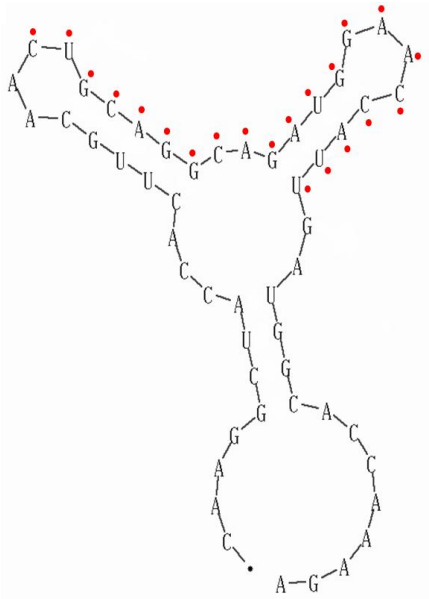

Target region 207-229 bp GC% 58

B

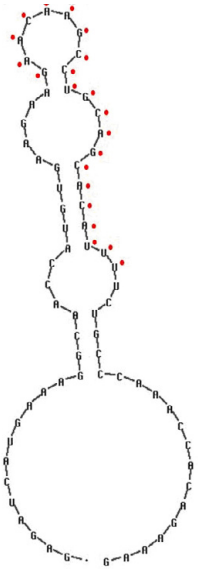

Target region 521-543 bp GC% 53

fhf2-siRNA#1

sense	CUGCAGGCAGAUGGAACCA	UU
antisense UU	GACGUCCGUCUACCUUGGU	

fhf2-siRNA#2

sense	GAACAAGCCUGCAGCACAU	UU
antisense UU	CUUGUUCGGACGUCGUGUA	

fhf2-siRNA negative#1

sense	TGTAGAGAGACGCACGCAC	UU
antisense UU	ACATCTCTCTGCGTGCGTG	

fhf2-siRNA negative#2

sense	ACGAGCATACATGCACACG	UU
antisense UU	TGCTCGTATGTACGTGTGC	

Figure 5-1.

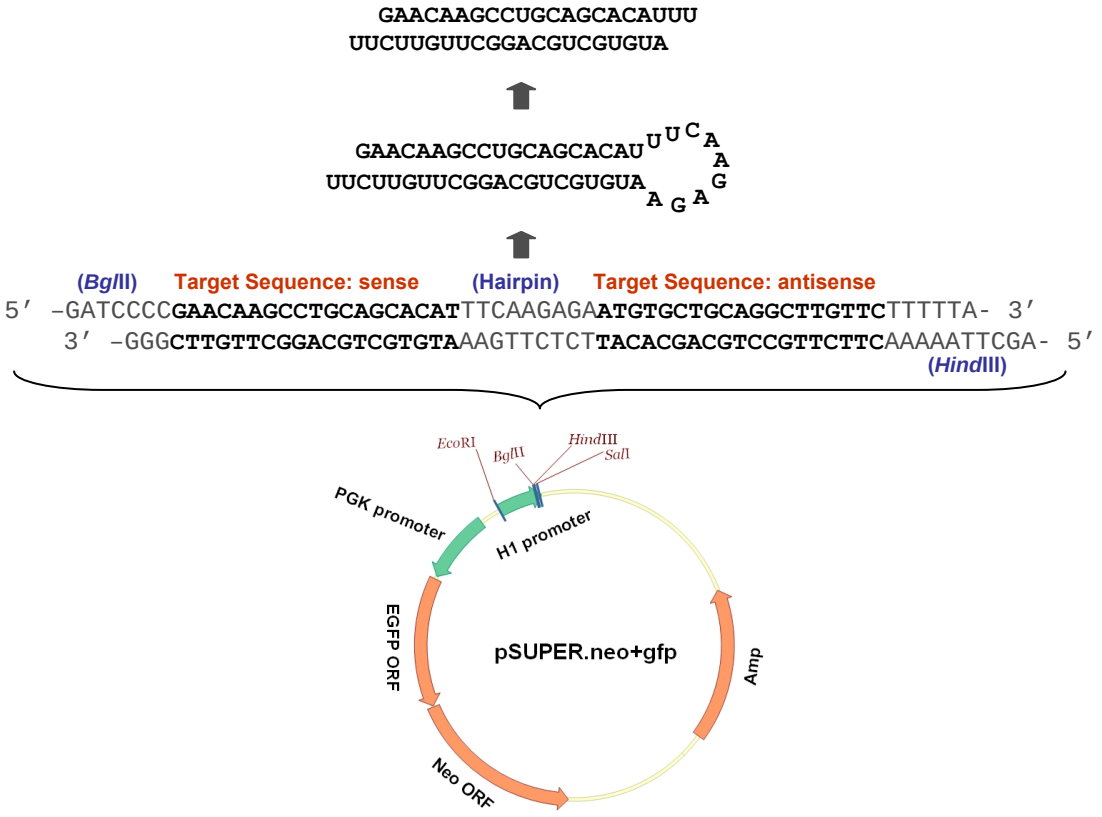

Figure 5-2. Mechanism of the pSUPER RNAi system

The pSUPER.neo+gfp-siFHF2#1 is taken as an example to show the 60-nt oligo is transcribed to hairpin RNA and processed to functional siRNA by the pSUPER RNAi system (modified from OligoEngine). The vector uses the polymerase-III H1-RNA gene promoter, as it produces a small RNA transcript lacking a polyadenosine tail and has a well-defined start of transcription and a termination signal consisting of five thymidines in a row (T5). The cleavage of the transcript at the termination site is after the second uridine, yielding a transcript resembling the ends of synthetic siRNAs, which also contain two 3' overhanging T or U nucleotides.

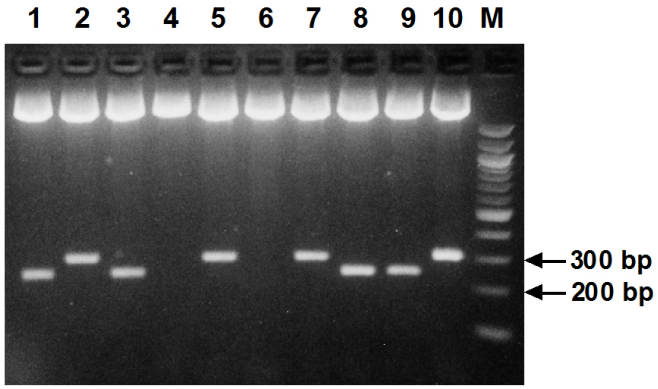

Figure 5-3. Confirmation of the presence of the correct insert within the pSUPER.neo+gfp vector with *EcoR*I and *Sal*I double digestion

Digested products were resolved in 2% agarose gel containing ethidium bromide. Double digestion of the negative clone released a 242 bp fragment, but double digestion of the positive clone produced a 302 bp fragment. M, 100 bp DNA ladder.

Figure 5-4. siRNA suppressed *fhf2* expression in rat hippocampal neurons without disrupting the AIS morphology

Cells were transfected with the *fhf2*-siRNA constructs (A, C), or the *fhf2*-siRNA negative constructs (B, D). After 72 hr, cells were fixed and double immunostained with antibodies: A, B, against FHF2 (green) and GFP (red); C, D, against GFP (green) and AnkG (red). Merged images include DAPI nuclear stain. Transfected cells show high background in the soma. Arrows denote the AIS of transfected cells. Arrow heads denote the AIS of nontransfected cells. Scale bar, 10 μm.

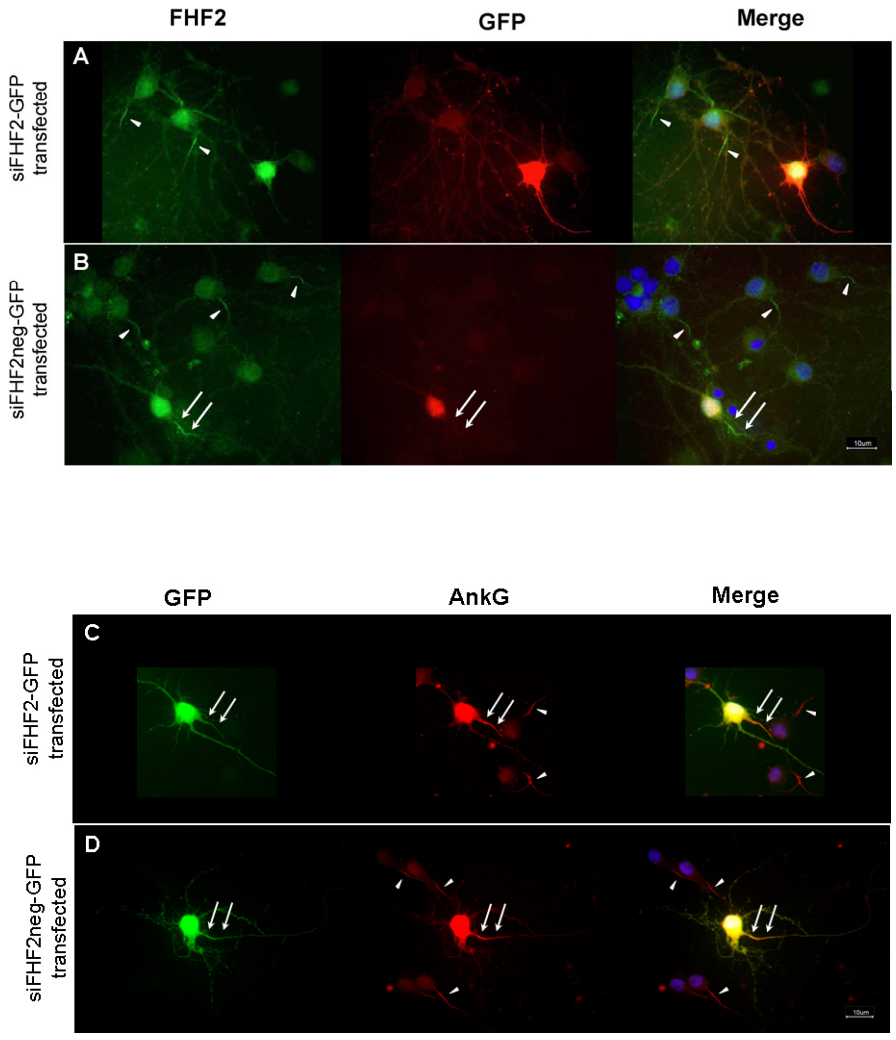
FHF2
GFP
Merge
A
siFHF2-GFP transfected
B
siFHF2neg-GFP transfected
GFP
AnkG
Merge
C
siFHF2-GFP transfected
D
siFHF2neg-GFP transfected

Figure 5-4.

Table 5-1. Summary of immunocytochemistry results of rat hippocampal neurons transfected with the *fhf2*-siRNA constructs

Cells were plated on 12-mm coverslips and transfected with the *fhf2*-siRNA constructs (1+ or 2+), or the *fhf2*-siRNA negative constructs (1- or 2-), respectively. After transfection, cells were fixed and double immunostained with antibodies against FHF2 and against GFP. GFP-expressing cells on the coverslip were examined for FHF2 staining signal.

hr after transfection	transfected with *fhf2*-siRNA construct	GFP-expressing cells	
		FHF2 staining positive in AIS	FHF2 staining negative in processes
56	1+	0	15
	1-	11	0
	2+	0	9
	2-	12	0
76	1+	0	7
	1-	10	0
	2+	0	13
	2-	12	0
113	1+	0	12
	1-	10	0
	2+	0	14
	2-	11	0

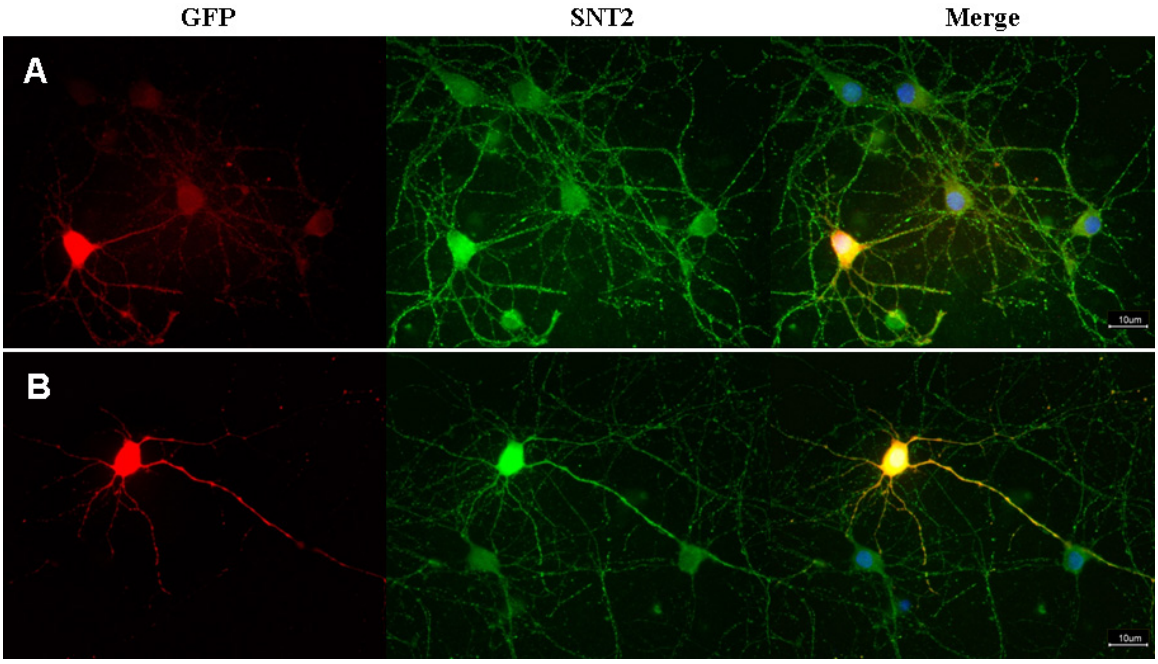

Figure 5-5. *Fhf2*-siRNA transfected cells show higher background than nontransfected cells as labeled by anti-SNT2$_{356}$ antibody

Hippocampal neurons were transfected with the *fhf2*-siRNA constructs (A), or the *fhf2*-siRNA negative constructs (B) by Lipofectamine^{TM} 2000 (Invitrogen). 72 hr after transfection, cells were fixed and double immunostained with antibodies against GFP (red) and SNT2$_{356}$ (green). Merged images include DAPI nuclear stain. Scale bar, 10 μm.

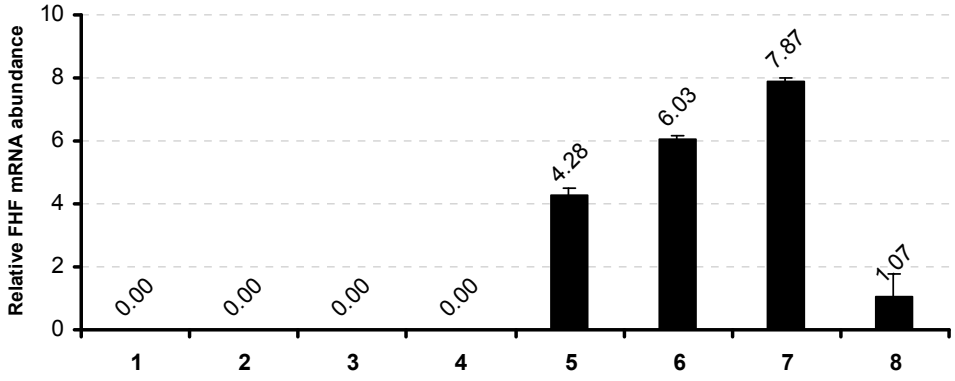

Figure 5-6. Single-cell real time PCR analysis of FHF2 expression in rat hippocampal neurons transfected with the *fhf2*-siRNA or its negative construct

Cell 1-4 were transfected with the *fhf2*-siRNA constructs, and cell 5-6 were transfected with the *fhf2*-siRNA negative constructs. 72 hr after transfection, cell contents harvested into the patch pipette at the end of each recording were subjected to first round One-step RT-PCR with the *fhf2* outer primer pairs (28 cycles). Aliquots of each first PCR product were diluted 100-fold, and subjected to a second round real time PCR (40 cycles) with the *fhf2* inner primer pair. β-actin was simultaneously amplified as a positive control in both rounds of PCR. All quantifications were normalized to β-actin amplified using the same conditions according to the $\Delta\Delta C_t$-method.

A

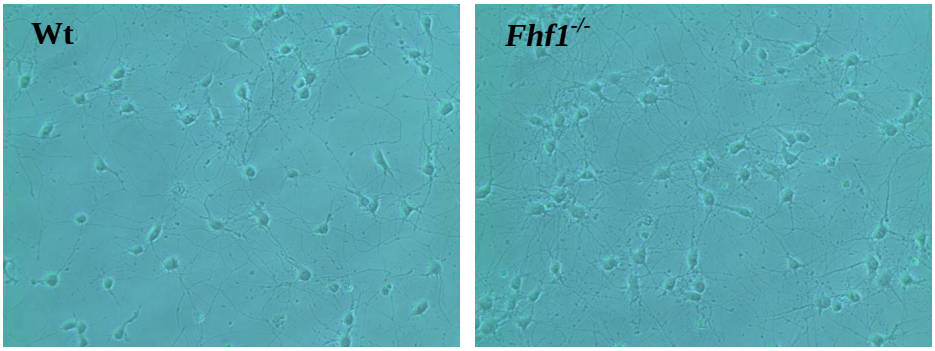

B

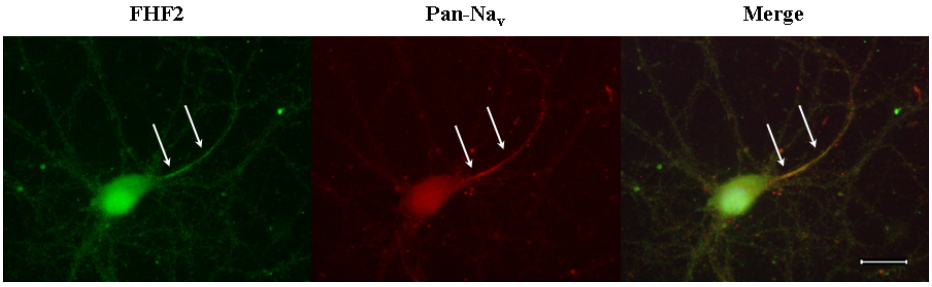

Figure 5-7. FHF2 and Na_v distribution in *Fhf1*$^{-/-}$ hippocampal culture were indistinguishable from wild-type

A, phase contrast micrographs of E18 hippocampal neurons cultured for 13 days. Left, wild-type neurons; right, *Fhf1*$^{-/-}$ neurons.

B, immunofluorescence analysis of *Fhf1*$^{-/-}$ hippocampal neurons cultured for 13 days. Cells were fixed and double immunostained with antibodies against FHF2 (green) and sodium channels (Pan-Na_v, red). Merged images include DAPI nuclear stain. Arrows denote AIS. Scale bar, 10 μm.

Figure 5-8. siRNA suppressed *fhf2* expression in *Fhf1*$^{-/-}$ hippocampal neurons without disrupting the Na_v localization

Cells were transfected with the *fhf2*-siRNA constructs (A, C, E), or the *fhf2*-siRNA negative constructs (B, D, F). After 48 hr (A, B) or 72 hr (C-F), cells were fixed and double immunostained with antibodies: A, B, C, D, against FHF2 (green) and GFP (red); E, F, against sodium channels (Pan-Na_v, green) and GFP (red). Merged images include DAPI nuclear stain. Arrows denote the AIS of transfected cells. Arrow heads denote the AIS of nontransfected cells. Scale bar in A, B, E, and F, 10 μm; in C and D, 5 μm.

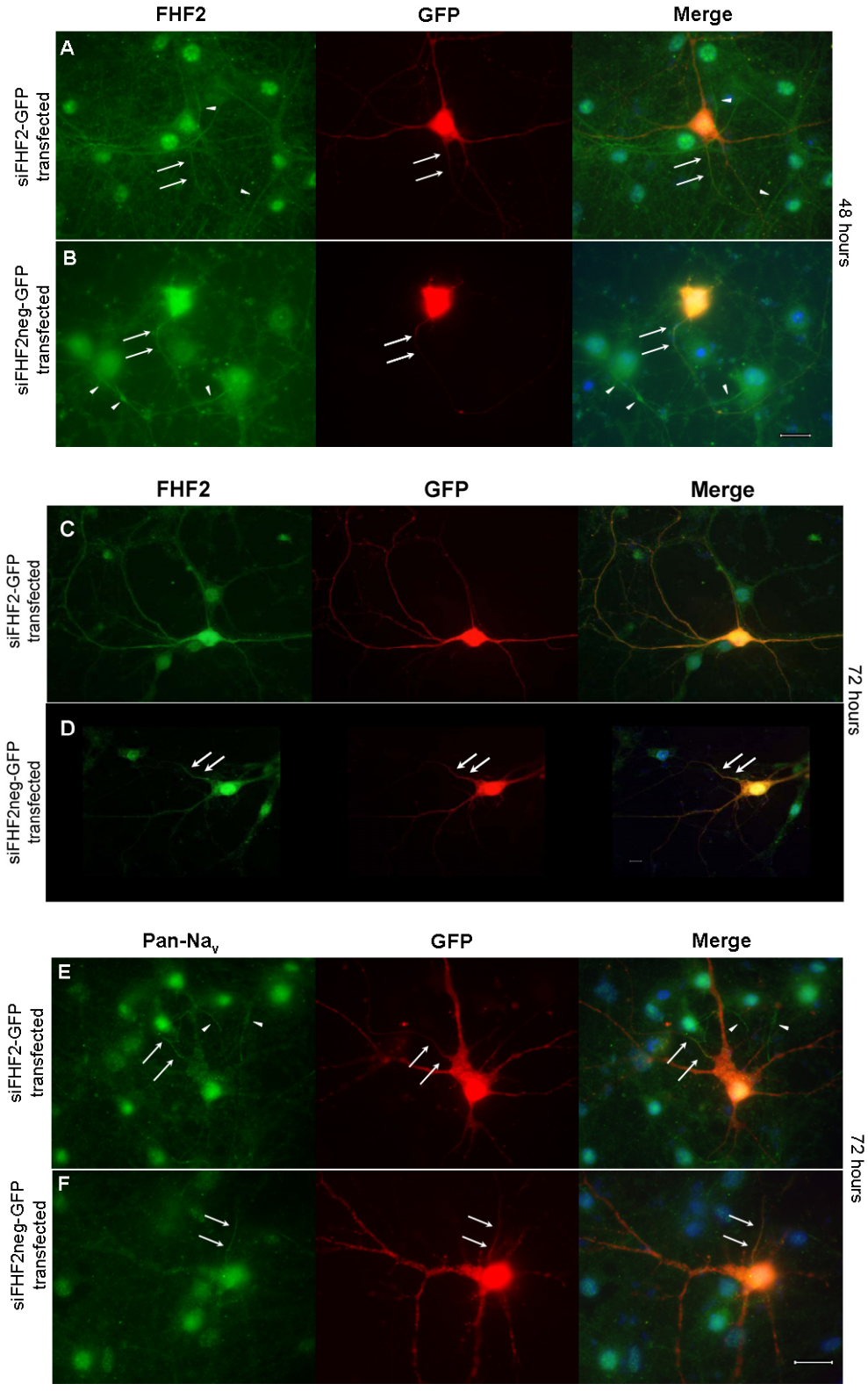
FHF2
GFP
Merge
A
siFHF2-GFP transfected
B
siFHF2neg-GFP transfected
48 hours
FHF2
GFP
Merge
C
siFHF2-GFP transfected
D
siFHF2neg-GFP transfected
72 hours
Pan-Na$_v$
GFP
Merge
E
siFHF2-GFP transfected
F
siFHF2neg-GFP transfected
72 hours

Figure 5-9. Single-cell real time PCR analysis and whole-cell patch-clamp recordings in *Fhf1*$^{-/-}$ hippocampal neurons transfected with the *fhf2*-siRNA or its negative construct

A, agarose gel analysis of the single-cell real time PCR products obtained on four representative transfected *Fhf1*$^{-/-}$ cells. Cell 1 and 2 were transfected with the *fhf2*-siRNA constructs, and cell 3 and 4 were transfected with the *fhf2*-siRNA negative constructs. 72 hr after transfection, cell contents harvested into the patch pipette at the end of each recording were subjected to first round One-step RT-PCR with an equal mix of *fhf1* and *fhf2* outer primer pairs (28 cycles). Aliquots of each first PCR product were diluted 100-fold, and subjected to a second round real time PCR (40 cycles) with the *fhf1* or *fhf2* inner primer pair. β-actin was simultaneously amplified as a positive control in both rounds of PCR. Products were resolved in 2% agarose gel containing ethidium bromide. M, 100 bp DNA ladder.

B, membrane voltage recordings of the corresponding cells during current injection. Arrows point to voltage spike thresholds. Note that repetitive firing is impaired in *Fhf1*$^{-/-}$ neurons transfected with the *fhf2*-siRNA.

A

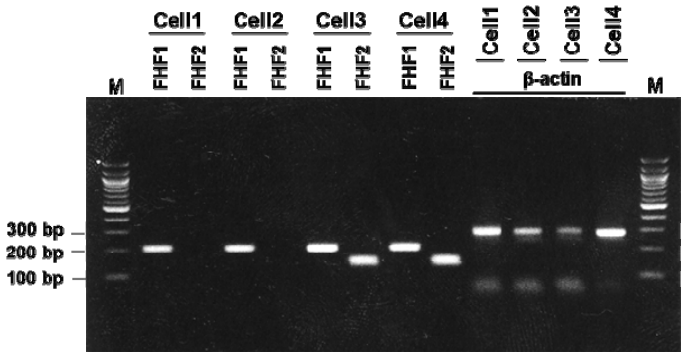
Cell1
Cell2
Cell3
Cell4
FHF1
FHF2
β-actin
M
300 bp
200 bp
100 bp

B

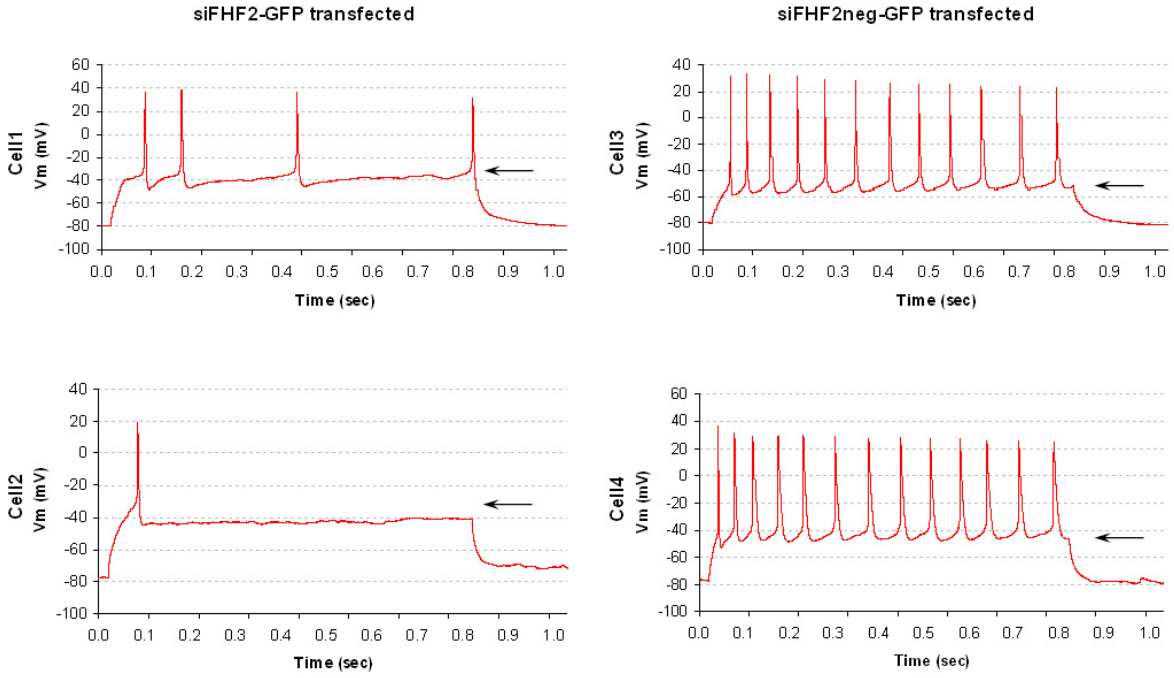
siFHF2-GFP transfected
siFHF2neg-GFP transfected
Cell1
Cell2
Cell3
Cell4
Vm (mV)
Time (sec)

Figure 5-9.

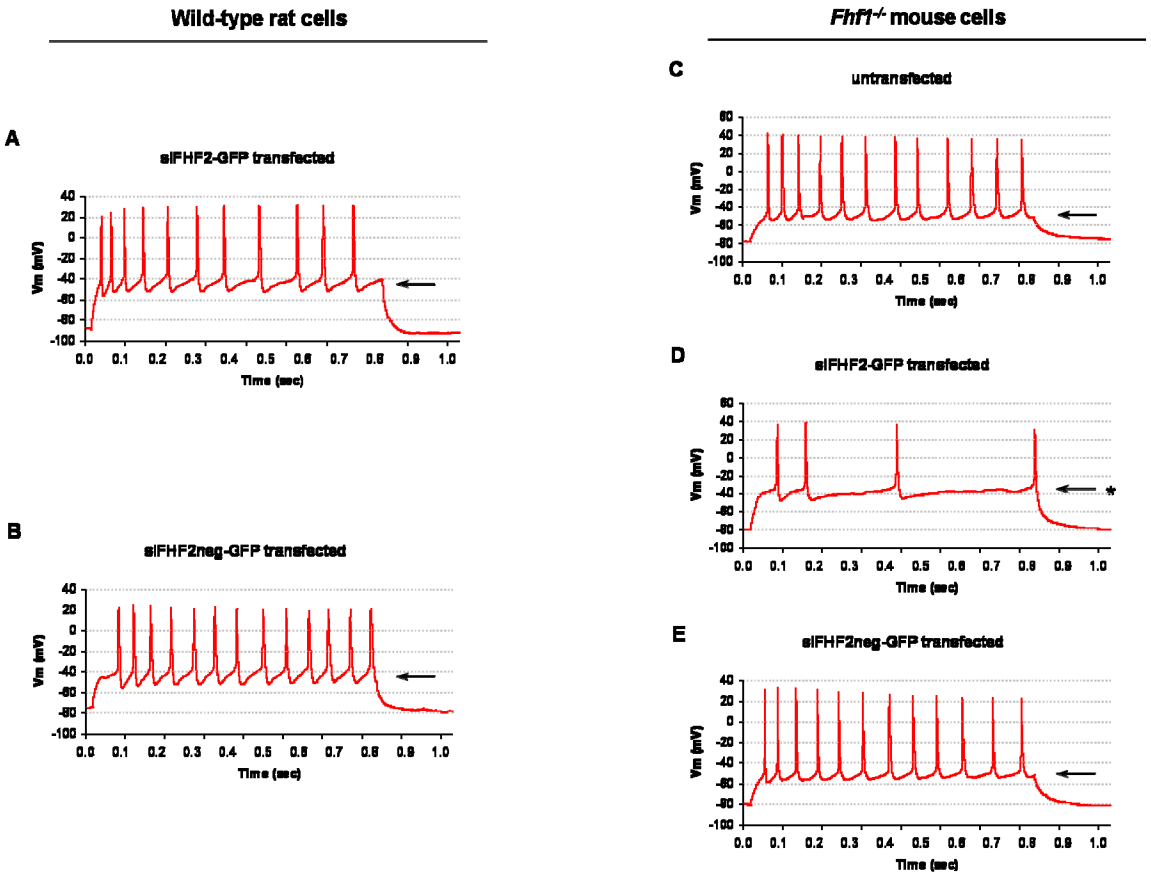

Figure 5-10. Membrane voltage recordings of representative hippocampal neurons during current injection

A, rat neuron transfected with the *fhf2*-siRNA; B, rat neuron transfected with the *fhf2*-siRNA negative construct; C, *Fhf1*$^{-/-}$ neuron; D, *Fhf1*$^{-/-}$ neuron transfected with the *fhf2*-siRNA; E, *Fhf1*$^{-/-}$ neuron transfected with the *fhf2*-siRNA negative construct. Arrows point to voltage spike thresholds. Repetitive firing is impaired in *Fhf1*$^{-/-}$ neuron transfected with the *fhf2*-siRNA. *, note significant elevated voltage spike threshold in D.

Table 5-2. Whole-cell patch-clamp recordings of hippocampal neurons in primary culture

	Wild-type rat cells		*Fhf1*$^{-/-}$ mouse cells			
	siFHF2-GFP transfected	**siFHF2 neg-GFP transfected**	**untransfected**	**siFHF2-GFP 48hr after transfected**	**siFHF2-GFP 72hr after transfected**	**siFHF2 neg-GFP 72hr after transfected**
No. of Cells recorded	8	7	7	5	5	5
R_{leak} (GΩ)	0.55 ± 0.25	0.49 ± 0.16	0.50 ± 0.16	0.57 ± 0.20	0.64 ± 0.18	0.36 ± 0.04
Cm (pF)	30.65 ± 11.55	35.55 ± 11.23	37.09 ± 10.27	26.31 ± 7.35	28.83 ± 10.13	47.33 ± 11.43
R_s (MΩ)	8.9 ± 4.7	7.1 ± 2.5	5.1 ± 1.8	7.8 ± 4.3	9.9 ± 4.8	5.3 ± 1.5
$I_{in\text{-}peak}$ at -10 mV (pA)	-1913 ± 465	-1607 ± 350	-2329 ± 760	-2098 ± 1041	-1938 ± 666	-3699 ± 1409
V_{rest} (mV)	-59.3 ± 6.6	-55.9 ± 10.7	-59.6 ± 10.7	-55.6 ± 6.3	-46.8 ± 7.0	-62.4 ± 8.6
$V_{thresold}$ (mV)	-43.8 ± 7.2 #	-48.3 ± 6.4	-46.0 ± 4.2	-45.0 ± 2.2	-36.1 ± 7.0 *	-49.6 ± 3.8 #
Maximum # spikes in 800ms	20.6 ± 10.1 #	14.0 ± 5.4	24.0 ± 6.1	28.6 ± 3.4	11.6 ± 8.0 **	25.4 ± 10.3 #

No deficit ($p < 0.2$) by *t*-test. * Significant deficit ($p < 0.005$) by *t*-test. ** Significant deficit ($p < 0.05$) by *t*-test.

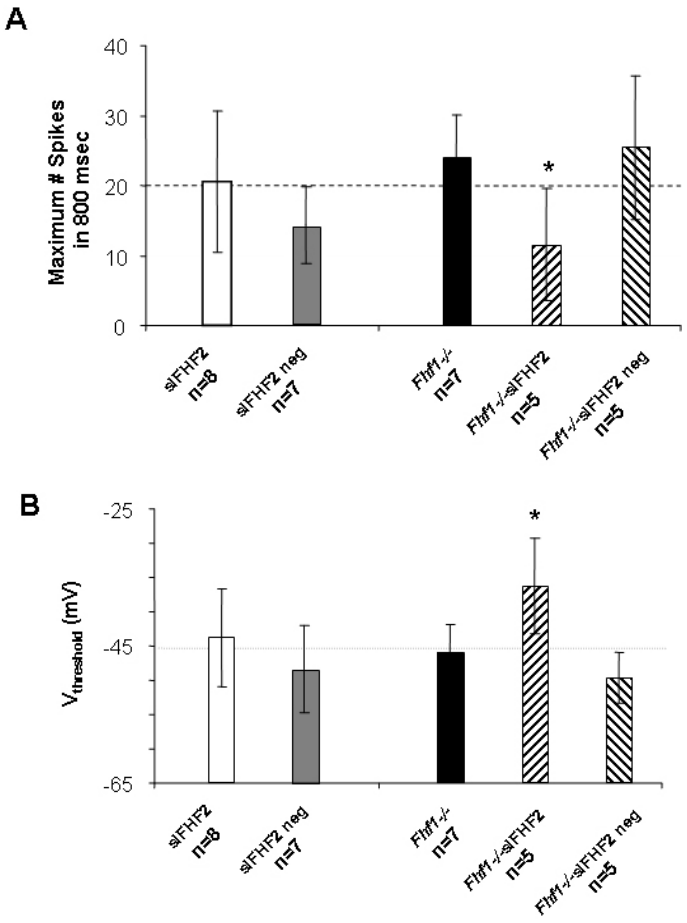

Figure 5-11. Intrinsic excitability of wild-type rat and *Fhf1*$^{-/-}$ mouse hippocampal neurons following FHF2 knockdown

A, maximal spike frequency. For each patched neuron, current injection command sweeps of 800 ms duration and of different amplitude were applied, action potentials recorded, and the maximum number spikes in any sweep determined. *n*, number of cells recorded. *, cells lacking for both FHFs less excitable than negative controls ($p < 0.05$ by *t* test). B, threshold voltage for spike generation ($V_{threshold}$). Significant elevated voltage spike thresholds in cells lacking for both FHFs compared to negative controls (* $p < 0.005$ by *t* test).

CHAPTER 6

SUMMARY AND FUTURE PERSPECTIVES

6.1 Summary

FHF modulation of Na_Vs inactivation has been demonstrated in cerebellar granule neurons of *Fhf1*$^{-/-}$*Fhf4*$^{-/-}$ mice. Loss of sodium channel modulation in *Fhf1*$^{-/-}$*Fhf4*$^{-/-}$ mice causes ataxia through impairment of granule neuron firing (Goldfarb et al., 2007). While the functional importance of FHF1 and FHF4 has been established through gene knockout studies, the roles of FHF2 and FHF3 have not been elucidated. My research efforts have focused on defining functional requirements for the FHF2 protein. Following my unsuccessful efforts to generate an *fhf2* knockout mouse (**Appendix**), I focused on the potential role of FHF2 in neuronal excitability. In this research, the hippocampal neuron was chosen as a model system to study the role of FHFs through investigating their subcellular localization, their transcript profiles, and the requirement of FHF2 for neuronal excitability.

I have investigated the localization of endogenous FHFs for which antibodies are available and the localization of FHF-GFP fusion proteins transfected into neurons (**Chapter 3**). I observed that endogenous FHF2 and FHF4 proteins colocalize at the AIS of hippocampal neurons. Transfected FHF1a, FHF2a, and FHF4b GFP fusion proteins

also localize to the AIS in both hippocampal and cerebellar granule neurons. By contrast, FHF1b-GFP associates with AIS to a far lesser extent than FHF1a-GFP, demonstrating that there is isoform specificity in FHF targeting. FHF2a octa-mutant (K67F/I69R/Y151N/Y152H/L195R/K197M/P198S/V201S) in the Na_v binding surface of the FHF2a core domain is deficient for channel binding and the AIS targeting, which suggests that the AIS targeting of an FHF requires the protein's sodium channel binding surface. Single mutant (R114G or Y155N) in the Na_v binding surface of the FHF1a core domain does not affect the AIS targeting of FHF1a. These findings show that sodium channel interaction is necessary, but not sufficient, for FHF colocalization with channels to the AIS.

To assess the roles of FHF paralogs in the nervous system, FHF transcript profiles were investigated using real time PCR (**Chapter 4**). The simultaneous amplification of the four FHFs reflects the initial proportions of their mRNA levels. I found that FHF2 is the most abundant among the FHF mRNAs in hippocampal neurons, making these cells attractive candidates for examining the potential role of FHF2 in neuronal excitability. Furthermore, I have confirmed earlier findings that FHF expression in the brain is far higher than in non-neuronal tissues. The present study also demonstrates the tissue-specific expression patterns of FHFs, which is in agreement with previous reports.

The requirement of FHF2 for hippocampal neuron excitability was analyzed using siRNA gene knockdown technology in conjunction with electrophysiological recordings

(**Chapter 5**). Loss of FHF1 or FHF2 function alone does not impair the intrinsic excitability of hippocampal neurons in terms of both maximum spike frequency and voltage threshold for spike induction. Hippocampal neurons of *Fhf1*$^{-/-}$ mice were transfected with the *fhf2*-siRNA constructs to generate a model imitating a double knockout of both genes. Hippocampal neurons lacking functional alleles for both of these genes display excitability deficits, with less maximum spike frequency and elevated voltage thresholds for spike induction. Sodium channel inactivation parameters are altered in *Fhf1*$^{-/-}$*Fhf4*$^{-/-}$ granule neurons (Goldfarb et al., 2007). In accordance, the colocalization and physical interaction of FHFs with sodium channels in hippocampal neurons suggest that intrinsic excitability deficits could reflect altered sodium channel physiology in cells lacking FHF1 and FHF2 function. These are the first data to indicate a role for FHF2 in neuronal excitability. These data suggest a widespread role for FHFs in the control of excitability across the CNS.

6.2 Future perspectives

6.2.1 Establishment of the rules for FHF localization

Transfection of neurons with FHF-GFP fusion proteins enables us to examine the subcellular localization of FHFs for which antibodies are unavailable or are not isoform-specific. As shown in Chapter 3, FHF1a-GFP concentrates in the AIS of hippocampal neurons, whereas FHF1b-GFP clusters at the node of Ranvier in the transfected and

myelinated DRG/Schwann coculture (Dover, et al., unpublished data). Differential subcellular localization of FHF1a and 1b suggests the isoform specificity in FHF targeting. The "a" isoforms for all four FHFs are very homologous in their N-terminal extensions. The "b" isoform N-termini are variable in sequence, and are very short in FHF1b and FHF2b (**Figure 1-2**). Moreover, single mutant (R114G) in the FHF1a core domain does not affect the AIS targeting, whereas the corresponding single mutant (R52G) in the FHF1b core domain is deficient for channel binding (Olsen et al., 2003). These findings suggest that the N-terminal region of FHF 1a may contribute to sodium channel binding or AIS targeting together with the core domain. More site-directed mutants of FHF1a in both the N-terminal region and the core domain are needed to study the role of the N-terminal region in channel binding or AIS targeting. The N-terminal region of FHF as an AIS targeting signal is also suggested by the localization studies of FHF4a and FHF4b. Despite their isoform difference, both FHF4a-GFP and FHF4b-GFP have been shown to preferentially colocalize with endogenous Na_vs at the AIS of fully differentiated hippocampal neurons (Lou et al., 2005). The FHF4b N-terminus contains two leucine-based motifs which have been implicated in protein trafficking (Bonifacino and Traub, 2003). Mutagenesis within the N-terminal extensions of "a" isoform and 4b isoform FHFs will be engineered to map the AIS localization signals.

Furthermore, FHF2a-GFP is found highly enriched at the AIS, whereas octa-mutant (K67F/I69R/Y151N/Y152H/L195R/K197M/P198S/V201S) in the FHF2a core domain does not interact with Na_vs or localize at the AIS. These findings show that

sodium channel interaction is necessary, but not sufficient, for FHF colocalization with channels to the AIS. The effect of the corresponding octa-mutant in the FHF2b core domain on channel binding or AIS targeting will be investigated in hippocampal neurons.

In the future, FHF localization analysis will be extended to all known FHF isoforms in order to establish the "rules for FHF localization".

6.2.2 Additional knockdown of FHF2 and/or FHF3 in *Fhf1*$^{-/-}$*Fhf4*$^{-/-}$ hippocampal neurons

FHF2 expression was not detected in cerebellar granule neurons (Goldfarb, 2005). Thus, the *Fhf1*$^{-/-}$*Fhf4*$^{-/-}$ cerebellar granule neuron is a model imitating a triple knockout of FHF1, 2, and 4 genes. It would be interesting to employ the *fhf2*-siRNA strategy in cultured hippocampal neurons of *Fhf1*$^{-/-}$*Fhf4*$^{-/-}$ mice to generate a model imitating a "triple knockout". With only FHF3 functioning, new or severe neuronal deficits would be expected in these hippocampal neurons. Furthermore, the siRNA specific for *fhf3* could be generated and simultaneously transfected with the *fhf2*-siRNA to the cultured hippocampal neurons of *Fhf1*$^{-/-}$*Fhf4*$^{-/-}$ mice. RNAi suppression of both *fhf2* and *fhf3* in *Fhf1*$^{-/-}$*Fhf4*$^{-/-}$ cells would imitate an *fhf*-null model to reveal the significance of FHFs in neuronal excitability.

However, RNAi only affect the transcriptional level of FHFs. The complex pattern of processing and control of expression of *fhf* detected might reflect different spatial and temporal expression of the *fhf* gene during development of the CNS (Smallwood et al., 1996). Despite prior technical difficulties, further efforts to generate mice with *fhf2* or *fhf3* disrupted in isolation or in combination with *fhf1* and/or *fhf4* are still of critical importance for uncovering the overall repertoire of FHF functions.

APPENDIX

TARGETING CONSTRUCT FOR ENGINEERING *Fhf2*$^{-/-}$ MICE

The chromosomal localization of *fhf2* gene is Xq26 A5 in house mouse. The length of *fhf2* gene is 72283 bp containing exon 1a, 1b, 2, 3, 4, and 5. This project involves engineering *fhf2*-knockout constructs in mouse embryonic stem (ES) cells, and generating mice harboring the corresponding genetic changes. The past efforts in our laboratory to obtain homologous recombination at the *fhf2* locus were unsuccessful due to using small targeting vector. Therefore, our new approach chose a very large vector to increase likelihood of homologous recombination.

Our new targeting vector BAC-FHF2-KO is engineered from a bacterial artificial chromosome (BAC). BAC clone RP23-469H13 containing *fhf2* exon 1a, 2, 3, 4, and 5 was purchased from BACPAC Resources. As shown in **Appendix Figure 1**, the DNA segment flanked by the outer *Mlu*I sites covers the coding region of *fhf2* exon 4 and 5. Our approach to generate a targeting vector in which this DNA segment is deleted and replaced by a 5.8-kb PGKNeo cassette, in which a selection gene *neo* encoding neomycin resistance that allows for positive selection in ES cells is under the control of the eukaryotic phosphoglycerate kinase (PGK) promoter. After the BAC-FHF2-KO is linearlized by *Not*I, this cassette is flanked in the 5' direction by a 34 kb homologous arm and in the 3' direction by a 39 kb homologous arm (**Appendix Figure 1**).

The BAC-FHF2-KO was constructed by the following steps. First, to generate *Mlu*I cleavage sites on both ends of the PGKNeo cassette, a pair of 18-nt oligonucleotides was synthesized for generating the *Not*I/*Mlu*I/*Xho*I adaptors (**Appendix Figure 2**), which includes the *Not*I, *Mlu*I, and *Xho*I cleavage sites and is phosphorylated at the *Xho*I end. The *Xho*I sites were used to ligate to both *Xho*I ends of PGKNeo cassette to generate a '*Not*I/*Mlu*I/*Xho*I-PGKNeo cassette-*Xho*I/*Mlu*I/*Not*I' fragment. This fragment was cloned into a *Not*I cleaved pBluescriptII SK(-)(Δ*Xho*I), and thereafter excised from this plasmid by *Mlu*I digestion and followed by gel purification. The PGKNeo cassette is now flanked by *Mlu*I sites. Second, RP23-469H13(Δ*Mlu*) vector was obtained by *Mlu*I digestion and religation of RP23-469H13 DNA deleting the coding region of exon 4 and 5 (**Appendix Figure 2**). Subsequently, RP23-469H13(Δ*Mlu*) was linearized by digestion with *Mlu*I and treated with calf intestinal phosphatase (CIP). Third, the linear '*Mlu*I/*Xho*I-PGKNeo cassette-*Xho*I/*Mlu*I' product derived from step one above was ligated to the *Mlu*I/CIP-treated RP23-469H13(Δ*Mlu*) vector from step two above. The ligation products were transformed into DH10B electrocompetent cells (Invitrogen). The bacteria in which the BAC had incorporated were selected by colony hybridization using the probe derived from *neo* gene with primers Neo-5'-S and Neo-3'-AS as depicted in **Appendix Figure 2**. The PGKNeo cassette was inserted in the same transcriptional direction as the endogenous mouse *fhf2* gene.

For disruption of the *fhf2* gene, BAC-FHF2-KO was linearized by digestion with *Not*I, and transformed into 129/SVEV-derived ES cells by electroporation (**Appendix Figure 3**). Transformants were selected with G418. Among the selected clones should be some in which homologous recombination between the BAC-FHF2-KO and the *fhf2* gene deleting exon 4 and 5. Since the *fhf2* gene is located in the X chromosome, a single homologous recombination event leads to complete loss of function in XY ES cells.

In a first transformation experiment, approximately 250 neomycin-resistant colonies were picked and expanded. Genomic DNAs from these clones were screened by PCR using two pairs of primers (**Appendix Figure 3**). One pair of primers corresponded to a segment in *fhf2* exon 4 with upstream primer E4-84555-S and downstream primer E4-84939-AS. The other pair served as an internal control, with primers IB2-IVS2-US2 and IB2-IVS2-DS4 specific for a portion of an unlinked gene, *IB2*. The PCR product of *fhf2* exon 4 was 385 bp for the wild-type allele, and that of *IB2* was 625 bp. The 385 bp band should be absent from any clone bearing a targeted allele. As shown in **Appendix Figure 4**, all genomic DNAs retained the *fhf2* exon 4 region, suggesting that none of these clones were the desired homologous recombinants.

There are several possible explanations for these first negative results. First, if homologous recombination does not occur between the BAC-FHF2-KO and the *fhf2* gene, the 385 bp band and the 625 bp band should have the same intensity since *fhf2* and *IB2* have the same copy number in XY ES cells. During the clone picking and expansion

stage, if the homologous recombinants were contaminated with the non-recombinants, a 385 bp band weaker than the 625 bp one would appear. Second, the selected clones were maintained on subconfluent mouse embryonic fibroblasts (MEFs) until clone lysis for DNA preparation stage. If the ratio of numbers between MEFs and ES cells was too high, the MEFs DNA maybe contribute to the presence and intensity of the *fhf2* 385 bp band.

I screened up to 576 ES clones in the later transformations, taking the precautions during clone expansion discussed above. Eight DNA samples with weaker *fhf2* exon4 band were obtained (as shown in **Appendix Figure 4** lane 8) and taken as candidate homologous recombinants. These candidates were further investigated by Southern blot hybridization using equal amount of the following two probes. One probe was from *fhf4*, yielding a 9.5 kb wild-type *EcoR*I digested fragment, the other was from *fhf2* exon4 region, yielding a 3.8 kb wild-type fragment. However, the 3.8 kb endogenous gene band remains in all the lanes of Southern blot hybridization results.

These unsuccessful efforts were an unfortunate and uncommon problem with gene knockout, which led me to pursue other approaches, including RNAi (**Chapter 5**).

Appendix Figure 1. Schematic depicting the *fhf2* gene and the targeting vector

The *fhf2* genomic locus in BAC RP23-469H13 (191 kb) shows the positions of the five coding exons (E1 through E5) and of *Mlu*I cleavage sites. The targeting vector replaces the genomic segment between outer *Mlu*I sites and containing exons E4+E5 with an IRES-lacZ:PGKNeo selection cassette. This targeting vector contains 5' and 3' homology segments of 34 kb and 39 kb, respectively.

The PGKNeo cassette contains the following in sequence: an internal ribosomal entry site (IRES), the *E. coli lacZ* gene, the SV40 late polyadenylation signal and a unit that consists of the promoter of the gene encoding mouse PGK, the neomycin resistance gene *neo* and the mouse PGK gene polyadenylation signal.

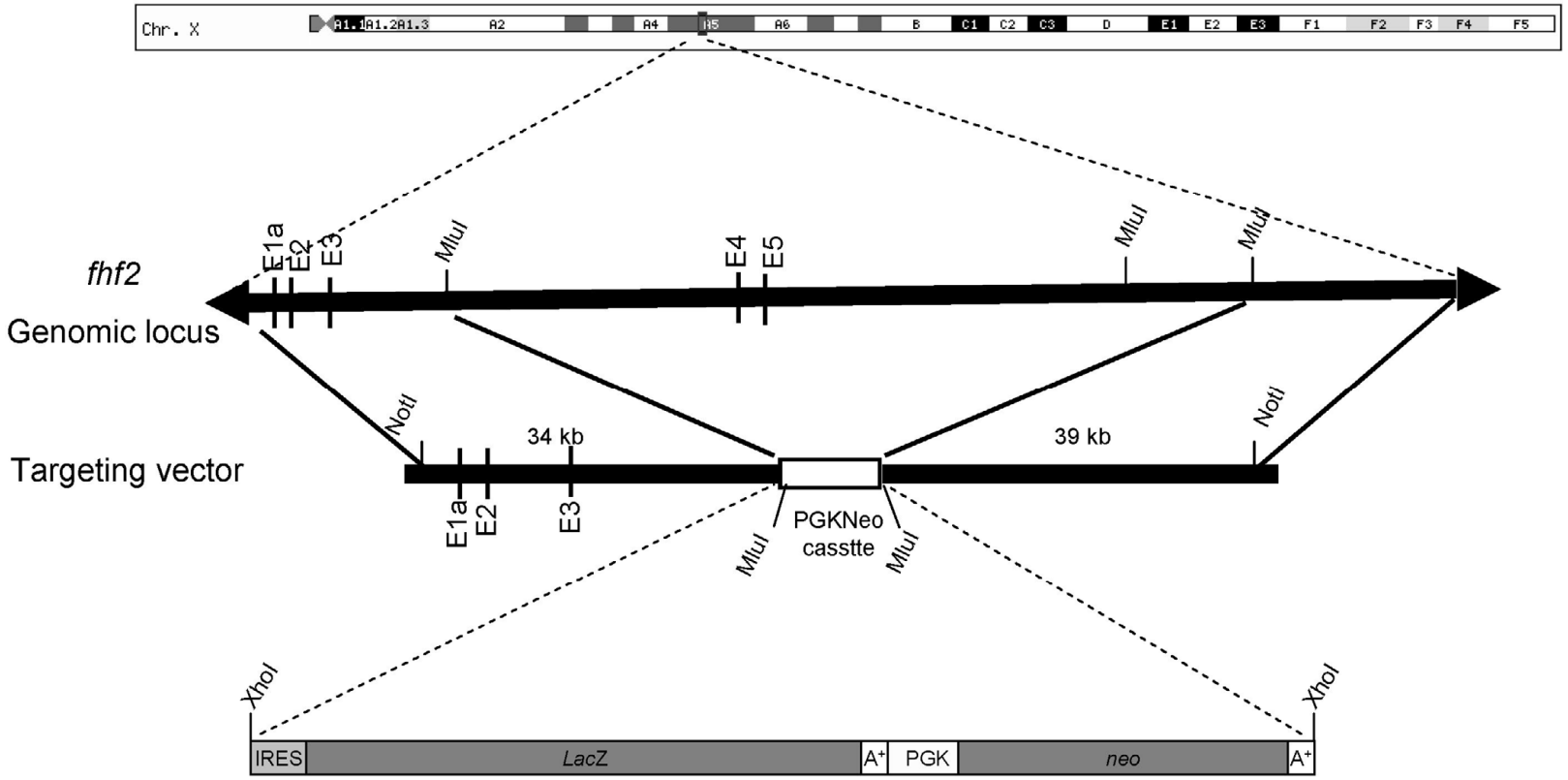

Appendix Figure 1.

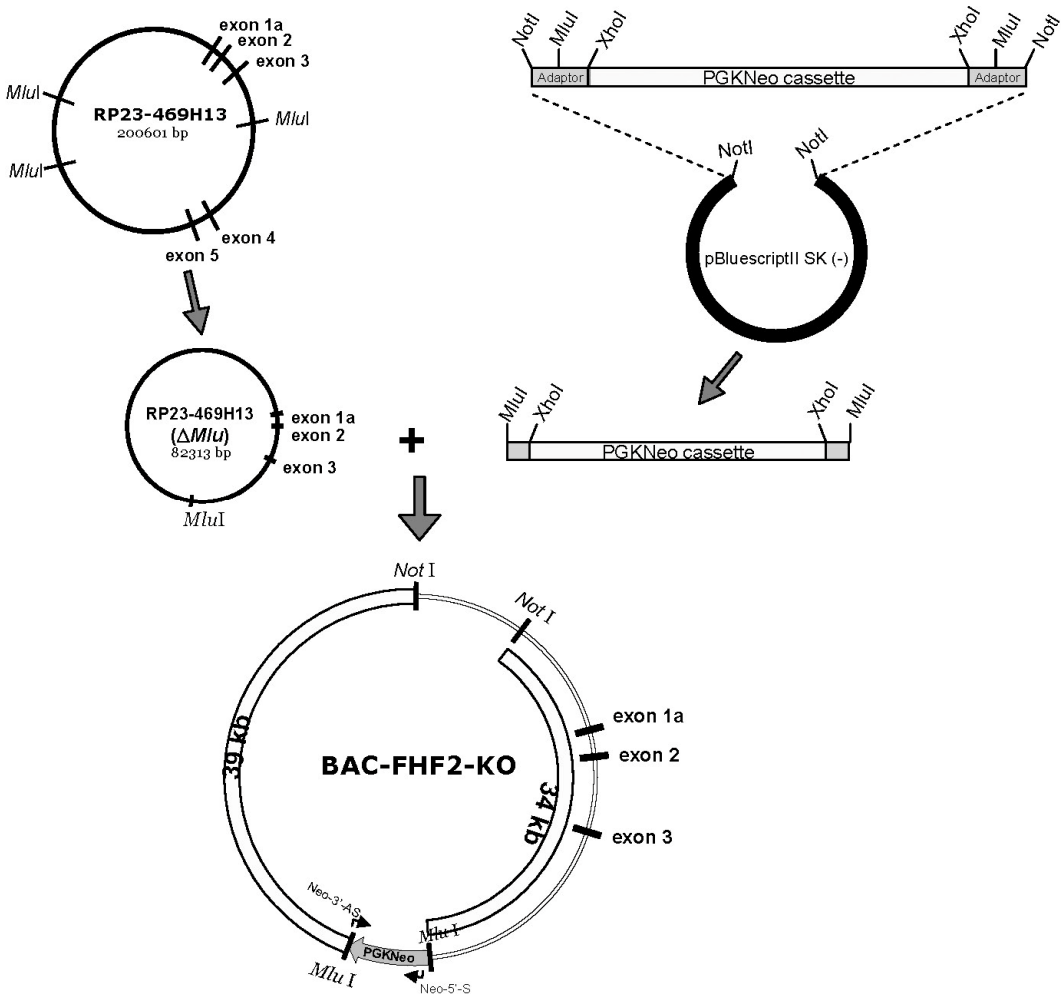

Appendix Figure 2. Schematic representation of approach used to generate BAC-based targeting vector

First, a PGKNeo cassette with *Mlu*I/*Xho*I adaptor (not drawn to scale) was generated. The targeting vector BAC-FHF2-KO replaces the genomic segment between outer *Mlu*I sites which contain exon 4 and 5 with PGKNeo cassette. The PGKNeo cassette is flanked in the 5' direction by a 34 kb homologous arm and in the 3' direction by a 39 kb homologous arm. The arrows show the oligonucleotide primers Neo-5'-S and Neo-3'-AS used for PCR detection of the PGKNeo cassette.

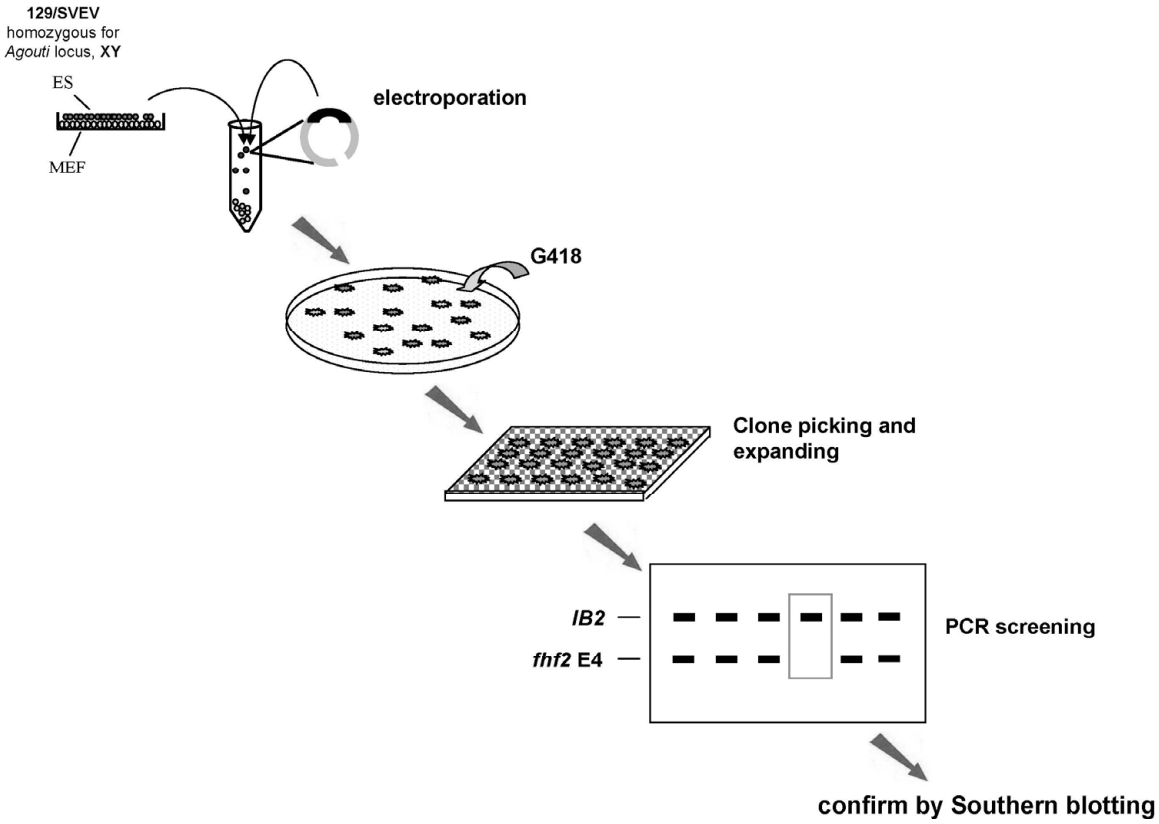

Appendix Figure 3. Gene targeting in murine ES cells

The linearized targeting vector BAC-FHF2-KO was transformed into ES cells by electroporation. The XY ES cells are 129/SVEV-derived, and homozygous for *Agouti* locus. Transformants were selected with G418. Neomycin-resistant clones were picked and expanded. Genomic DNAs from these clones were screened by PCR using two pairs of primers. One pair of primers corresponded to a segment in *fhf2* exon 4. The other pair served as an internal control, with primers specific for a portion of an unlinked gene, *IB2*. The band corresponded to exon 4 should be absent from any clone bearing a targeted allele. Candidate homologous recombinants identified by PCR will be confirmed by Southern blotting.

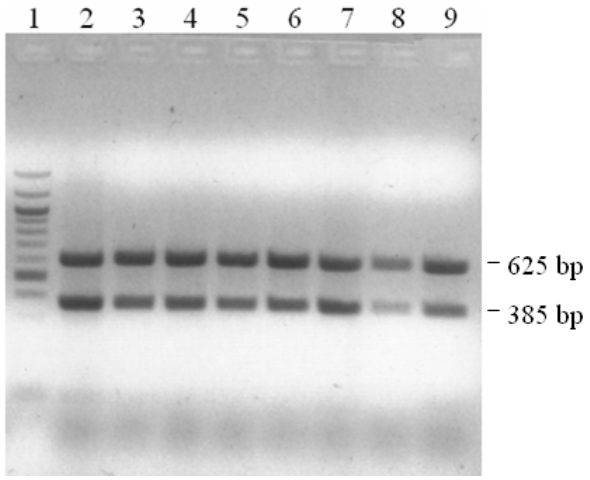

Appendix Figure 4. PCR analysis of the representative ES clones with two pairs of primers specific for *fhf2* exon 4 and *IB2* separately

Products were resolved in 2% agarose gel containing ethidium bromide. 1, 100 bp DNA ladder; 2-9, ES clones. Note that the sample in lane 8 had a weaker *fhf2* exon4 band and was taken as a candidate homologous recombinant to be further investigated by Southern blot hybridization.

BIBLIOGRAPHY

Abriel, H., Cabo, C., Wehrens, X.H., Rivolta, I., Motoike, H.K., Memmi, M., Napolitano, C., Priori, S.G., and Kass, R.S. (2001). Novel arrhythmogenic mechanism revealed by a long-QT syndrome mutation in the cardiac Na(+) channel. Circ Res **88,** 740-745.

Banker, G., Goslin, K., and Hannelore, A. (1998). Rat hippocampal neurons in low density culture. . In Culturing nerve cells, G. Banker and K. Goslin, eds (Cambridge, Mass.: MIT Press), pp. 339–370.

Beckh, S., Noda, M., Lubbert, H., and Numa, S. (1989). Differential regulation of three sodium channel messenger RNAs in the rat central nervous system during development. Embo J **8,** 3611-3616.

Benhorin, J., Goldmit, M., MacCluer, J.W., Blangero, J., Goffen, R., Leibovitch, A., Rahat, A., Wang, Q., Medina, A., Towbin, J., and Kerem, B. (1998). Identification of a new SCN5A mutation, D1840G, associated with the long QT syndrome. Mutations in brief no. 153. Online. Hum Mutat **12,** 72.

Bennett, V., and Lambert, S. (1999). Physiological roles of axonal ankyrins in survival of premyelinated axons and localization of voltage-gated sodium channels. J Neurocytol **28,** 303-318.

Bochet, P., Audinat, E., Lambolez, B., Crepel, F., Rossier, J., Iino, M., Tsuzuki, K., and Ozawa, S. (1994). Subunit composition at the single-cell level explains functional properties of a glutamate-gated channel. Neuron **12,** 383-388.

Boiko, T., Rasband, M.N., Levinson, S.R., Caldwell, J.H., Mandel, G., Trimmer, J.S., and Matthews, G. (2001). Compact myelin dictates the differential targeting of two sodium channel isoforms in the same axon. Neuron **30,** 91-104.

Bonifacino, J.S., and Traub, L.M. (2003). Signals for sorting of transmembrane proteins to endosomes and lysosomes. Annu Rev Biochem **72,** 395-447.

Brown, T.H., and Zador, A.M. (1990). The hippocampus. In Synaptic Organization of the Brain, G. Shepherd, ed (New York: Oxford University Press), pp. 346-388.

Burack, M.A., Silverman, M.A., and Banker, G. (2000). The role of selective transport in neuronal protein sorting. Neuron **26,** 465-472.

Burgess, D.L., Kohrman, D.C., Galt, J., Plummer, N.W., Jones, J.M., Spear, B., and Meisler, M.H. (1995). Mutation of a new sodium channel gene, Scn8a, in the mouse mutant 'motor endplate disease'. Nat Genet **10,** 461-465.

Caceres, A., Banker, G.A., and Binder, L. (1986). Immunocytochemical localization of tubulin and microtubule-associated protein 2 during the development of hippocampal neurons in culture. J Neurosci **6,** 714-722.

Catterall, W.A. (2000). From ionic currents to molecular mechanisms: the structure and function of voltage-gated sodium channels. Neuron **26,** 13-25.

Chang, C.C., Kuo, I.C., Ling, I.F., Chen, C.T., Chen, H.C., Lou, P.J., Lin, J.J., and Chang, T.C. (2004). Detection of quadruplex DNA structures in human telomeres by a fluorescent carbazole derivative. Anal Chem **76,** 4490-4494.

Coulier, F., Pontarotti, P., Roubin, R., Hartung, H., Goldfarb, M., and Birnbaum, D. (1997). Of worms and men: an evolutionary perspective on the fibroblast growth factor (FGF) and FGF receptor families. J Mol Evol **44,** 43-56.

Craig, A.M. (1998). Transfecting cultured neurons. In Culturing. Nerve Cells, G. Banker and K. Goslin, eds (Boston: MIT Press), pp. 79-111.

Dargent, B.M., I.; Shah, R.M.; Spooner, E.T.; Boudier, J.A.; Le Bivic, A.; Maue, R.; Sampo, B. . (1998). Targeting of the voltage-dependent sodium channel to the axon of cultured hippocampal neurons. . Soc. Neurosci. Abstr. **24,** 1078.

Dotti, C.G., Sullivan, C.A., and Banker, G.A. (1988). The establishment of polarity by hippocampal neurons in culture. J Neurosci **8,** 1454-1468.

Elbashir, S.M., Lendeckel, W., and Tuschl, T. (2001). RNA interference is mediated by 21- and 22-nucleotide RNAs. Genes Dev **15,** 188-200.

Ferrero, G.B., Gebbia, M., Pilia, G., Witte, D., Peier, A., Hopkin, R.J., Craigen, W.J., Shaffer, L.G., Schlessinger, D., Ballabio, A., and Casey, B. (1997). A submicroscopic deletion in Xq26 associated with familial situs ambiguus. Am J Hum Genet **61,** 395-401.

Garrido, J.J., Fernandes, F., Giraud, P., Mouret, I., Pasqualini, E., Fache, M.P., Jullien, F., and Dargent, B. (2001). Identification of an axonal determinant in the C-terminus of the sodium channel Na(v)1.2. Embo J **20,** 5950-5961.

Gecz, J., Baker, E., Donnelly, A., Ming, J.E., McDonald-McGinn, D.M., Spinner, N.B., Zackai, E.H., Sutherland, G.R., and Mulley, J.C. (1999). Fibroblast growth factor homologous factor 2 (FHF2): gene structure, expression and mapping to the Borjeson-Forssman-Lehmann syndrome region in Xq26 delineated by a duplication breakpoint in a BFLS-like patient. Hum Genet **104,** 56-63.

Gedeon, A.K., Glass, I.A., Connor, J.M., and Mulley, J.C. (1996). Genetic localisation of MRX27 to Xq24-26 defines another discrete gene for non-specific X-linked mental retardation. Am J Med Genet **64,** 121-124.

Gee, S.H., Madhavan, R., Levinson, S.R., Caldwell, J.H., Sealock, R., and Froehner, S.C. (1998). Interaction of muscle and brain sodium channels with multiple members of the syntrophin family of dystrophin-associated proteins. J Neurosci **18,** 128-137.

Goetz, R., Dover, K., Laezza, F., Shtraizent, N., Huang, X., Tchetchik, D., Eliseenkova, A.V., Xu, C.F., Neubert, T., Ornitz, D.M., Goldfarb, M., and Mohammadi, M. (manuscript submitted). Crystal structure of a fibroblast growth factor homologous factor define conserved surface for binding and modulation of voltage-gated sodium channels. J Biol Chem.

Goldfarb, M. (2005). Fibroblast growth factor homologous factors: evolution, structure, and function. Cytokine Growth Factor Rev **16,** 215-220.

Goldfarb, M., Schoorlemmer, J., Williams, A., Diwakar, S., Wang, Q., Huang, X., Giza, J., Tchetchik, D., Kelley, K., Vega, A., Matthews, G., Rossi, P., Ornitz, D.M., and D'Angelo, E. (2007). Fibroblast growth factor homologous factors control neuronal excitability through modulation of voltage-gated sodium channels. Neuron **55,** 449-463.

Goldin, A.L. (2001). Resurgence of sodium channel research. Annu Rev Physiol **63,** 871-894.

Goldin, A.L., Barchi, R.L., Caldwell, J.H., Hofmann, F., Howe, J.R., Hunter, J.C., Kallen, R.G., Mandel, G., Meisler, M.H., Netter, Y.B., Noda, M., Tamkun, M.M., Waxman, S.G., Wood, J.N., and Catterall, W.A. (2000). Nomenclature of voltage-gated sodium channels. Neuron **28,** 365-368.

Gong, B., Rhodes, K.J., Bekele-Arcuri, Z., and Trimmer, J.S. (1999). Type I and type II Na(+) channel alpha-subunit polypeptides exhibit distinct spatial and temporal patterning, and association with auxiliary subunits in rat brain. J Comp Neurol **412,** 342-352.

Hartung, H., Feldman, B., Lovec, H., Coulier, F., Birnbaum, D., and Goldfarb, M. (1997). Murine FGF-12 and FGF-13: expression in embryonic nervous system, connective tissue and heart. Mech Dev **64,** 31-39.

Hille, B. (2001). Ion channels of excitable membranes. (Sunderland, Mass.: Sinauer).

Inda, M.C., DeFelipe, J., and Munoz, A. (2006). Voltage-gated ion channels in the axon initial segment of human cortical pyramidal cells and their relationship with chandelier cells. Proc Natl Acad Sci U S A **103,** 2920-2925.

Isom, L.L. (2001). Sodium channel beta subunits: anything but auxiliary. Neuroscientist **7,** 42-54.

Kordeli, E., Lambert, S., and Bennett, V. (1995). AnkyrinG. A new ankyrin gene with neural-specific isoforms localized at the axonal initial segment and node of Ranvier. J Biol Chem **270,** 2352-2359.

Laezza, F., Gerber, B.R., Lou, J.Y., Kozel, M.A., Hartman, H., Craig, A.M., Ornitz, D.M., and Nerbonne, J.M. (2007). The FGF14(F145S) mutation disrupts the interaction of FGF14 with voltage-gated Na+ channels and impairs neuronal excitability. J Neurosci **27,** 12033-12044.

Lambolez, B., Audinat, E., Bochet, P., Crepel, F., and Rossier, J. (1992). AMPA receptor subunits expressed by single Purkinje cells. Neuron **9,** 247-258.

Li, B.W., Rush, A.C., Tan, J., and Weil, G.J. (2004). Quantitative analysis of gender-regulated transcripts in the filarial nematode Brugia malayi by real-time RT-PCR. Mol Biochem Parasitol **137,** 329-337.

Liu, C., Dib-Hajj, S.D., and Waxman, S.G. (2001a). Fibroblast growth factor homologous factor 1B binds to the C terminus of the tetrodotoxin-resistant sodium channel rNav1.9a (NaN). J Biol Chem **276,** 18925-18933.

Liu, C.J., Dib-Hajj, S.D., Renganathan, M., Cummins, T.R., and Waxman, S.G. (2003). Modulation of the cardiac sodium channel Nav1.5 by fibroblast growth factor homologous factor 1B. J Biol Chem **278,** 1029-1036.

Liu, C.J., Dib-Hajj, S.D., Black, J.A., Greenwood, J., Lian, Z., and Waxman, S.G. (2001b). Direct interaction with contactin targets voltage-gated sodium channel Na(v)1.9/NaN to the cell membrane. J Biol Chem **276,** 46553-46561.

Lou, J.Y., Laezza, F., Gerber, B.R., Xiao, M., Yamada, K.A., Hartmann, H., Craig, A.M., Nerbonne, J.M., and Ornitz, D.M. (2005). Fibroblast growth factor 14 is an intracellular modulator of voltage-gated sodium channels. J Physiol **569,** 179-193.

Malmgren, H., Sundvall, M., Dahl, N., Gustavson, K.H., Anneren, G., Wadelius, C., Steen-Bondeson, M.L., and Pettersson, U. (1993). Linkage mapping of a severe X-linked mental retardation syndrome. Am J Hum Genet **52,** 1046-1052.

Matsumoto, E., and Rosenbluth, J. (1985). Plasma membrane structure at the axon hillock, initial segment and cell body of frog dorsal root ganglion cells. J Neurocytol **14,** 731-747.

McPhee, J.C., Ragsdale, D.S., Scheuer, T., and Catterall, W.A. (1995). A critical role for transmembrane segment IVS6 of the sodium channel alpha subunit in fast inactivation. J Biol Chem **270,** 12025-12034.

Mechaly, I., Scamps, F., Chabbert, C., Sans, A., and Valmier, J. (2005). Molecular diversity of voltage-gated sodium channel alpha subunits expressed in neuronal and non-neuronal excitable cells. Neuroscience **130,** 389-396.

Munoz-Sanjuan, I., Fallon, J.F., and Nathans, J. (2000a). Expression and regulation of chicken fibroblast growth factor homologous factor (FHF)-4 at the base of the developing limbs. Mech Dev **95,** 101-112.

Munoz-Sanjuan, I., Smallwood, P.M., and Nathans, J. (2000b). Isoform diversity among fibroblast growth factor homologous factors is generated by alternative promoter usage and differential splicing. J Biol Chem **275,** 2589-2597.

Munoz-Sanjuan, I., Simandl, B.K., Fallon, J.F., and Nathans, J. (1999). Expression of chicken fibroblast growth factor homologous factor (FHF)-1 and of differentially spliced isoforms of FHF-2 during development and involvement of FHF-2 in chicken limb development. Development **126,** 409-421.

Munoz-Sanjuan, I., Cooper, M.K., Beachy, P.A., Fallon, J.F., and Nathans, J. (2001). Expression and regulation of chicken fibroblast growth factor homologous factor (FHF)-4 during craniofacial morphogenesis. Dev Dyn **220,** 238-245.

Nether, E. (1992). Correction for liquid junction potentials in patch clamp experiments. In Methods in Enzymol, B.R.a.L. Iverson, ed (San Diego: Academic Press), pp. 123-131.

Noda, M., Ikeda, T., Kayano, T., Suzuki, H., Takeshima, H., Kurasaki, M., Takahashi, H., and Numa, S. (1986). Existence of distinct sodium channel messenger RNAs in rat brain. Nature **320,** 188-192.

Nolan, T., Hands, R.E., and Bustin, S.A. (2006). Quantification of mRNA using real-time RT-PCR. Nat Protoc **1,** 1559-1582.

Olsen, S.K., Garbi, M., Zampieri, N., Eliseenkova, A.V., Ornitz, D.M., Goldfarb, M., and Mohammadi, M. (2003). Fibroblast growth factor (FGF) homologous factors share structural but not functional homology with FGFs. J Biol Chem **278,** 34226-34236.

Ornitz, D.M., and Itoh, N. (2001). Fibroblast growth factors. Genome Biol **2,** REVIEWS3005.

Rasband, M.N., Peles, E., Trimmer, J.S., Levinson, S.R., Lux, S.E., and Shrager, P. (1999). Dependence of nodal sodium channel clustering on paranodal axoglial contact in the developing CNS. J Neurosci **19,** 7516-7528.

Ratcliffe, C.F., Westenbroek, R.E., Curtis, R., and Catterall, W.A. (2001). Sodium channel beta1 and beta3 subunits associate with neurofascin through their extracellular immunoglobulin-like domain. J Cell Biol **154,** 427-434.

Rush, A.M., Wittmack, E.K., Tyrrell, L., Black, J.A., Dib-Hajj, S.D., and Waxman, S.G. (2006). Differential modulation of sodium channel Na(v)1.6 by two members of the fibroblast growth factor homologous factor 2 subfamily. Eur J Neurosci **23,** 2551-2562.

Schaller, K.L., Krzemien, D.M., Yarowsky, P.J., Krueger, B.K., and Caldwell, J.H. (1995). A novel, abundant sodium channel expressed in neurons and glia. J Neurosci **15,** 3231-3242.

Schoorlemmer, J., and Goldfarb, M. (2001). Fibroblast growth factor homologous factors are intracellular signaling proteins. Curr Biol **11,** 793-797.

Schoorlemmer, J., and Goldfarb, M. (2002). Fibroblast growth factor homologous factors and the islet brain-2 scaffold protein regulate activation of a stress-activated protein kinase. J Biol Chem **277,** 49111-49119.

Shakkottai, V.G., Xiao, M., Xu, L., Wong, M., Nerbonne, J.M., Ornitz, D.M., and Yamada, K.A. (2009). FGF14 regulates the intrinsic excitability of cerebellar Purkinje neurons Neurobiol Dis **33,** 81-88.

Shiloh, Y., Litvak, G., Ziv, Y., Lehner, T., Sandkuyl, L., Hildesheimer, M., Buchris, V., Cremers, F.P., Szabo, P., White, B.N., and et al. (1990). Genetic mapping of X-linked albinism-deafness syndrome (ADFN) to Xq26.3-q27.I. Am J Hum Genet **47,** 20-27.

Smallwood, P.M., Munoz-Sanjuan, I., Tong, P., Macke, J.P., Hendry, S.H., Gilbert, D.J., Copeland, N.G., Jenkins, N.A., and Nathans, J. (1996). Fibroblast growth factor (FGF) homologous factors: new members of the FGF family implicated in nervous system development. Proc Natl Acad Sci U S A **93,** 9850-9857.

Stuart, G., Spruston, N., Sakmann, B., and Hausser, M. (1997). Action potential initiation and backpropagation in neurons of the mammalian CNS. Trends Neurosci **20,** 125-131.

Sugawara, T., Tsurubuchi, Y., Fujiwara, T., Mazaki-Miyazaki, E., Nagata, K., Montal, M., Inoue, Y., and Yamakawa, K. (2003). Nav1.1 channels with mutations of severe myoclonic epilepsy in infancy display attenuated currents. Epilepsy Res **54,** 201-207.

Tsuzuki, K., Isa, T., and Ozawa, S. (2000). Subunit composition of AMPA receptors expressed by single hippocampal neurons. Neuroreport **11,** 3583-3587.

van Swieten, J.C., Brusse, E., de Graaf, B.M., Krieger, E., van de Graaf, R., de Koning, I., Maat-Kievit, A., Leegwater, P., Dooijes, D., Oostra, B.A., and Heutink, P. (2003). A mutation in the fibroblast growth factor 14 gene is associated with autosomal dominant cerebellar ataxia [corrected]. Am J Hum Genet **72,** 191-199.

Verdier, A.S., Mattei, M.G., Lovec, H., Hartung, H., Goldfarb, M., Birnbaum, D., and Coulier, F. (1997). Chromosomal mapping of two novel human FGF genes, FGF11 and FGF12. Genomics **40,** 151-154.

Wang, Q., McEwen, D.G., and Ornitz, D.M. (2000). Subcellular and developmental expression of alternatively spliced forms of fibroblast growth factor 14. Mech Dev **90,** 283-287.

Wang, Q., Bardgett, M.E., Wong, M., Wozniak, D.F., Lou, J., McNeil, B.D., Chen, C., Nardi, A., Reid, D.C., Yamada, K., and Ornitz, D.M. (2002). Ataxia and

paroxysmal dyskinesia in mice lacking axonally transported FGF14. Neuron **35,** 25-38.

Winckler, B., and Mellman, I. (1999). Neuronal polarity: controlling the sorting and diffusion of membrane components. Neuron **23,** 637-640.

Wittmack, E.K., Rush, A.M., Craner, M.J., Goldfarb, M., Waxman, S.G., and Dib-Hajj, S.D. (2004). Fibroblast growth factor homologous factor 2B: association with Nav1.6 and selective colocalization at nodes of ranvier of dorsal root axons. J Neurosci **24,** 6765-6775.

Xiao, M., Xu, L., Laezza, F., Yamada, K., Feng, S., and Ornitz, D.M. (2007). Impaired hippocampal synaptic transmission and plasticity in mice lacking fibroblast growth factor 14. Mol Cell Neurosci **34,** 366-377.

Yamamoto, S., Mikami, T., Konishi, M., and Itoh, N. (2000). Stage-specific expression of a novel isoform of mouse FGF-14 (FHF-4) in spermatocytes. Biochim Biophys Acta **1490,** 121-124.